Cell

A commonly inherited human *PCSK9* germline variant drives breast cancer metastasis via LRP1 receptor

Graphical abstract

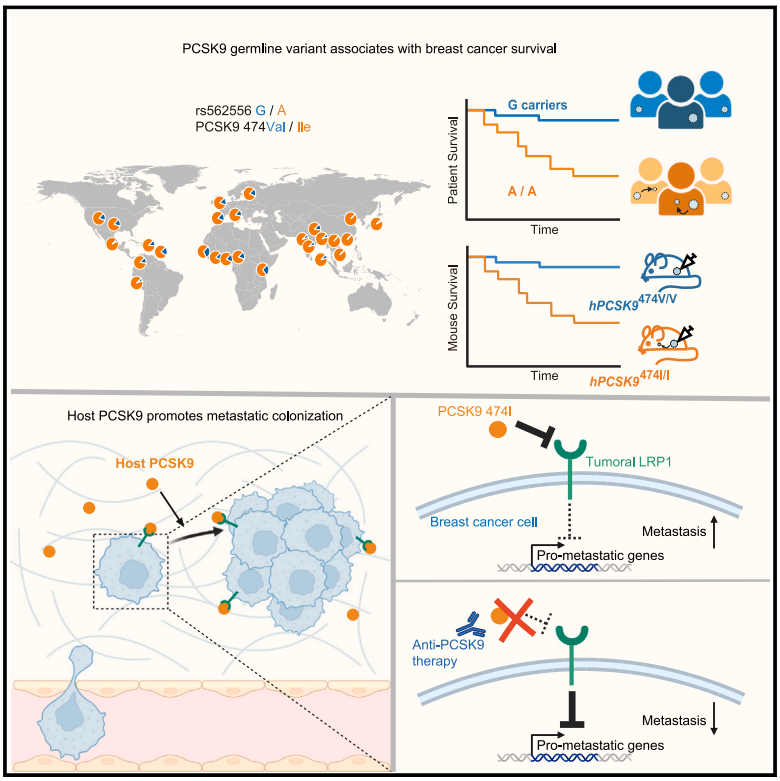

Highlights

- A human germline variant in *PCSK9* (V474I) associates with breast cancer survival
- Host PCSK9 V474I causally drives breast cancer metastasis
- Host PCSK9 targets tumoral LRP1 and induces somatic pro-metastatic gene expression
- Therapeutic inhibition of PCSK9 suppresses breast cancer metastasis

Authors

Wenbin Mei (梅文彬), Schayan Faraj Tabrizi, Christopher Godina, Anthea F. Lovisa, Karolin Isaksson, Helena Jernström, Sohail F. Tavazoie

Correspondence

sohail.tavazoie@rockefeller.edu

In brief

Characterization of a common germline variant in *PCSK9* unveils a hereditary basis underlying breast cancer metastasis and suggests that PCSK9 inhibition therapy could be a promising strategy for breast cancer metastasis prevention.

Mei et al., 2025, Cell *188*, 371–389
January 23, 2025
https://doi.org/10.1016/j.cell.2024.11.009

CellPress

Cell

CellPress

Article

A commonly inherited human *PCSK9* germline variant drives breast cancer metastasis via LRP1 receptor

Wenbin Mei (梅文彬),[1] Schayan Faraj Tabrizi,[1,4] Christopher Godina,[2,4] Anthea F. Lovisa,[1,4] Karolin Isaksson,[3] Helena Jernström,[2] and Sohail F. Tavazoie[1,5,*]

[1]Laboratory of Systems Cancer Biology, The Rockefeller University, New York, NY, USA
[2]Division of Oncology, Department of Clinical Sciences in Lund, Lund University Cancer Center/Kamprad, Lund, Sweden
[3]Division of Surgery, Department of Clinical Sciences in Lund, Lund University and Department of Surgery Kristianstad Hospital, Lund, Sweden
[4]These authors contributed equally
[5]Lead contact
*Correspondence: sohail.tavazoie@rockefeller.edu
https://doi.org/10.1016/j.cell.2024.11.009

SUMMARY

Identifying patients at risk for metastatic relapse is a critical medical need. We identified a common missense germline variant in proprotein convertase subtilisin/kexin type 9 (*PCSK9*) (rs562556, V474I) that is associated with reduced survival in multiple breast cancer patient cohorts. Genetic modeling of this gain-of-function single-nucleotide variant in mice revealed that it causally promotes breast cancer metastasis. Conversely, host PCSK9 deletion reduced metastatic colonization in multiple breast cancer models. Host PCSK9 promoted metastatic initiation events in lung and enhanced metastatic proliferative competence by targeting tumoral low-density lipoprotein receptor related protein 1 (LRP1) receptors, which repressed metastasis-promoting genes *XAF1* and *USP18*. Antibody-mediated therapeutic inhibition of PCSK9 suppressed breast cancer metastasis in multiple models. In a large Swedish early-stage breast cancer cohort, rs562556 homozygotes had a 22% risk of distant metastatic relapse at 15 years, whereas non-homozygotes had a 2% risk. Our findings reveal that a commonly inherited genetic alteration governs breast cancer metastasis and predicts survival—uncovering a hereditary basis underlying breast cancer metastasis.

INTRODUCTION

Metastasis formation is the most critical determinant of cancer survival outcome.[1] It has long been thought that specific somatic mutations emerge during tumorigenesis and drive metastatic progression. However, unlike tumorigenesis[2–4] or drug resistance,[5,6] such postulated emergent somatic "metastasis driver mutations" have not been identified by extensive tumor sequencing efforts[7–10]—with similar patterns of driver mutations observed in metastases and matched primary tumors.[11,12] While these findings do not rule out the possibility that rare emergent somatic "driver" mutations may exist in metastases, they motivate the search for alternative mechanisms.

One alternative mechanism is that germline genetic differences between individuals underlie distinct metastatic outcomes. This could explain observations thus far since (1) germline genetic alterations are already present at the primary tumor site and do not need to "emerge" at the metastatic site—explaining similar genetic mutational landscapes of metastases and primary tumors—and (2) germline genetics would produce similar host-derived proteins at the primary and metastatic sites that would signal to cancer cells[13–15] and give rise to concordant pro-metastatic gene expression programs at both locations. This could account for the similar gene expression programs observed in matched primary and metastatic tumors.[16–19]

Historical observations in mice support the role of germline genetics in affecting metastasis. For example, it has long been observed that genetic background can influence the efficiency of metastasis in the polyoma middle T oncogene (PyMT) murine breast cancer model.[20,21] Identifying germline genetic differences that could influence human metastatic outcomes is a far greater challenge, as the substantial genetic variation within the human population limits the statistical power for identifying genetic associations with cancer outcomes.[22,23] One way to increase the statistical power for detecting associations is to focus on common germline variants. Indeed, recent studies have found that common germline variants of *APOE* differentially impact melanoma progression and metastasis and associate with human melanoma survival.[24,25]

We herein hypothesized that common germline variants could underlie breast cancer metastatic outcomes and devised a systematic approach to search for such a causal variant. We identified the common missense variant rs562556 in the proprotein convertase subtilisin/kexin type 9 (*PCSK9*) gene to be

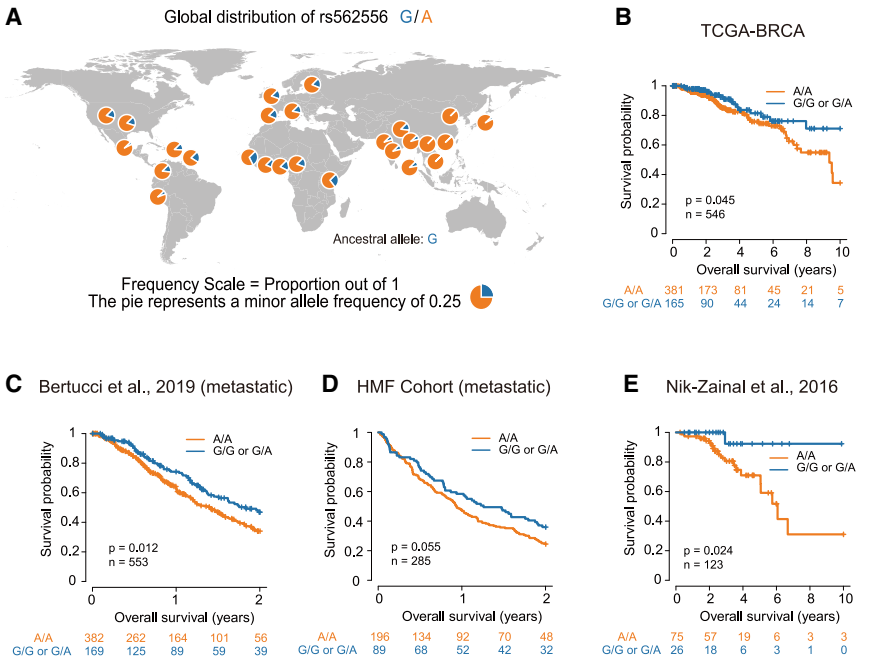

Figure 1. PCSK9 germline variant rs562556 associates with breast cancer survival

(A) Geographical distribution of rs562556 allele frequency.

(B–E) Kaplan-Meier curves of breast cancer patients in cohorts stratified by rs562556 genotype (two-sided log-rank test). TCGA-BRCA (n = 546): patients with high-risk breast cancer as defined by stage II/III and over 50 (B) Bertucci et al.[26] (n = 553): patients with metastatic breast cancer (C). Hartwig Medical Foundation (HMF) cohort (n = 285): patients over 50 with metastatic breast cancer from the HMF cohort (D). Nik-Zainal et al.[29] (n = 123): patients with high-risk breast cancer as defined by grade II/III and over 50 (E). Number at risk tables are shown.

See also Figure S1.

associated with reduced survival outcomes in multiple breast cancer patient cohorts. We found that the *PCSK9* rs562556 variant drives breast cancer metastasis by targeting tumoral low-density lipoprotein (LDL) receptor (LDLR) related protein 1 (LRP1) receptors, consequently leading to the induction of genes that we implicate as metastatic colonization promoters.

RESULTS

Common germline variant rs562556 of the human *PCSK9* gene associates with breast cancer prognosis

Previous genome-wide association study (GWAS) efforts had identified very few germline variants that associate with breast cancer prognosis, likely due to limited statistical power for identifying small effect size variants when surveying the large landscape of genome-wide variants.[22] We focused on a set of common missense variants with known disease associations, which would *a priori* be more likely to exhibit phenotypic consequences. This set also included missense variants of ligand, receptor, and transporter genes, as they would be more likely to mediate communication between microenvironmental cells and cancer cells. This approach identified 8 single-nucleotide polymorphisms (SNPs) that are associated with breast cancer overall survival in both the Cancer Genome Atlas Breast Invasive Carcinoma (TCGA-BRCA) and Bertucci et al. US cohorts[26] (Figures S1A and S1B). *PCSK9*, a well-known therapeutic target in cardiovascular disease and hypercholesterolemia,[27] was among the 8 identified genes harboring a candidate SNP. We focused on this gene given the availability of approved therapeutics that inhibit its protein product.

The rs562556 SNP (1240G>A; allele frequency = 0.83) affects exon 9 of *PCSK9*, causing an amino acid substitution (V474I) thought to be hypermorphic in cholesterol regulation.[28] The allele frequency of this variant varies geographically, with approximately 70% of individuals of European ancestry being A/A homozygotes (Figure 1A). When a recessive genetic model was applied, beyond the two cohorts from the US (TCGA-BRCA and Bertucci et al.) (Figures 1B and 1C), rs562556 was associated with reduced breast cancer patient survival outcomes in two additional independent cohorts from the Netherlands[12] and the UK,[29] respectively (Figures 1D and 1E). In contrast to patients carrying the ancestral G allele, women homozygous for the gain-of-function A allele exhibited reduced overall survival. This association remained significant after adjusting for common clinical confounders, including pathological stage, tumor grade, treatment status, and breast cancer subtype (Figures S1C–S1F).

The Bertucci et al. and TCGA-BRCA cohorts enrolled US patients of Asian ancestry who are enriched for the rs562556 A/A genotype, which is associated with reduced overall survival (Figure 1A). This is unlikely to bias the results as Asian women have higher breast cancer survival rates compared with other ethnic groups in the US.[30] Moreover, the association between rs562556 and breast cancer prognosis remained significant when focusing solely on individuals of European ancestry[31] or adjusting for the principal components of genetic variation (Figures S1G–S1I). Adjusting for the status of the other two common missense mutations in *PCSK9* did not abrogate the significance of rs562556 either (Figure S1J). The rs562556 A allele has also been associated with a modest increase in cardiovascular disease risk.[32,33] However, we observed no correlation between rs562556 and overall mortality in an age-matched breast cancer-free general population in the UK biobank[34] (Figure S1K). Moreover, rs562556 did not associate with overall survival in melanoma or lung cancer (Figures S1L–S1N). These findings reveal that the association between rs562556 and breast cancer survival outcomes is not confounded by ancestry or non-cancer mortality.

Host PCSK9 promotes breast cancer metastasis

Because cancer metastasis is the primary determinant of breast cancer survival,[35] we hypothesized that the *PCSK9* rs562556

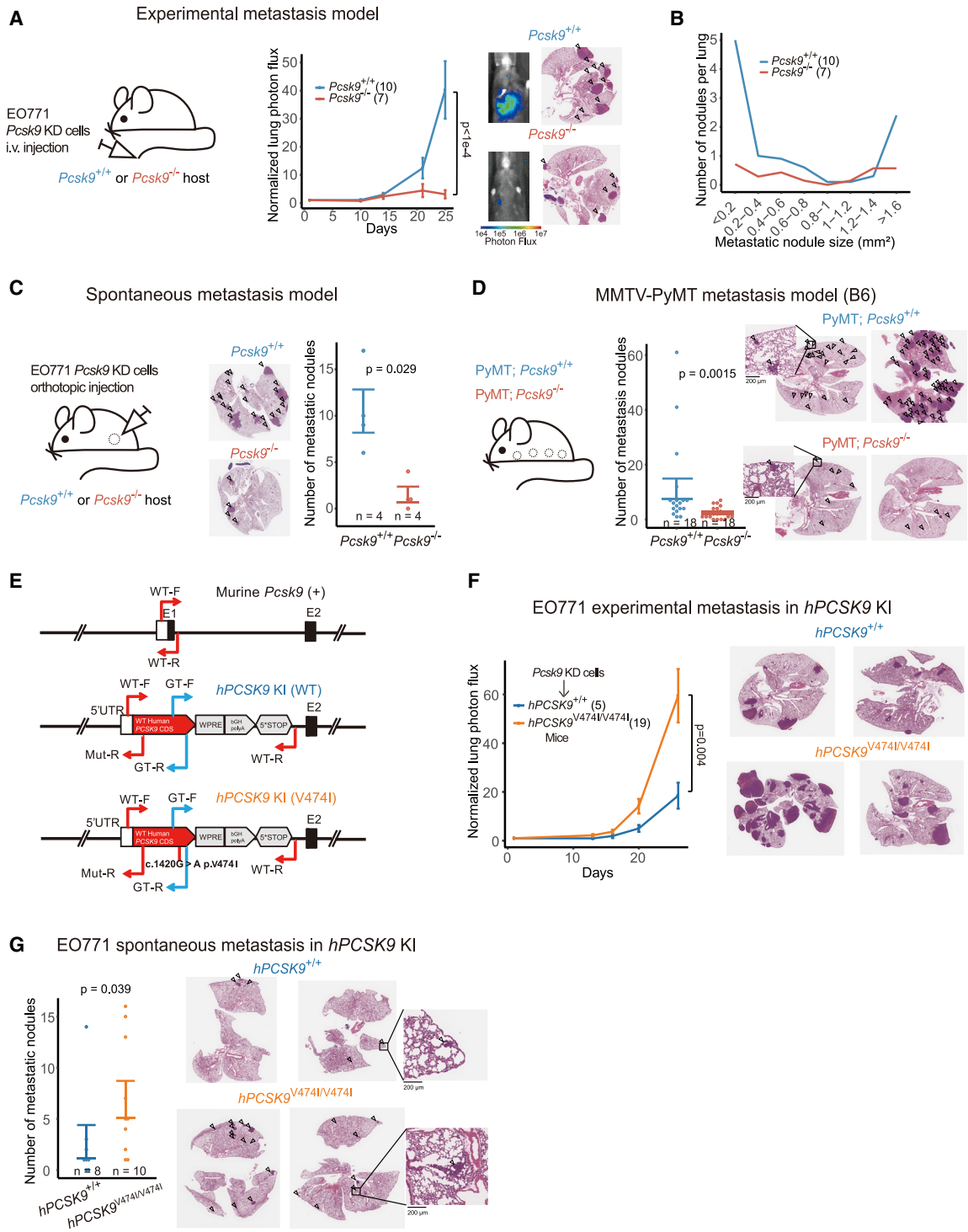

Figure 2. Host PCSK9 promotes breast cancer metastasis

(A) Bioluminescence imaging of metastatic progression of *Pcsk9* knockdown (KD) EO771-LM2-shPcsk9 cells intravenously injected into wild-type or *Pcsk9* knockout mice (F test).

(B) Distribution of lung metastasis foci size and number in wild-type and *Pcsk9* knockout mice.

(C) Spontaneous lung metastasis quantification in wild-type and *Pcsk9* knockout mice with mammary fat pad implantation of EO771-LM2-shPcsk9 cells (two-sided Wilcoxon rank-sum test).

(D) Lung metastasis number in wild-type and *Pcsk9* knockout mice with MMTV-PyMT transgene in C57BL/6J (B6) background (two-sided Wilcoxon rank-sum test).

(legend continued on next page)

variant may impact survival by affecting metastasis formation. PCSK9 is normally mainly expressed in the liver, lung, esophagus, pancreas, and colon (www.proteinatlas.org).[36] PCSK9 has been observed to be highly expressed in human gastrointestinal and lung cancers but poorly expressed in breast tumors and normal mammary tissues (Figure S2A).

Despite its low expression, we first assessed the role of tumoral PCSK9 in breast cancer, as a prior study reported that tumoral PCSK9 could promote primary tumor growth by suppressing the immune response,[37] whereas another study implicated a role for tumoral PCSK9 in regulation of cholesterol synthesis in colorectal cancer cells.[38] shRNA or CRISPR-Cas9-mediated depletion of tumoral PCSK9 did not impact breast cancer metastatic colonization after intravenous injection of PCSK9-depleted EO771 murine breast cancer cells in an immune-competent model (Figures S2B–S2D). Moreover, tumoral *Pcsk9* deletion did not impact murine breast tumor growth (Figure S2E). Similarly, *PCSK9* deletion in MDA-MB-231 human breast cancer cells did not affect metastasis (Figures S2B, bottom and S2F). Consistent with this, PCSK9 expression was not detected in another highly metastatic triple-negative murine breast cancer cell line, 4T1 (Figure S2B, right). These findings reveal that tumoral PCSK9 does not impact breast cancer progression in multiple models.

To test the impact of host PCSK9 on metastatic colonization, we intravenously injected *Pcsk9*-depleted EO771 cells into wild-type or *Pcsk9* knockout mice, which were generated by CRISPR-Cas9 targeting (Figure S2G). The use of *Pcsk9*-depleted cells allowed us to study the role of host PCSK9 specifically and avoid potential immune-mediated rejection of PCSK9-expressing cells in *Pcsk9* knockout mice. We observed markedly reduced breast cancer lung metastatic colonization in *Pcsk9* knockout mice relative to wild-type counterparts (Figure 2A), with reduced numbers of small and large lung metastatic nodules (Figure 2B). Intracardiac injections revealed reduced systemic metastasis to multiple organs in *Pcsk9* knockout mice as quantified by bioluminescence imaging (Figure S2H). EO771 breast cancer cells implanted into the mammary fat pads exhibited reduced spontaneous metastasis in *Pcsk9* knockout mice (Figure 2C) without a significant difference in primary tumor growth (Figure S2I). Similarly, *Pcsk9* deletion significantly reduced lung metastasis in the mouse mammary tumor virus-PyMT (MMTV-PyMT)[39] genetically engineered model (Figure 2D), without observable effects on primary tumor growth (Figure S2J). These findings from multiple models reveal that host PCSK9 promotes breast cancer metastasis.

The amino acid altered by rs562556, valine 474, is conserved from hominoids to Old World monkeys but not conserved in mice.[40,41] To directly model the effect of PCSK9 variant rs562556, we generated human *PCSK9* wild-type and rs562556 mutant (c.1420G>A, p.V474I) knockin (KI) mice in the C57BL/6J background, with the human *PCSK9* alleles knocked into the murine *Pcsk9* locus (Figures 2E and S2K top). The expression levels of PCSK9 were similar in human *PCSK9* wild-type and V474I mutant mice (Figure S2K bottom). This single nucleotide/amino acid change in host PCSK9 caused a significant enhancement in lung metastatic colonization by murine *Pcsk9*-silenced EO771 breast cancer cells (Figure 2F), consistent with its association with worse prognosis in human breast cancer patients. EO771 breast cancer cells implanted into the mammary fat pads also exhibited enhanced spontaneous metastasis in h*PCSK9*$^{V474I/V474I}$ relative to h*PCSK9*$^{+/+}$ mice without significant change in primary tumor growth (Figures 2G and S2L). These findings reveal that inherited PCSK9 genetic status modulates breast cancer metastasis outcomes in mice.

Metastasis promotion by PCSK9 is independent of host cholesterol reduction

Obesity and hypercholesterolemia have been shown to promote breast cancer progression in experimental models.[42–44] Epidemiological studies have shown both positive and negative correlations between high cholesterol and increased breast cancer risk and death.[45] PCSK9 increases serum cholesterol levels by promoting the degradation of LDLRs and reducing LDL clearance.[27,46] One study proposed that hypercholesterolemia due to hepatic PCSK9 and the alteration of liver tissue increased melanoma liver metastasis.[47] To determine if the metastasis-suppressive effect of host PCSK9 deficiency in breast cancer was due to its associated cholesterol reduction effect (total cholesterol = 39.7 mg/dL for *Pcsk9* knockout versus 80.64 mg/dL for wild-type mice; Figure S3A), we fed mice a high cholesterol diet (HCD) starting 10 days before tumor implantation. This dietary intervention scheme brought the LDL of *Pcsk9* knockout mice to a similar level as wild-type mice and their total cholesterol to a comparable level as mice on a regular chow diet (Figure S3A). Under this condition, *Pcsk9* knockout mice continued to exhibit reduced breast cancer lung metastasis relative to littermates under HCD or regular chow diet, while HCD modestly increased lung metastasis in wild-type mice (Figure S3B). Our results indicate that the metastasis-suppressive effect of PCSK9 deficiency is not mediated by LDL cholesterol reduction.

We also measured cholesterol levels of human *PCSK9* KI mice on regular chow diet. h*PCSK9*$^{V474I/V474I}$ mice showed a trend toward slightly higher total cholesterol and LDL levels (total cholesterol = 151.5 mg/dL versus 148.6 mg/dL; LDL = 36.3 mg/dL versus 32.4 mg/dL) than h*PCSK9*$^{+/+}$ mice (Figures S3C and S3D). The lack of meaningful differences in circulating cholesterol and LDL levels, despite substantial differences in metastatic progression outcomes, further argues against cholesterol being the causal downstream mediator of the effects of the h*PCSK9*$^{V474I/V474I}$ variant on metastasis formation.

(E) Human *PCSK9* knockin mice generation strategy. Arrows indicate genotyping primers.
(F) Bioluminescence imaging of metastatic progression of EO771-LM2-shPcsk9 cells intravenously injected into h*PCSK9*$^{+/+}$ or h*PCSK9*$^{V474I/V474I}$ mice (F test).
(G) Spontaneous lung metastasis quantification in h*PCSK9*$^{+/+}$ and h*PCSK9*$^{V474I/V474I}$ mice with mammary fat pad implantation of EO771-LM2-shPcsk9 cells (two-sided Wilcoxon rank-sum test). In (A)–(D), (F), and (G), mice numbers per group are indicated. In (A), (C), (D), (F), and (G), representative H&E images of lung metastasis are shown. Arrows indicate metastatic nodules.
See also Figure S2.

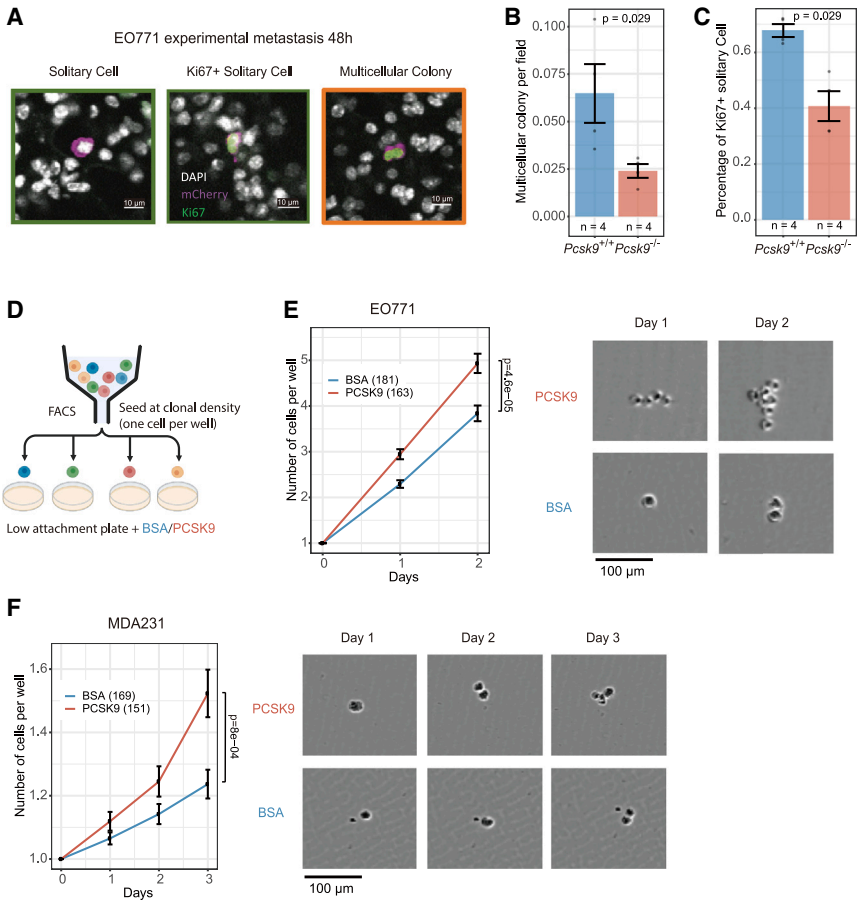

Figure 3. PCSK9 enhances breast cancer metastatic initiation in the lung

(A) Representative immunofluorescence images of single and multicellular lung metastases formed by EO771-LM2-shPcsk9 cells intravenously injected into wild-type or *Pcsk9* knockout mice (48 h after injection). DAPI staining in white, Ki-67 staining in green, and mCherry staining in purple.

(B) Multicellular lung metastasis quantification in wild-type or *Pcsk9* knockout mice. Mice numbers per group are indicated.

(C) Percentage of solitary single cells that stained positively for Ki-67.

(D) Schematic of colony initiation assay in low-attachment plate.

(E and F) Colony initiation assay in low-attachment 96-well plates of EO771-LM2-shPcsk9 (E) and MDA231-LM3-sgPCSK9-2 (F) cells treated with 2 μg/mL recombinant PCSK9 or BSA. Number of wells is indicated. Representative Incucyte images are shown.

p values were calculated with two-sided Wilcoxon rank-sum test. The number of fields of view of each mouse examined in (B) and (C) were: $Pcsk9^{+/+}$ (212, 141, 200, and 200), $Pcsk9^{-/-}$ (391, 285, 304, and 350).

See also Figure S3.

Adaptive immunity is not required for PCSK9-mediated metastasis promotion

We next sought to test whether host PCSK9 promotes breast cancer metastasis formation by regulating adaptive immunity, as a previous study proposed that tumoral PCSK9 reduced MHCI levels.[37] *Pcsk9*-deficient mice continued to exhibit markedly reduced lung metastatic colonization burden relative to wild-type mice in the context of CD4+ and CD8+ T cell depletion using antibodies (Figures S3E and S3F). These findings, in addition to data from therapeutic PCSK9 inhibition studies in immune-deficient mice described below, reveal that enhancement of metastatic progression by host PCSK9 can occur independent of functional adaptive immunity.

Macrophage function is not required for PCSK9-mediated metastasis promotion

We next compared metastasis progression in wild-type and *Pcsk9* knockout mice upon treatment with clodronate liposomes, a well-established method for depleting tissue-resident macrophages.[48] Clodronate treatment successfully depleted macrophages in the lung ($CD45^{+}CD24^{-}$ $F4/80^{+}$)[49] (Figures S3G and S3H). Metastatic progression was similarly reduced in *Pcsk9* knockout mice under control or clodronate treatment compared with wild-type mice receiving the same treatment (Figure S3I). This suggests that macrophage function is not required for PCSK9-mediated lung metastasis enhancement.

PCSK9 promotes breast cancer metastatic initiation events

We next tested the impact of a physiological concentration of recombinant PCSK9 (2 μg/mL)[50] on various metastatic phenotypes *in vitro*. PCSK9 treatment did not affect breast cancer cell proliferation (Figure S3J), invasion through Matrigel (Figures S3K and S3L), or resistance to anoikis (Figure S3M). To study PCSK9's impact on metastatic colonization, we injected mCherry-labeled EO771 cells intravenously into wild-type or *Pcsk9* knockout mice. We observed no discernible difference in the total number of solitary cells that had seeded in the lungs of mice at 48 h after injection (Figure S3N), arguing against a role for PCSK9 in regulating extravasation. Importantly, breast cancer cells formed fewer multicellular colonies in *Pcsk9* knockout mice than in wild-type counterparts (Figures 3A and 3B). *Pcsk9* deletion also reduced the number of solitary cells that stained for the proliferative marker Ki67 (Figures 3A and 3C), supporting a role for PCSK9 in proliferative competence. At a later time point of 18 days post injection, this distinction continued as a fewer number of seeded EO771 cells developed into multicellular colonies or macro-metastases in *Pcsk9* knockout mice (Figures S3O and S3P). We observed no

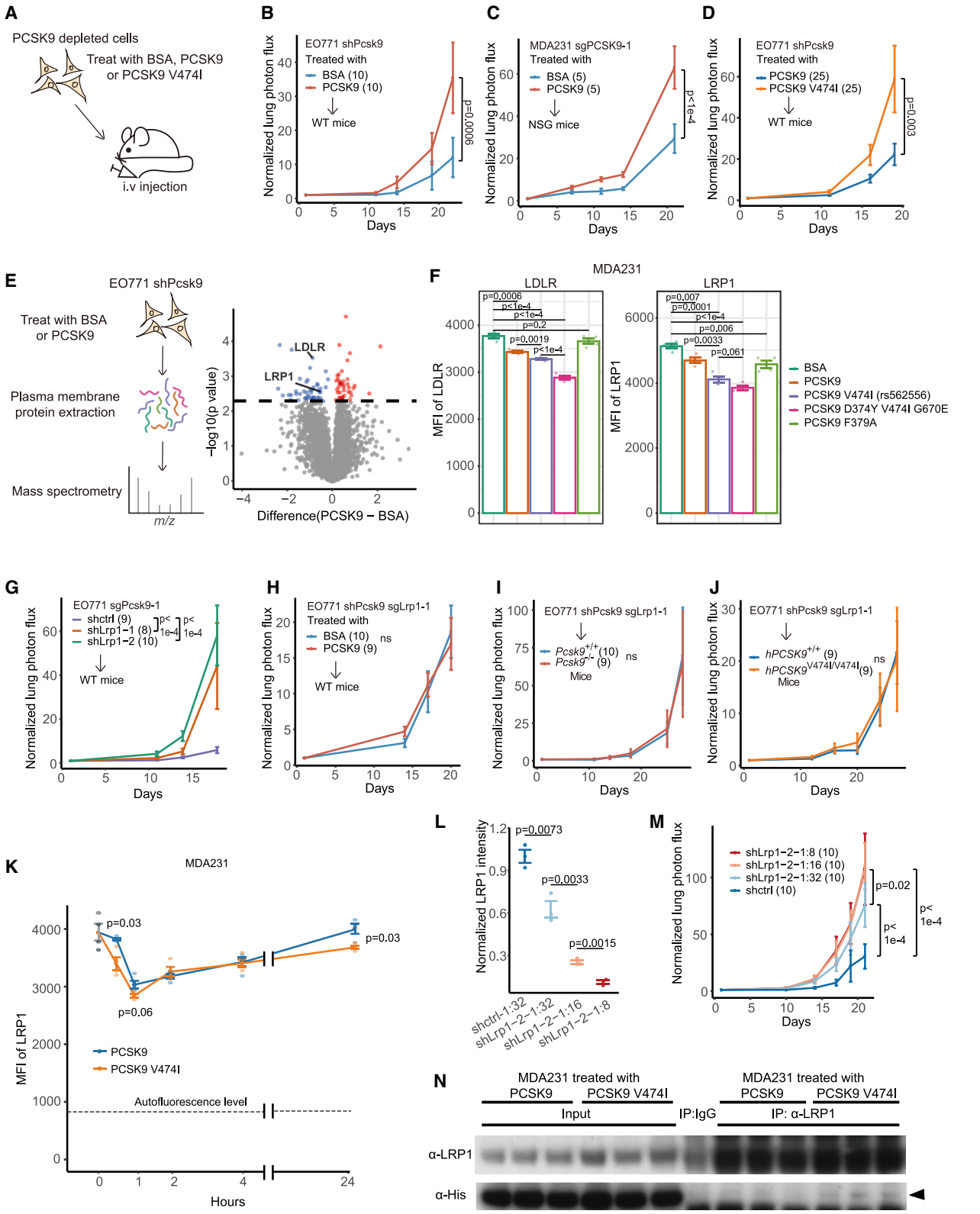

(legend on next page)

difference between wild-type and *Pcsk9* knockout animals in *in vivo* caspase-3/-7 reporter signal, suggesting that the differences in metastatic initiation events were not caused by differences in apoptosis rates (Figure S3Q). These results reveal that host PCSK9 increases the fraction of breast cancer cells that progress to multicellular and macroscopic colonies. The observed increase in proliferative cells at the single-cell and multicellular stages is consistent with a role for PCSK9 in promoting metastatic initiation events by driving proliferative competence, which is a major bottleneck in metastasis formation.[51–53]

To initiate metastatic colonies, disseminated cancer cells must proliferate in the setting of absent or reduced attachment to underlying extracellular matrix, which provides proliferative and survival cues. The lack of such signals can lead to protracted cell-cycle arrest or dormancy.[51,54,55] To model this phase of metastatic colony initiation,[51,56] we flow-sorted single *Pcsk9*-silenced breast cancer cells into individual wells of low-attachment plates, supplemented with bovine serum albumin (BSA) or PCSK9 at physiological levels (Figure 3D). Physiological levels of extrinsic recombinant PCSK9 were sufficient to enhance proliferation of both murine and human breast cancer cells (Figures 3E and 3F). Taken together, these results reveal that host PCSK9 promotes metastatic initiation and proliferation and that extrinsic PCSK9 is sufficient to enhance proliferative capacity in the setting of substratum detachment.

PCSK9 promotes breast cancer metastasis by targeting tumoral LRP1

We next pretreated PCSK9-depleted breast cancer cells with recombinant wild-type or V474I PCSK9 protein and assessed the capacity of cells to form metastases (Figure 4A). Pretreatment of murine EO771 and human MDA-MB-231 breast cancer cells with recombinant PCSK9 for 24 h *in vitro* prior to injection was sufficient to increase these cells' metastatic capacity *in vivo* (Figures 4B and 4C). Importantly, the PCSK9 V474I variant enhanced metastatic capacity to a greater extent than wild-type PCSK9 protein (Figure 4D). These findings suggest that extrinsic PCSK9 can act on breast cancer cells to alter cell state toward one that is more proficient in metastatic initiation.

As PCSK9 is known to promote the degradation of plasma membrane proteins in normal or pathological contexts,[57,58] we used mass spectrometry-based proteomics to identify plasma membrane protein targets on EO771 breast cancer cells that reduced in abundance upon recombinant PCSK9 treatment. Of the 3,880 proteins detected, 59 were downregulated upon PCSK9 treatment (false discovery rate [FDR] < 0.1; Table S1). Importantly, the well-established PCSK9 target LDLR was among the top downregulated proteins (Figure 4E). LRP1, a member of the LDLR family[59] previously reported to be a target of PCSK9[60,61] as well as a regulator of melanoma progression[62] was also found to be downregulated. To validate these findings using an orthogonal approach, we performed flow cytometry to assess the impact of recombinant PCSK9 or its hypermorphic and loss-of-function mutants on plasma membrane protein levels in MDA-MB-231 cells. As expected, while PCSK9 V474I and a triple mutant with three gain-of-function variants (D374Y V474I G670E) both degraded LDLR to a greater extent than wild-type PCSK9,[63,64] the loss-of-function mutant F379A[65] did not suppress membrane LDLR levels (Figure 4F left). Interestingly, while PCSK9 V474I acted as a gain-of-function variant in reducing LRP1 levels, other PCSK9 gain-of-function or loss-of-function variants had a less pronounced effect on plasma membrane LRP1 levels (Figure 4F right). As PCSK9 V474I was hypermorphic in degrading LDLR and LRP1, we studied these two receptors as potential downstream mediators of PCSK9 in breast cancer.

We hypothesized that silencing the downstream target of PCSK9 in breast cancer cells should phenocopy the effects of PCSK9 treatment, as PCSK9 degrades its targets. Such

Figure 4. PCSK9 modulates metastatic colonization through tumoral LRP1

(A) PCSK9 treatment scheme.

(B and C) Bioluminescence imaging of metastatic progression of EO771-LM2-shPcsk9 (B) or MDA231-LM3-sgPCSK9-2 cells (C) treated with 2 μg/mL BSA or PCSK9 for 24 h before intravenous injection.

(D) Bioluminescence imaging of metastatic progression of EO771-LM2-shPcsk9 cells treated with 2 μg/mL PCSK9 wild type or V474I for 24 h before intravenous injection.

(E) Mass spectrometry quantification of plasma membrane proteins of EO771-LM2-shPcsk9 cells treated with 2 μg/mL BSA or PCSK9 for 24 h. Dash line indicates FDR = 0.1.

(F) Flow cytometry quantification of LDLR (left) and LRP1 (right) plasma membrane level on MDA231-LM3-sgPCSK9-2 cells treated with 2 μg/mL BSA or PCSK9 variants for 24 h (two-tailed Student's t test). 4 replicates per group.

(G) Bioluminescence imaging of metastatic progression of EO771-LM2-sgPcsk9-1 shctrl or shLrp1 cells injected intravenously into C57BL/6J mice.

(H) Bioluminescence imaging of metastatic progression of EO771-LM2-shPcsk9-sgLrp1 cells treated with 2 μg/mL BSA or PCSK9 for 24 h before intravenous injection.

(I and J) Bioluminescence imaging of metastatic progression of EO771-LM2-shPcsk9-sgLrp1 cells intravenously injected into wild-type or *Pcsk9* knockout mice (I) or *PCSK9*$^{+/+}$ and h*PCSK9*$^{V474I/V474I}$ mice (J).

(K) Flow cytometry quantification of LRP1 plasma membrane levels on MDA231-LM3-sgPCSK9-2 cells following addition of 2 μg/mL wild-type PCSK9 or V474I. Time points of 0, 0.5, 1, 2, 4, and 24 h were measured (two-tailed Student's t test). 4 replicates per condition.

(L) Western blot quantification of LRP1 levels on EO771 cells transduced with different doses of shctrl or shLrp1-2 virus (two-tailed Student's t test). 3 replicates per group.

(M) Bioluminescence imaging of metastatic progression of EO771-LM2 cells transduced with different doses of shctrl or shLrp1-2 virus intravenously injected into C57BL/6J mice.

(N) Co-immunoprecipitation of LRP1 and exogenously added 2 μg/mL His-tagged wild-type PCSK9 or PCSK9 V474I protein from MDA231-LM3-sgPCSK9-2 cells (3 replicates per condition). Arrow indicates the expected sized band.

p values in (B)–(D), (G)–(J), and (M) were calculated with F test, and mice numbers per group are indicated.

See also Figure S4.

silencing of a PCSK9 target should also rescue the metastasis reduction phenotype observed in *Pcsk9* knockout mice. We first depleted tumoral LDLR in breast cancer cells using shRNA or CRISPR interference and performed experimental metastasis assays (Figure S4A). Tumoral LDLR depletion did not rescue the metastasis repression phenotype observed in *Pcsk9* knockout mice (Figures S4B and S4C), suggesting that LDLR is not the mediator of the metastasis phenotype downstream of PCSK9.

By contrast, shRNA-mediated depletion of *Lrp1* significantly increased the metastatic capacity of EO771 cells in wild-type mice (Figures 4G and S4D), phenocopying the effect of PCSK9 pretreatment. LRP1 depletion in breast cancer cells was also sufficient to enhance colony-forming capacity under low adherence conditions (Figure S4E) but did not alter proliferation rates under basal tissue culture conditions (Figure S4F). CRISPR-mediated deletion of *Lrp1* in EO771 cells abolished the metastasis-promoting effect of PCSK9 pretreatment *in vivo* (Figures 4H and S4G). CRISPR targeting of *LRP1* also abolished the colony initiation enhancement phenotype of PCSK9 treatment in EO771 and MDA-MB-231 cells *in vitro*, while guides targeting the intergenic region did not (Figures S4H and S4I). Most importantly, deletion of tumoral *Lrp1* rescued the ability of breast cancer cells to form metastases in *Pcsk9* knockout mice (Figure 4I). These experiments were repeated using an independent LRP1 guide and a control guide targeting the intergenic region (Figures S4J–S4M). Moreover, deletion of tumoral *Lrp1* abolished the difference in metastasis between h*PCSK9*$^{+/+}$ and h*PCSK9*$^{V474I/V474I}$ KI mice (Figure 4J). These data reveal that the metastasis promotion and colony initiation effects of PCSK9 are mediated through the LRP1 receptor.

V474I may increase PCSK9's binding to and suppression of tumoral LRP1

We next examined the kinetics of PCSK9's action by performing a time course experiment. We observed a ~38% reduction in plasma membrane LRP1 level at 1 h post PCSK9 treatment. LRP1 levels then gradually rebounded, with PCSK9 V474I exhibiting faster kinetics and being more potent at suppressing LRP1 at steady state than wild-type PCSK9 (Figure 4K). To determine if the magnitude of LRP1 reduction observed upon PCSK9 treatment is sufficient to drive metastasis, we titrated viral shRNA transduction of EO771 cells and achieved a range of LRP1 depletions (Figure 4L). We observed that depletion of LRP1 to a similar extent mediated by PCSK9 (~37%) was sufficient to significantly enhance metastasis (Figure 4M), revealing that breast cancer metastasis is highly sensitive to LRP1 levels.

Alteration in ligand-receptor binding properties can change the kinetics and strength of downstream signaling.[66,67] Recombinant His-tagged PCSK9 added to cells was able to pull down endogenous LDLR and LRP1, while endogenous LRP1 pulled down exogenous PCSK9 (Figures S4N and S4O). This is consistent with a prior report that described an interaction between PCSK9 and LRP1 in human Huh7 cells and mouse liver.[61] Importantly, endogenous LRP1 was able to pull down more PCSK9 V474I than wild-type PCSK9 (Figure 4N). This data suggests a model whereby the V474I variant enhances the interaction between PCSK9 and LRP1—thus enhancing PCSK9-mediated suppression of tumoral LRP1.

PCSK9 induces the expression of a set of pro-metastatic genes

LRP1 is known to regulate gene expression in health and disease contexts.[68–70] We thus searched for transcripts that were differentially expressed upon perturbation of this axis as breast cancer cells gained enhanced metastatic activity. We conducted mRNA-seq analysis of (1) breast cancer cells treated with PCSK9 versus BSA *in vitro*, (2) primary breast tumors formed in wild-type versus *Pcsk9* knockout mice, and (3) *Lrp1*-depleted versus control breast cancer cells. Interferon (IFN) signaling was a pathway recurrently found to be differentially regulated (Figures S5A–S5D). Specifically, IFN pathways were among the top upregulated pathways induced in breast cancer cells in the presence of PCSK9.

IFN pathways play critical roles in anti-tumor immunity,[71] and cancer patients display impaired IFN signaling in immune cells.[72] However, activation of tumor cell-intrinsic IFN-stimulated genes has been shown to associate with reduced survival outcomes in breast cancer patients.[73,74] Moreover, such tumor cell-intrinsic IFN-stimulated genes can promote cancer cell survival[75] or resistance to chemotherapy,[73] independent of the adaptive immune response. To further define the expression signature of the PCSK9-LRP1 axis, we overlapped the differentially expressed genes in the aforementioned experiments wherein PCSK9 or LRP1 were modulated and identified 6 genes that were upregulated in all contexts, 5 of which have human orthologs (Figures 5A, S5E, and S5F). All 5 genes (*Xaf1*, *Oas1a*, *Isg15*, *Usp18*, and *Rtp4*) were previously reported to be IFN stimulated.[76–80] The expression levels of these human orthologs exhibited high correlation across human breast cancers (Figure S5G), suggesting coordinate regulation. Importantly, genes differentially expressed between breast cancers from *PCSK9* rs562556 A/A homozygotes versus G/A and G/G homozygote patients were also enriched in IFN signaling (Figure 5B). Similarly, tumors from h*PCSK9*$^{V474I/V474I}$ mice exhibited upregulation of IFN-associated pathways compared with h*PCSK9*$^{+/+}$ mice (Figure 5C). The expression of this 5-gene signature also significantly correlated with the patients' rs562556 genotype, with tumors from the gain-of-function A/A homozygotes exhibiting higher expression of this gene set (Figure 5D). The 5-gene signature also trended higher in h*PCSK9*$^{V474I/V474I}$ mice (Figure S5H). Patients whose tumors overexpressed this 5-gene PCSK9-dependent signature experienced reduced distant metastasis-free survival outcomes in two independent breast cancer cohorts (KMplot and SCAN-B) (Figures 5E and S5I). These findings uncover a set of genes that are coordinately induced by PCSK9, associate with the *PCSK9* rs562556 genotype, and associate with risk of distant metastasis in human breast cancer.

We next transduced EO771 breast cancer cells with a pool of 60 CRISPR guides targeting the 5 genes as well as intergenic targeting controls, treated the cells with recombinant PCSK9, and conducted experimental metastasis colonization assays (Figure 5F). CRISPR guides targeting *Xaf1* and *Usp18* were depleted in lung metastatic samples relative to control guides but were not depleted during *in vitro* cellular growth (Figure 5G). The "drop

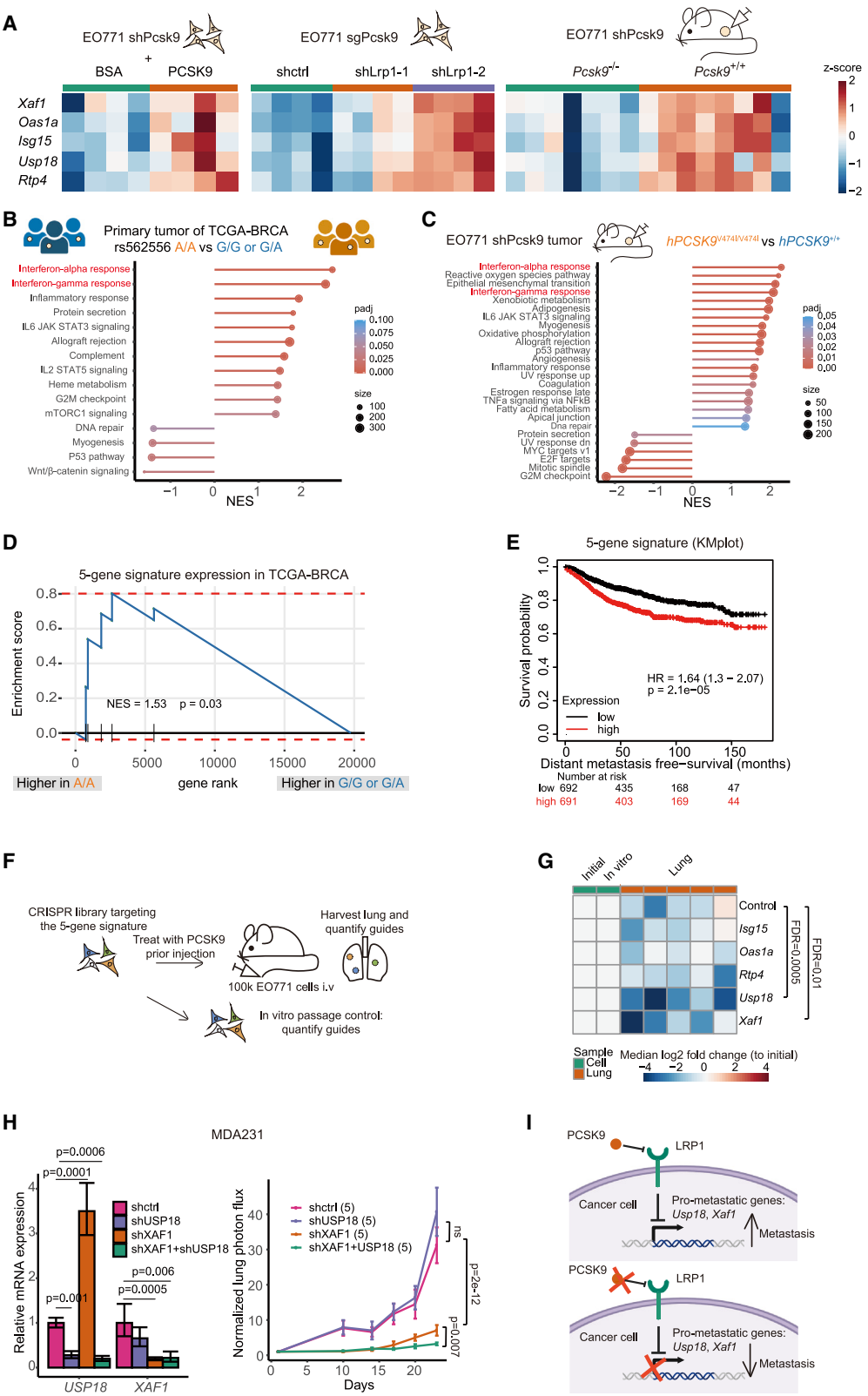

(legend on next page)

out'' of guides targeting *Xaf1* and *Usp18* implicates these genes as metastasis promoters. We also depleted *XAF1* and *USP18* individually and combinatorially in MDA-MB-231 cells (Figure 5H left). Depletion of *XAF1* but not *USP18* as a single gene was sufficient to suppress breast cancer metastasis, and combinatorial depletion of both genes further reduced metastatic colonization *in vivo*, indicating cooperativity (Figure 5H right). Depletion of *XAF1* or *USP18* also significantly suppressed colony initiation under low adherence conditions *in vitro* (Figure S5J). These findings support a model whereby host PCSK9 promotes metastasis formation by inhibiting tumoral LRP1—leading to induction of the expression of *Xaf1* and *Usp18* (Figure 5I), which promote metastasis.

LRP1 ICD suppresses pro-metastatic gene expression

Lastly, we studied the mechanism by which LRP1 inhibits the expression of the 5-gene signature. LRP1 was previously found to suppress inflammatory pathways through inhibition of JNK and nuclear factor (NF)-κB pathways in microglia,[81] activation of Akt/mTOR signaling in macrophages,[82] or via the translocation of the LRP1 intracellular domain (ICD) into the nucleus of fibroblasts.[68] To determine if LRP1 regulates these pathways in breast cancer cells, we depleted LRP1 and assessed changes in these previously characterized signaling pathways. Depletion of LRP1 in EO771 breast cancer cells did not alter the phosphorylation levels of NF-κB or mitogen-activated protein kinase (MAPK) pathways (p38-MAPK, ERK, and JNK) (Figures S6A–S6C) or phosphorylation levels of Akt, mTOR, or downstream targets (Figures S6D and S6E). We did detect the nuclear localization of endogenous LRP1-ICD in EO771 breast cancer cells, which was lost upon shRNA-mediated LRP1 depletion (Figure S6F). We next attempted stable overexpression of HA-tagged LRP1-ICD that was designed to be resistant to the LRP1 targeting shRNA (Figure 6A). This weak re-expression of LRP1-ICD partially reduced the expression of the 5-gene signature *in vitro* and partially suppressed metastasis *in vivo* (Figures 6B and 6C).

It was reported that LRP1-ICD produced by LRP1 cleavage is unstable and subject to proteasomal degradation.[68,83] To overcome this, we implemented a doxycycline-inducible overexpression system to express LRP1-ICD. Interestingly, while the expression of LRP1-ICD increased as the concentration of doxycycline increased, LRP1-ICD expression was lost upon treatment with longer or higher concentrations of doxycycline (Figure 6D), indicating a likely negative feedback regulatory pathway. We then treated cells with PCSK9 and induced LRP1-ICD expression for 24 h to assess if the LRP1-ICD could rescue the gene expression change upon PCSK9 treatment. LRP1-ICD overexpression suppressed the upregulation of the 5-gene signature induced by PCSK9 treatment (Figure 6E). Depletion of *XAF1* and *USP18* also abolished the pro-metastatic effect of PCSK9 treatment (Figure 6F). Conversely, overexpression of *Xaf1* and *Usp18* enhanced the ability of breast cancer cells to form metastases in *Pcsk9* knockout mice (Figures S6G–S6I). Collectively, these data suggest that the LRP1-ICD suppresses the pro-metastatic gene expression program driven by PCSK9 via repression of *XAF1* and *USP18*.

Therapeutic inhibition of PCSK9 suppresses breast cancer metastasis

The discovery of rare loss-of-function human germline genetic variants in *PCSK9* that associate with reduced cholesterol[84] led to the development and approval of two neutralizing antibodies for the treatment of hypercholesterolemia.[85] Administration of the PCSK9 blocking antibody evolocumab, which also recognizes murine PCSK9,[86] prior to intravenous injection of EO771 or 4T1 breast cancer cells significantly reduced lung metastatic colonization in syngeneic C57BL/6 and BALB/c mice, respectively (Figures 7A–7C), and metastatic colonization by human MDA-MB-231 breast cancer cells in immune-deficient mice (Figure 7D). In pretreatment experiments, PCSK9 V474I also enhanced the metastatic capacity of EMT6, an ER+ line that colonizes the lung,[87] and SKBR3, a HER2+ cell line that metastasizes to the bone,[88] to a greater extent than wild-type PCSK9 (Figures S7A and S7B). Anti-PCSK9 treatment also reduced the metastatic progression of these two cell lines, representing additional breast cancer subtypes (Figures S7C and S7D).

The cholesterol-lowering effect of evolocumab is unlikely to underlie the metastasis inhibition effects observed as similar levels of cholesterol reduction achieved by statin administration did not reduce breast cancer lung metastasis formation (Figures S7E and S7F). Evolocumab treatment markedly

Figure 5. PCSK9 induces a pro-metastatic gene expression program

(A) Heatmap showing the expression (*Z* score) of the 5-gene signature (*Xaf1*, *Oas1a*, *Isg15*, *Usp18*, and *Rtp4*) as measured by RNA-seq in EO771-LM2-shPcsk9 treated with 2 μg/mL BSA or PCSK9 for 24 h (left), EO771-LM2-sgPcsk9 with shctrl or shLrp1 (center), or EO771-LM2-shPcsk9 primary tumors when implanted into the mammary fat pads of wild-type or *Pcsk9* knockout mice (right). Red/blue indicates high/low expression, respectively.

(B and C) NES of the top differentially expressed pathways revealed by gene set enrichment analysis (GSEA) in TCGA-BRCA primary tumors comparing rs562556 A/A homozygotes to G/A or G/G patients (B) and EO771-LM2-shPcsk9 primary tumors from the mammary fat pads of h$PCSK9^{V474I/V474I}$ (n = 7) and h$PCSK9^{+/+}$ (n = 6) mice (C).

(D) Gene set enrichment analysis of the 5-gene signature in TCGA-BRCA breast cancer primary tumor RNA-seq. NES, normalized enrichment score. p value was calculated with permutation test.

(E) Kaplan-Meier curve of distant metastasis-free survival of breast cancer patients documented by KM plotter stratified by the mean expression of the 5-gene signature (top quantile versus bottom quantile). Hazard ratio (HR) and p value were calculated with two-sided Cox proportional hazard model.

(F) Scheme of the *in vivo* CRISPR competition assay.

(G) Heatmap of the CRISPR guide abundance in different conditions. Color key indicates the median $\log_2$ fold change of guide abundance compared with the initial conditions. FDR was calculated with permutation test and Benjamini-Hochberg procedure.

(H) qPCR quantification of *XAF1* and *USP18* expression (left) (n = 4 per group; two-tailed Student's t test) and bioluminescence imaging of metastatic progression (right) of MDA231-LM3-sgPCSK9-2 shctrl, shXAF1, shUSP18, and shXAF+USP18 cells injected intravenously into NSG mice (F test). 5 mice per group.

(I) Experimentally derived model depicting that PCSK9 targets LRP1 and de-represses pro-metastatic gene expression, drawn with BioRender.com.

See also Figure S5.

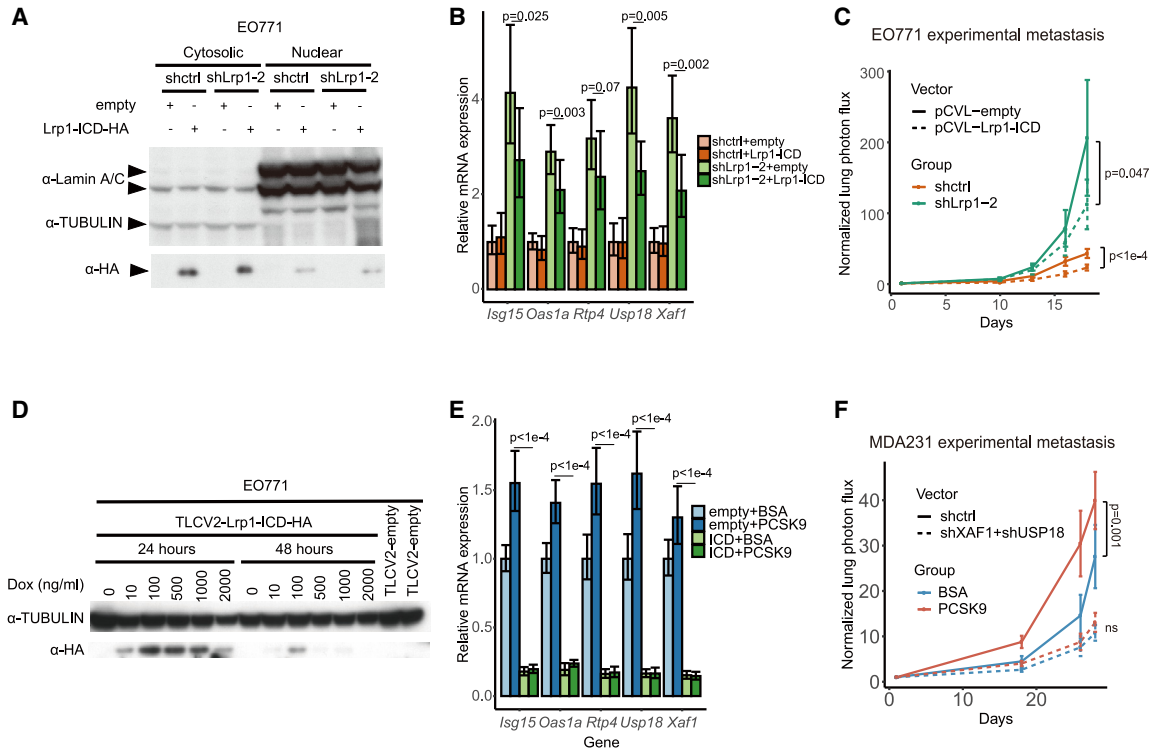

Figure 6. LRP1-ICD suppresses the pro-metastatic gene expression program

(A) Cytosolic and nuclear extracts prepared from EO771-LM2-sgPcsk9-1 shctrl or shLrp1-2 with empty vector or Lrp1-ICD-HA overexpression. Western blotting with antibodies against lamin A/C (nuclear marker), beta-IV-TUBULIN (cytosolic marker), and HA-tag. Arrows indicate the expected band.

(B) qPCR quantification of the 5-gene signature expression in EO771-LM2-sgPcsk9-1 shctrl or shLrp1-2 with pCVL-empty vector or pCVL-Lrp1-ICD-HA overexpression (two-tailed Student's t test). $n = 6$ per group.

(C) Bioluminescence imaging of metastatic progression of EO771-LM2-sgPcsk9-1 shctrl or shLrp1-2 with pCVL-empty vector or pCVL-Lrp1-ICD-HA overexpression injected intravenously into C57BL/6J mice (F test). 10 mice per group.

(D) Inducible Lrp1-ICD-HA EO771 cells treated with increasing concentrations of doxycycline for 24 or 48 h. Induced ICD-HA expression was quantified by western blot.

(E) qPCR quantification of the 5-gene signature expression in EO771-LM2 cells expressing TLCV2-empty vector or TLCV2-Lrp1-ICD-HA and treated with 500 ng/mL doxycycline and 2 μg/mL BSA or PCSK9 for 24 h (two-tailed Student's t test). $n = 4$ per group.

(F) Bioluminescence imaging of metastatic progression of MDA231-LM3-sgPCSK9-2 shctrl or shXAF + shUSP18 cells treated with 2 μg/mL BSA or PCSK9 for 24 h before intravenous injection (F test). 5 mice per group.

See also Figure S6.

reduced lung metastatic colonization by a triple-negative patient-derived organoid (PDO)[89] (Figures 7E and 7F). Evolocumab treatment also significantly inhibited spontaneous metastasis formation by 4T1 breast cancer cells from the orthotopic site (Figure 7G), with minimal effect on tumor growth (Figure S7G). Evolocumab treatment also substantially reduced lung metastasis formation in the MMTV-PyMT genetically initiated breast cancer model[21] with little impact on primary tumor size (Figures 7H and S7H).

Because PCSK9 inhibition suppressed metastatic initiation events and reduced the number of macrometastases, we speculated that PCSK9 inhibition may exhibit activity in animals with established metastases. We next began treating cohorts of mice injected with EO771 or MDA-MB-231 cells with evolocumab or control IgG antibody after incipient metastasis signals were detected by bioluminescence imaging and observed a modest but significant suppressive effect on metastatic colonization in both murine and human breast cancer models upon evolocumab treatment (Figures 7I and S7I). These findings reveal that in a variety of murine, human, transplantable, and genetically initiated models of breast cancer, antibody-mediated PCSK9 inhibition suppressed metastasis formation. While we observed a suppressive effect on the progression of established metastases, the effect of evolocumab on metastasis prevention was more pronounced. These results provide proof-of-concept efficacy for antibody-based inhibition of PCSK9 for the prevention and perhaps treatment of metastatic breast cancer.

PCSK9 rs562556 as a putative prognostic biomarker in early-stage breast cancer

Identifying which patients are at risk for metastatic relapse could enable their treatment with adjuvant or targeted therapies to improve survival outcomes. We thus performed a blinded analysis by genotyping patients in a large Swedish early-stage breast cancer cohort, BC-blood.[90] *PCSK9* rs562556 A/A genotype predicted a higher risk of developing distant metastasis, with ~22% of the

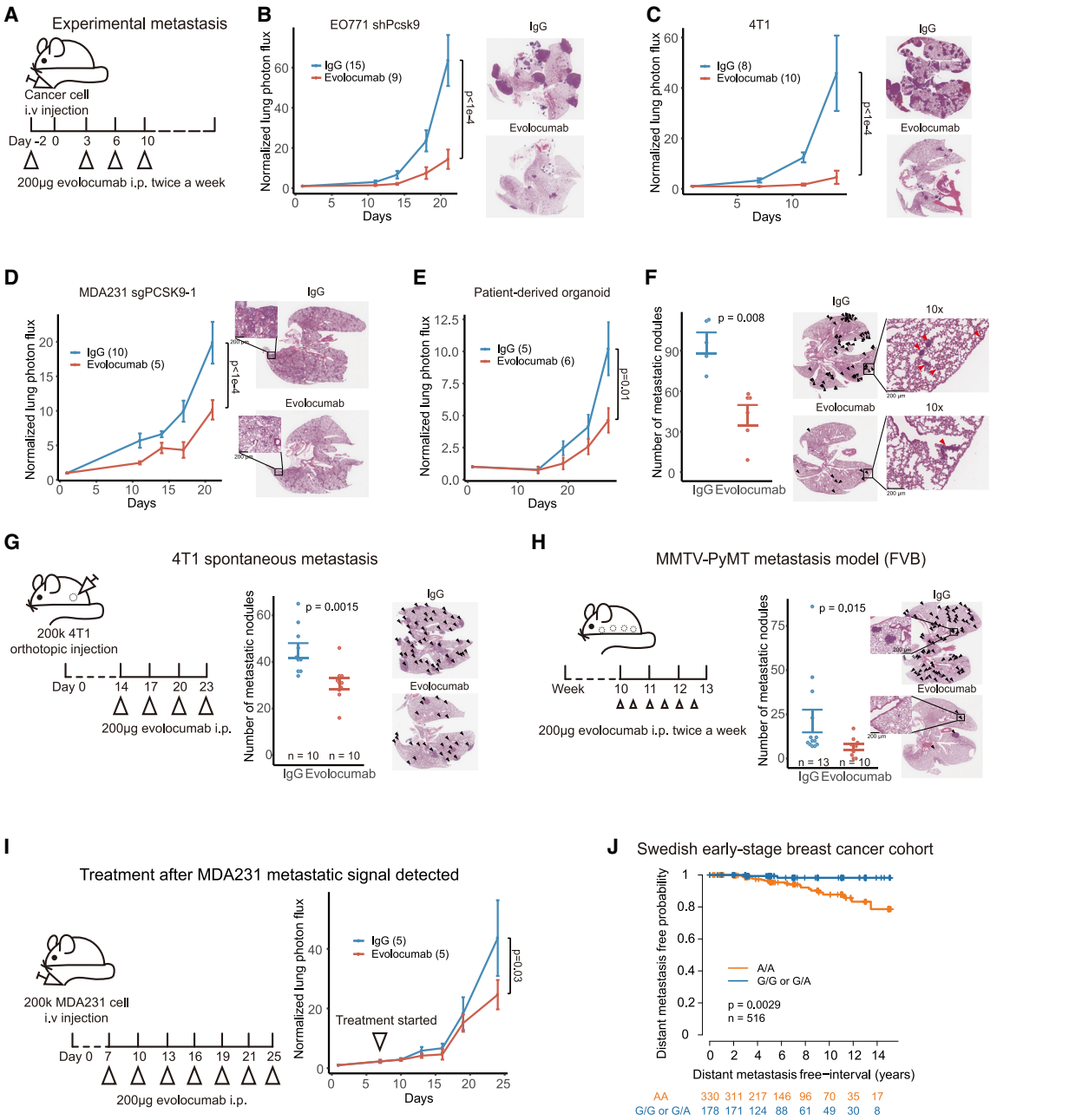

Figure 7. Inhibition of PCSK9 suppresses breast cancer metastatic colonization

(A) Treatment scheme of evolocumab in experimental metastasis assays.

(B–E) Bioluminescence imaging of metastatic progression of breast cancer EO771-LM2-shPcsk9 (B), 4T1 (C), MDA231-LM3-sgPCSK9-2 cells (D) or patient-derived HCI012 organoid (PDO) (E) intravenously injected into mice treated with evolocumab or isotype antibody control.

(F) Quantification of lung metastasis nodules formed by HCI012 PDO (two-sided Wilcoxon rank-sum test).

(G) Treatment scheme and spontaneous metastasis quantification in BALB/c mice upon mammary fat pad implantation of 4T1 cells treated with evolocumab or isotype control (two-sided Wilcoxon rank-sum test).

(H) Treatment scheme and spontaneous metastasis numbers in FVB/NJ mice harboring MMTV-PyMT transgene (two-sided Wilcoxon rank-sum test).

(I) Treatment scheme and bioluminescence imaging of metastatic progression of MDA231-LM3-sgPCSK9-2 cells intravenously injected into NSG mice treated with evolocumab or isotype control started as indicated.

(J) Kaplan-Meier curve of distant metastasis-free survival of early-stage breast cancer patients (defined as stage I, lymph node negative and grades 2 or 3, over 50 when diagnosed) from the BC-blood cohort. *p* value was calculated with two-sided log-rank test.

In (B)–(H), representative H&E images of lung metastasis are shown. Arrows on H&E images indicate metastatic nodules. *p* values in (B)–(E) and (I) were calculated with F test, and mice numbers per group are indicated.

See also Figure S7.

A/A patients developing metastatic relapse compared with that of ~2% in the G/A or G/G group at 15 years post diagnosis (p = 0.0029, hazard ratio [HR] = 7.66, 95% confidence interval [CI] 1.78–32.90, Figure 7J). An increased risk of metastasis or recurrence was associated with PCSK9 rs562556 A/A patients in multivariable analysis with clinical features (Figures S7J and S7K). The association between the PCSK9 rs562556 allele and reduced metastasis-free survival held for both in ER+ patients (p = 0.024) and ER- patients (p = 0.051) and trended in TNBC and HER2 groups, which had lower patient numbers (Figures S7L and S7M). We performed an analysis that controlled for the competing risk of death from cardiovascular mortality. A competing risk regression analysis confirmed the results of the Cox regression models (p = 0.01, SHR = 2.32, 95% CI 1.15–4.68). These findings reveal that rs562556 can stratify early-stage breast cancer patients into those with higher versus lower risk for distant metastatic recurrence, motivating future prospective trials.

DISCUSSION

Despite extensive genomic sequencing of metastases, emergent somatic metastasis driver mutations have not been identified,[7] suggesting that alternative or additional mechanisms may be at play. We reasoned that because germline-encoded host proteins can act on cancer cells in end-organs, germline genetic variation in such proteins might underlie variation in metastatic colonization and survival outcomes. Our unbiased genetic analysis identified an association between *PCSK9* germline variant rs562556 and reduced survival of breast cancer patients from multiple countries. This variant is prevalent, with 70% of breast cancer patients of European ancestry being A/A homozygotes.

We observed a causal role for PCSK9 and its rs562556 variant in transplantable and genetically initiated breast cancer models as well as in cellular and biochemical assays. Genetic deletion of PCSK9 in the host but not in cancer cells suppressed breast cancer metastatic colonization. The dependence of metastasis on host-derived rather than tumoral PCSK9 likely stems from its low expression in human breast tumors, which would cause a higher degree of organ-derived relative to tumoral PCSK9 impacting rare, disseminated cancer cells in a distant organ. Extrinsic PCSK9 enhanced proliferative competence of cells during reduced substratum attachment and enhanced metastatic initiation events.

Through biochemical and genetic approaches, we implicated tumoral LRP1 as the downstream mediator of PCSK9's effects on metastatic progression. LRP1 was previously characterized as a melanoma invasiveness suppressor,[62] but the downstream molecular mechanisms of metastatic colonization suppression by LRP1 remained to be defined. We observed that PCSK9 reduced the abundance of LRP1 on the plasma membranes of breast cancer cells, and deletion of tumoral LRP1 enhanced metastatic colonization. We also found that the V474I mutation may increase PCSK9's binding to tumoral LRP1, which may underlie enhanced LRP1 repression. The PCSK9/LRP1 axis was found to regulate genes associated with IFN signaling.

Importantly, the PCSK9/LRP1 5-gene signature we identified predicted increased risk of metastasis in two large breast cancer cohorts. The expression of this gene signature also correlated with *PCSK9* rs562556 variant status in patients, with the gain-of-function V474I allele conferring higher pro-metastatic gene expression. The finding that a single-nucleotide germline alteration can substantially alter the somatic tumoral gene expression program and shape the metastasis trajectory of the tumor suggests that germline genetics constitutes a major constraint for tumor evolution. This also reveals a hereditary basis underlying cancer metastasis, which means the progression outcome of future breast cancer is in part pre-destined at birth, decades before the onset of the actual malignancy.

Our study raises evolutionary questions. The total cholesterol and LDL levels of the h*PCSK9* KI mice were higher than that of C57BL/6J wild-type mice (Figures S3A, S3C, and S3D), suggesting that perhaps human *PCSK9* may have evolved to maintain higher plasma LDL levels than the distant ancestral allele. The gain-of-function A allele of rs562556 is nearly fixed in multiple populations and is under positive selection in African Americans.[40,91] This may seem paradoxical as rs562556 promotes worse outcomes in cardiovascular disease and breast cancer. However, late-onset diseases, including cancer progression and cardiovascular disease, exert weak effects on reproductive fitness.[92,93] Future studies are needed to explore the evolutionary pressures that may have selected *PCSK9*/rs562556 throughout human history.

Pioneering studies in mice and humans mechanistically linked PCSK9 deficiency to reduced cholesterol levels via its degradation of LDLRs,[57,65,94] leading to the approval of highly effective PCSK9 inhibition therapy for hypercholesterolemia. By administering the FDA-approved PCSK9 neutralizing antibody to mice, we observed significant metastatic colonization suppressive effects across a variety of models bearing murine and human breast cancer cells. Targeted therapies have been most successful when paired with predictive biomarkers that are enriched in patients in whom the targeted pathway is active. The association of rs562556 with significantly reduced survival and distant metastasis-free interval in early-stage breast cancer patients from a large Swedish cancer cohort provides an ideal genetic biomarker for selecting early-stage breast cancer patients for a future metastasis prevention trial with anti-PCSK9. Future work is needed to assess the prognostic ability of rs562556 in patients treated with recently approved therapies that may interact with the PCSK9-LRP1 axis. The impact of PCSK9 inhibition on future metastasis could also be tested even earlier on patients with inherited breast cancer susceptibility disorders. The great safety profile of anti-PCSK9 antibody therapy, its reduced cost stemming from patent expiration, coupled with the availability of a companion genetic biomarker for patient selection, motivate consideration of such trials.

In sum, our findings reveal a key role for hereditary genetics in driving breast cancer metastasis, providing new insights into the interplay between germline genetics and somatic tumor gene expression and progression programs with potential implications for the management of this prevalent disease.

Limitations of the study

Although we identified tumoral LRP1 as a downstream mediator of PCSK9's effect on breast cancer metastasis through a series of genetic and biochemical experiments, this cannot rule out the

possibility that other PCSK9 targets on other cell type(s) also play roles. Proteins in the LDLR family are structurally similar, and many were reported as PCSK9 targets.[58] Future studies are needed to explore the role of other PCSK9's targets in breast cancer metastasis.

The identification of additional germline variants that associate with survival outcome could further refine our ability to guide therapeutic decision-making. This is especially important in ethnic populations in whom a given germline genetic variant is "fixed" and thus uninformative. The rs562556 A allele, for example, is nearly fixed in Asia and South America—revealing another limitation of our study in its application to these populations (Figure 1A). Future work is needed to collect well-annotated cancer specimens along with germline sequence information to enable identification of prognostic and causal variants in these ethnic groups, which may also offer insights into cancer survival disparities in different ethnic groups. Such studies will be greatly enabled by the open sharing of patient cancer outcomes and germline DNA sequence data from multiple international cohorts.

RESOURCE AVAILABILITY

Lead contact

Requests for information and reagents should be directed to and will be fulfilled by the lead contact, Sohail F. Tavazoie (sohail.tavazoie@rockefeller.edu).

Materials availability

All unique reagents and data generated in this study are available from the lead contact. Questions regarding the BC-blood cohort should be directed to Dr. Jernström (helena.jernstrom@med.lu.se).

Data and code availability

Newly generated sequencing data were deposited to GEO: GSE255558, GSE255559, GSE255560, GSE273936. The mass spectrometry proteomics data was deposited to the ProteomeXchange Consortium via the PRIDE[95] with identifier PXD049279. Western blot data was deposited to Mendeley Data: https://data.mendeley.com/preview/32369gyznm?a=34ba66b3-a90f-4c36-9b44-a653bf3cfd7b. This paper does not report original code. Additional information required to reanalyze the data reported in this paper is available from the lead contact upon request.

ACKNOWLEDGMENTS

We thank the members of our laboratory for their thoughtful comments on previous versions of this manuscript. We thank Dr. Mengwei Hu (Merck & Co.) and Dr. Norihiro Yamaguchi (NCI) for proofreading this manuscript. We thank the following Rockefeller University Resource Center staff for assistance: V. Francis, C. Zhao, C. Lai, S. Heissel, S. Mazel, R. Norinsky, and the Laboratory of Comparative Pathology at MSKCC. We acknowledge Clinical Genomics Lund, SciLifeLab, and the Center for Translational Genomics (CTG), Lund University, for genotyping. We thank the patients who consented, the central SCAN-B laboratory at Lund University, the Swedish National Quality Register for Breast Cancer for clinical and histopathological data, the Regional Cancer Center South, and the South Swedish Breast Cancer Group. This publication and the underlying study have been made possible partly based on data that Hartwig Medical Foundation has made available to the study through the Hartwig Medical Database. UK Biobank analyses were conducted using the UK Biobank Resource under application number 62709. The results published here are also in whole or part based upon data generated by the TCGA Research Network. We also want to acknowledge the contribution of lab animals to this study. W.M. was supported by the David Rockefeller Graduate Program in Bioscience and the Shapiro-Silverberg Fund for the Advancement of Translational Research. S. Faraj Tabrizi was supported by a scholarship from the German National Academic Foundation. A.F.L. was supported by Boehringer Ingelheim Fonds. This work was supported by the Marlene Hess Center for Research on Women's Health and Biomedicine at Rockefeller University. S.F. Tavazoie was supported for this work by an NCI R35 Outstanding Investigator award CA274446. S.F. Tavazoie was supported by the NCI MetNet CA261701 award, the Black Family Center for Human Metastasis, and the Breast Cancer Research Foundation. K.I. was supported by the South Swedish Health Care Region junior investigator award. K.I. received funding from the Skåne University Hospital Fund. C.G., H.J., K.I., and the BC-blood cohort received funding from the Swedish Cancer Society, the Faculty of Medicine at Lund University, the Mrs Berta Kamprad Foundation, the South Swedish Health Care Region (Region Skåne ALF 40620), and the Skåne University Hospital fund.

AUTHOR CONTRIBUTIONS

S.F. Tavazoie conceived the study. W.M. and S.F. Tavazoie supervised all research and wrote the manuscript. W.M., S. Faraj Tabrizi, and A.F.L. performed experiments. K.I. and H.J. were responsible for the BC-blood cohort. H.J. supervised the statistical analysis of the SCAN-B and BC-blood cohorts. C.G. and H.J. conducted statistical analyses of the SCAN-B and BC-blood cohorts. W.M. performed bioinformatic and statistical analyses of all other datasets.

DECLARATION OF INTERESTS

S.F. Tavazoie is a cofounder, shareholder, and member of the scientific advisory board of Inspirna.

STAR★METHODS

Detailed methods are provided in the online version of this paper and include the following:

- KEY RESOURCES TABLE
- EXPERIMENTAL MODEL AND STUDY PARTICIPANT DETAILS
  - Animal studies
  - Tissue culture
  - Three-dimensional culture
- METHOD DETAILS
  - Selection of candidate SNPs
  - Analysis of the TCGA cohort
  - Analysis of the Bertucci et al. cohort
  - Analysis of the Nik-Zainal et al. cohort
  - Analysis of the Hartwig Medical Foundation (HMF) cohort
  - Analysis of the UK Biobank
  - Analysis of population structure
  - Analysis of the BC-Blood cohort
  - Analysis of the SCAN-B cohort
  - KM plotter
  - Expression of PCSK9 in human tissues
  - Generation of *Pcsk9* knockout mice
  - Generation of human PCSK9 KI mice
  - Genotyping of transgenic mouse lines
  - *In vivo* selection of PDO
  - Vector Construction
  - Lentiviral production, transduction and cell line construction
  - siRNA transfection
  - Protein isolation
  - Nuclear and cytoplasmic fractionation
  - Western blotting
  - Quantitative reverse transcription PCR
  - Analysis of cell surface protein expression
  - Co-immunoprecipitation (co-IP) analysis
  - Matrigel Invasion Assay
  - Cell Proliferation Assay
  - Anoikis Assay
  - Colony initiation in the absence of substratum attachment
  - Experimental metastasis assay

- Mouse diet and serum chemistry
- T cell depletion
- Macrophage depletion
- Intracardiac injection
- Primary tumor growth and spontaneous metastasis
- PCSK9 inhibition therapeutics
- Immunofluorescence
- Mass spectroscopy of plasma membrane protein
- Bulk RNASeq
- *In vivo* CRISPR competition assay

- QUANTIFICATION AND STATISTICAL ANALYSIS

SUPPLEMENTAL INFORMATION

Supplemental information can be found online at https://doi.org/10.1016/j.cell.2024.11.009.

Received: February 12, 2024
Revised: August 12, 2024
Accepted: November 10, 2024
Published: December 9, 2024

REFERENCES

1. Gerstberger, S., Jiang, Q., and Ganesh, K. (2023). Metastasis. Cell *186*, 1564–1579. https://doi.org/10.1016/j.cell.2023.03.003.
2. Visvader, J.E. (2011). Cells of origin in cancer. Nature *469*, 314–322. https://doi.org/10.1038/nature09781.
3. Boutelle, A.M., and Attardi, L.D. (2021). p53 and tumor suppression: it takes a network. Trends Cell Biol. *31*, 298–310. https://doi.org/10.1016/j.tcb.2020.12.011.
4. Sherman, M.A., Yaari, A.U., Priebe, O., Dietlein, F., Loh, P.R., and Berger, B. (2022). Genome-wide mapping of somatic mutation rates uncovers drivers of cancer. Nat. Biotechnol. *40*, 1634–1643. https://doi.org/10.1038/s41587-022-01353-8.
5. O'Brien, N.A., Browne, B.C., Chow, L., Wang, Y., Ginther, C., Arboleda, J., Duffy, M.J., Crown, J., O'Donovan, N., and Slamon, D.J. (2010). Activated phosphoinositide 3-kinase/AKT signaling confers resistance to trastuzumab but not lapatinib. Mol. Cancer Ther. *9*, 1489–1502. https://doi.org/10.1158/1535-7163.MCT-09-1171.
6. Riaz, N., Havel, J.J., Kendall, S.M., Makarov, V., Walsh, L.A., Desrichard, A., Weinhold, N., and Chan, T.A. (2016). Recurrent SERPINB3 and SERPINB4 mutations in patients who respond to anti-CTLA4 immunotherapy. Nat. Genet. *48*, 1327–1329. https://doi.org/10.1038/ng.3677.
7. Vogelstein, B., Papadopoulos, N., Velculescu, V.E., Zhou, S., Diaz, L.A., and Kinzler, K.W. (2013). Cancer genome landscapes. Science *339*, 1546–1558. https://doi.org/10.1126/science.1235122.
8. Turajlic, S., and Swanton, C. (2016). Metastasis as an evolutionary process. Science *352*, 169–175. https://doi.org/10.1126/science.aaf2784.
9. Patel, S.A., Rodrigues, P., Wesolowski, L., and Vanharanta, S. (2021). Genomic control of metastasis. Br. J. Cancer *124*, 3–12. https://doi.org/10.1038/s41416-020-01127-6.
10. Garcia-Recio, S., Hinoue, T., Wheeler, G.L., Kelly, B.J., Garrido-Castro, A.C., Pascual, T., De Cubas, A.A., Xia, Y., Felsheim, B.M., McClure, M.B., et al. (2023). Multiomics in primary and metastatic breast tumors from the Aurora US network finds microenvironment and epigenetic drivers of metastasis. Nat. Cancer *4*, 128–147. https://doi.org/10.1038/s43018-022-00491-x.
11. Reiter, J.G., Makohon-Moore, A.P., Gerold, J.M., Heyde, A., Attiyeh, M.A., Kohutek, Z.A., Tokheim, C.J., Brown, A., DeBlasio, R.M., Niyazov, J., et al. (2018). Minimal functional driver gene heterogeneity among untreated metastases. Science *361*, 1033–1037. https://doi.org/10.1126/science.aat7171.
12. Priestley, P., Baber, J., Lolkema, M.P., Steeghs, N., de Bruijn, E., Shale, C., Duyvesteyn, K., Haidari, S., van Hoeck, A., Onstenk, W., et al. (2019). Pan-cancer whole-genome analyses of metastatic solid tumours. Nature *575*, 210–216. https://doi.org/10.1038/s41586-019-1689-y.
13. Malanchi, I., Santamaria-Martínez, A., Susanto, E., Peng, H., Lehr, H.A., Delaloye, J.F., and Huelsken, J. (2011). Interactions between cancer stem cells and their niche govern metastatic colonization. Nature *481*, 85–89. https://doi.org/10.1038/nature10694.
14. Risom, T., Glass, D.R., Averbukh, I., Liu, C.C., Baranski, A., Kagel, A., McCaffrey, E.F., Greenwald, N.F., Rivero-Gutiérrez, B., Strand, S.H., et al. (2022). Transition to invasive breast cancer is associated with progressive changes in the structure and composition of tumor stroma. Cell *185*, 299–310.e18. https://doi.org/10.1016/j.cell.2021.12.023.
15. de Visser, K.E., and Joyce, J.A. (2023). The evolving tumor microenvironment: from cancer initiation to metastatic outgrowth. Cancer Cell *41*, 374–403. https://doi.org/10.1016/j.ccell.2023.02.016.
16. Weigelt, B., Glas, A.M., Wessels, L.F.A., Witteveen, A.T., Peterse, J.L., and Van'T Veer, L.J. (2003). Gene expression profiles of primary breast tumors maintained in distant metastases. Proc. Natl. Acad. Sci. USA *100*, 15901–15905. https://doi.org/10.1073/pnas.2634067100.
17. Suzuki, M., and Tarin, D. (2007). Gene expression profiling of human lymph node metastases and matched primary breast carcinomas: clinical implications. Mol. Oncol. *1*, 172–180. https://doi.org/10.1016/j.molonc.2007.03.005.
18. Vignot, S., Lefebvre, C., Frampton, G.M., Meurice, G., Yelensky, R., Palmer, G., Capron, F., Lazar, V., Hannoun, L., Miller, V.A., et al. (2015). Comparative analysis of primary tumour and matched metastases in colorectal cancer patients: evaluation of concordance between genomic and transcriptional profiles. Eur. J. Cancer *51*, 791–799. https://doi.org/10.1016/j.ejca.2015.02.012.
19. Krøigård, A.B., Larsen, M.J., Thomassen, M., and Kruse, T.A. (2016). Molecular concordance between primary breast cancer and matched metastases. Breast J. *22*, 420–430. https://doi.org/10.1111/tbj.12596.
20. Freund, R., Dubensky, T., Bronson, R., Sotnikov, A., Carroll, J., and Benjamin, T. (1992). Polyoma tumorigenesis in mice: evidence for dominant resistance and dominant susceptibility genes of the host. Virology *191*, 724–731. https://doi.org/10.1016/0042-6822(92)90248-N.
21. Davie, S.A., Maglione, J.E., Manner, C.K., Young, D., Cardiff, R.D., MacLeod, C.L., and Ellies, L.G. (2007). Effects of FVB/NJ and C57BL/6J strain backgrounds on mammary tumor phenotype in inducible nitric oxide synthase deficient mice. Transgen. Res. *16*, 193–201. https://doi.org/10.1007/s11248-006-9056-9.
22. Azzato, E.M., Pharoah, P.D.P., Harrington, P., Easton, D.F., Greenberg, D., Caporaso, N.E., Chanock, S.J., Hoover, R.N., Thomas, G., Hunter, D.J., et al. (2010). A genome-wide association study of prognosis in breast cancer. Cancer Epidemiol. Biomarkers Prev. *19*, 1140–1143. https://doi.org/10.1158/1055-9965.EPI-10-0085.
23. Escala-Garcia, M., Guo, Q., Dörk, T., Canisius, S., Keeman, R., Dennis, J., Beesley, J., Lecarpentier, J., Bolla, M.K., Wang, Q., et al. (2019). Genome-wide association study of germline variants and breast cancer-specific mortality. Br. J. Cancer *120*, 647–657. https://doi.org/10.1038/s41416-019-0393-x.
24. Ostendorf, B.N., Bilanovic, J., Adaku, N., Tafreshian, K.N., Tavora, B., Vaughan, R.D., and Tavazoie, S.F. (2020). Common germline variants of the human APOE gene modulate melanoma progression and survival. Nat. Med. *26*, 1048–1053. https://doi.org/10.1038/s41591-020-0879-3.
25. Adaku, N., Ostendorf, B.N., Mei, W., and Tavazoie, S.F. (2023). Apolipoprotein E2 stimulates protein synthesis and promotes melanoma progression and metastasis. Cancer Res. *83*, 3013–3025. https://doi.org/10.1158/0008-5472.CAN-23-1252.
26. Bertucci, F., Ng, C.K.Y., Patsouris, A., Droin, N., Piscuoglio, S., Carbuccia, N., Soria, J.C., Dien, A.T., Adnani, Y., Kamal, M., et al. (2019). Genomic characterization of metastatic breast cancers. Nature *569*, 560–564. https://doi.org/10.1038/s41586-019-1056-z.

27. Seidah, N.G., Awan, Z., Chrétien, M., and Mbikay, M. (2014). PCSK9: A key modulator of cardiovascular health. Circ. Res. *114*, 1022–1036. https://doi.org/10.1161/CIRCRESAHA.114.301621.

28. Burke, A.C., Dron, J.S., Hegele, R.A., and Huff, M.W. (2017). PCSK9: regulation and target for drug development for dyslipidemia. Annu. Rev. Pharmacol. Toxicol. *57*, 223–244. https://doi.org/10.1146/annurev-pharmtox-010716-104944.

29. Nik-Zainal, S., Davies, H., Staaf, J., Ramakrishna, M., Glodzik, D., Zou, X., Martincorena, I., Alexandrov, L.B., Martin, S., Wedge, D.C., et al. (2016). Landscape of somatic mutations in 560 breast cancer whole-genome sequences. Nature *534*, 47–54. https://doi.org/10.1038/nature17676.

30. Yedjou, C.G., Sims, J.N., Miele, L., Noubissi, F., Lowe, L., Fonseca, D.D., Alo, R.A., Payton, M., and Tchounwou, P.B. (2019). Health and racial disparity in breast cancer. Adv. Exp. Med. Biol. *1152*, 31–49. https://doi.org/10.1007/978-3-030-20301-6_3.

31. Teo, Y.Y. (2008). Common statistical issues in genome-wide association studies: a review on power, data quality control, genotype calling and population structure. Curr. Opin. Lipidol. *19*, 133–143. https://doi.org/10.1097/MOL.0b013e3282f5dd77.

32. Ferreira, J.P., Xhaard, C., Lamiral, Z., Borges-Canha, M., Neves, J.S., Dandine-Roulland, C., Lefloch, E., Deleuze, J.F., Bacq-Daian, D., Bozec, E., et al. (2020). Pcsk9 protein and rs562556 polymorphism are associated with arterial plaques in healthy middle-aged population: the stanislas cohort. J. Am. Heart Assoc. *9*, e014758. https://doi.org/10.1161/JAHA.119.014758.

33. Gai, M.T., Adi, D., Chen, X.C., Liu, F., Xie, X., Yang, Y.N., Gao, X.M., Ma, X., Fu, Z.Y., Ma, Y.T., et al. (2021). Polymorphisms of rs2483205 and rs562556 in the PCSK9 gene are associated with coronary artery disease and cardiovascular risk factors. Sci. Rep. *11*, 11450. https://doi.org/10.1038/s41598-021-90975-0.

34. Sudlow, C., Gallacher, J., Allen, N., Beral, V., Burton, P., Danesh, J., Downey, P., Elliott, P., Green, J., Landray, M., et al. (2015). UK Biobank: an open access resource for identifying the causes of a Wide Range of complex diseases of middle and old age. PLOS Med. *12*, e1001779. https://doi.org/10.1371/journal.pmed.1001779.

35. Cardoso, F., Spence, D., Mertz, S., Corneliussen-James, D., Sabelko, K., Gralow, J., Cardoso, M.J., Peccatori, F., Paonessa, D., Benares, A., et al. (2018). Global analysis of advanced/metastatic breast cancer: decade report (2005–2015). Breast *39*, 131–138. https://doi.org/10.1016/j.breast.2018.03.002.

36. Uhlén, M., Fagerberg, L., Hallström, B.M., Lindskog, C., Oksvold, P., Mardinoglu, A., Sivertsson, Å., Kampf, C., Sjöstedt, E., Asplund, A., et al. (2015). Proteomics. Tissue-based map of the human proteome. Science *347*, 1260419. https://doi.org/10.1126/science.1260419.

37. Liu, X., Bao, X., Hu, M., Chang, H., Jiao, M., Cheng, J., Xie, L., Huang, Q., Li, F., and Li, C.Y. (2020). Inhibition of PCSK9 potentiates immune checkpoint therapy for cancer. Nature *588*, 693–698. https://doi.org/10.1038/s41586-020-2911-7.

38. Wong, C.C., Wu, J.L., Ji, F., Kang, W., Bian, X., Chen, H., Chan, L.S., Luk, S.T.Y., Tong, S., Xu, J., et al. (2022). The cholesterol uptake regulator PCSK9 promotes and is a therapeutic target in APC/KRAS-mutant colorectal cancer. Nat. Commun. *13*, 3971. https://doi.org/10.1038/s41467-022-31663-z.

39. Guy, C.T., Cardiff, R.D., and Muller, W.J. (1992). Induction of mammary tumors by expression of polyomavirus middle T oncogene: a transgenic mouse model for metastatic disease. Mol. Cell. Biol. *12*, 954–961. https://doi.org/10.1128/mcb.12.3.954-961.1992.

40. Ding, K., McDonough, S.J., and Kullo, I.J. (2007). Evidence for positive selection in the C-terminal domain of the cholesterol metabolism gene PCSK9 based on phylogenetic analysis in 14 primate species. PLoS One *2*, e1098. https://doi.org/10.1371/journal.pone.0001098.

41. Cameron, J., Holla, Ø.L., Berge, K.E., Kulseth, M.A., Ranheim, T., Leren, T.P., and Laerdahl, J.K. (2008). Investigations on the evolutionary conservation of PCSK9 reveal a functionally important protrusion. FEBS Journal *275*, 4121–4133. https://doi.org/10.1111/j.1742-4658.2008.06553.x.

42. Nelson, E.R., Wardell, S.E., Jasper, J.S., Park, S., Suchindran, S., Howe, M.K., Carver, N.J., Pillai, R.V., Sullivan, P.M., Sondhi, V., et al. (2013). 27-hydroxycholesterol links hypercholesterolemia and breast cancer pathophysiology. Science *342*, 1094–1098. https://doi.org/10.1126/science.1241908.

43. Ringel, A.E., Drijvers, J.M., Baker, G.J., Catozzi, A., García-Cañaveras, J.C., Gassaway, B.M., Miller, B.C., Juneja, V.R., Nguyen, T.H., Joshi, S., et al. (2020). Obesity shapes metabolism in the tumor microenvironment to suppress anti-tumor immunity. Cell *183*, 1848–1866.e26. https://doi.org/10.1016/j.cell.2020.11.009.

44. Jin, X., Demere, Z., Nair, K., Ali, A., Ferraro, G.B., Natoli, T., Deik, A., Petronio, L., Tang, A.A., Zhu, C., et al. (2020). A metastasis map of human cancer cell lines. Nature *588*, 331–336. https://doi.org/10.1038/s41586-020-2969-2.

45. Garcia-Estevez, L., and Moreno-Bueno, G. (2019). Updating the role of obesity and cholesterol in breast cancer. Breast Cancer Res. *21*, 35. https://doi.org/10.1186/s13058-019-1124-1.

46. Goldstein, J.L., and Brown, M.S. (1974). Binding and degradation of low density lipoproteins by cultured human fibroblasts. Comparison of cells from a normal subject and from a patient with homozygous familial hypercholesterolemia. J. Biol. Chem. *249*, 5153–5162. https://doi.org/10.1016/s0021-9258(19)42341-7.

47. Sun, X., Essalmani, R., Day, R., Khatib, A.M., Seidah, N.G., and Prat, A. (2012). Proprotein convertase subtilisin/kexin type 9 deficiency reduces melanoma metastasis in liver. Neoplasia *14*, 1122–1131. https://doi.org/10.1593/neo.121252.

48. Nguyen, T., Du, J., and Li, Y.C. (2021). A protocol for macrophage depletion and reconstitution in a mouse model of sepsis. Star Protoc. *2*, 101004. https://doi.org/10.1016/j.xpro.2021.101004.

49. Misharin, A.V., Morales-Nebreda, L., Mutlu, G.M., Budinger, G.R.S., and Perlman, H. (2013). Flow cytometric analysis of macrophages and dendritic cell subsets in the mouse lung. Am. J. Respir. Cell Mol. Biol. *49*, 503–510. https://doi.org/10.1165/rcmb.2013-0086MA.

50. Lakoski, S.G., Lagace, T.A., Cohen, J.C., Horton, J.D., and Hobbs, H.H. (2009). Genetic and metabolic determinants of plasma PCSK9 levels. J. Clin. Endocrinol. Metab. *94*, 2537–2543. https://doi.org/10.1210/jc.2009-0141.

51. Ross, J.B., Huh, D., Noble, L.B., and Tavazoie, S.F. (2015). Identification of molecular determinants of primary and metastatic tumour re-initiation in breast cancer. Nat. Cell Biol. *17*, 651–664. https://doi.org/10.1038/ncb3148.

52. Al-Hajj, M., Wicha, M.S., Benito-Hernandez, A., Morrison, S.J., and Clarke, M.F. (2003). Prospective identification of tumorigenic breast cancer cells. Proc. Natl. Acad. Sci. USA *100*, 3983–3988. https://doi.org/10.1073/pnas.0530291100.

53. Gkountela, S., and Aceto, N. (2016). Stem-like features of cancer cells on their way to metastasis. Biol. Direct *11*, 33. https://doi.org/10.1186/s13062-016-0135-4.

54. Elgundi, Z., Papanicolaou, M., Major, G., Cox, T.R., Melrose, J., Whitelock, J.M., and Farrugia, B.L. (2019). Cancer metastasis: the role of the extracellular matrix and the heparan sulfate proteoglycan perlecan. Front. Oncol. *9*, 1482. https://doi.org/10.3389/fonc.2019.01482.

55. Giancotti, F.G. (2013). Mechanisms governing metastatic dormancy and reactivation. Cell *155*, 750–764. https://doi.org/10.1016/j.cell.2013.10.029.

56. Pavlova, N.N., Pallasch, C., Elia, A.E.H., Braun, C.J., Westbrook, T.F., Hemann, M., and Elledge, S.J. (2013). A role for PVRL4-driven cell-cell interactions in tumorigenesis. eLife *2*, e00358. https://doi.org/10.7554/eLife.00358.

57. Horton, J.D., Cohen, J.C., and Hobbs, H.H. (2007). Molecular biology of PCSK9: its role in LDL metabolism. Trends Biochem. Sci. *32*, 71–77. https://doi.org/10.1016/j.tibs.2006.12.008.

58. Poirier, S., Mayer, G., Benjannet, S., Bergeron, E., Marcinkiewicz, J., Nassoury, N., Mayer, H., Nimpf, J., Prat, A., and Seidah, N.G. (2008). The proprotein convertase PCSK9 induces the degradation of low density lipoprotein receptor (LDLR) and its closest family members VLDLR and ApoER2. J. Biol. Chem. *283*, 2363–2372. https://doi.org/10.1074/jbc.M708098200.

59. Herz, J., Hamann, U., Rogne, S., Myklebost, O., Gausepohl, H., and Stanley, K.K. (1988). Surface location and high affinity for calcium of a 500-kd liver membrane protein closely related to the LDL-receptor suggest a physiological role as lipoprotein receptor. EMBO J. *7*, 4119–4127. https://doi.org/10.1002/j.1460-2075.1988.tb03306.x.

60. Canuel, M., Sun, X., Asselin, M.C., Paramithiotis, E., Prat, A., and Seidah, N.G. (2013). Proprotein convertase subtilisin/Kexin Type 9 (PCSK9) can mediate degradation of the low density lipoprotein receptor-related Protein 1 (LRP-1). PLoS One *8*, e64145. https://doi.org/10.1371/journal.pone.0064145.

61. Fu, T., Guan, Y.Y., Xu, J., and Wang, Y. (2017). APP, APLP2 and LRP1 interact with PCSK9 but are not required for PCSK9-mediated degradation of the LDLR in vivo. Biochim. Biophys. Acta Mol. Cell Biol. Lipids *1862*, 883–889. https://doi.org/10.1016/j.bbalip.2017.05.002.

62. Pencheva, N., Tran, H., Buss, C., Huh, D., Drobnjak, M., Busam, K., and Tavazoie, S.F. (2012). Convergent multi-miRNA targeting of ApoE grives LRP1/LRP8-dependent melanoma metastasis and angiogenesis. Cell *151*, 1068–1082. https://doi.org/10.1016/j.cell.2012.10.028.

63. Naoumova, R.P., Tosi, I., Patel, D., Neuwirth, C., Horswell, S.D., Marais, A.D., Van Heyningen, C., and Soutar, A.K. (2005). Severe hypercholesterolemia in four British families with the D374Y mutation in the PCSK9 gene: long-term follow-up and treatment response. Arterioscler. Thromb. Vasc. Biol. *25*, 2654–2660. https://doi.org/10.1161/01.ATV.0000190668.94752.ab.

64. Chen, S.N., Ballantyne, C.M., Gotto, A.M., Tan, Y., Willerson, J.T., and Marian, A.J. (2005). A common PCSK9 haplotype, encompassing the E670G coding single nucleotide polymorphism, is a novel genetic marker for plasma low-density lipoprotein cholesterol levels and severity of coronary atherosclerosis. J. Am. Coll. Cardiol. *45*, 1611–1619. https://doi.org/10.1016/j.jacc.2005.01.051.

65. Kwon, H.J., Lagace, T.A., McNutt, M.C., Horton, J.D., and Deisenhofer, J. (2008). Molecular basis for LDL receptor recognition by PCSK9. Proc. Natl. Acad. Sci. USA *105*, 1820–1825. https://doi.org/10.1073/pnas.0712064105.

66. Spangler, J.B., Moraga, I., Mendoza, J.L., and Garcia, K.C. (2015). Insights into cytokine-receptor interactions from cytokine engineering. Annu. Rev. Immunol. *33*, 139–167. https://doi.org/10.1146/annurev-immunol-032713-120211.

67. Martinez-Fabregas, J., Wilmes, S., Wang, L., Hafer, M., Pohler, E., Lokau, J., Garbers, C., Cozzani, A., Fyfe, P.K., Piehler, J., et al. (2019). Kinetics of cytokine receptor traffi 1 cking determine signaling and functional selectivity. eLife *8*, e49314. https://doi.org/10.7554/eLife.49314.

68. Zurhove, K., Nakajima, C., Herz, J., Bock, H.H., and May, P. (2008). γ-secretase limits the inflammatory response through the processing of LRP1. Sci. Signal. *1*, ra15. https://doi.org/10.1126/scisignal.1164263.

69. Boucher, P., and Herz, J. (2011). Signaling through LRP1: protection from atherosclerosis and beyond. Biochem. Pharmacol. *81*, 1–5. https://doi.org/10.1016/j.bcp.2010.09.018.

70. Gonias, S.L., and Campana, W.M. (2014). LDL receptor-related protein-1: A regulator of inflammation in atherosclerosis, cancer, and injury to the nervous system. Am. J. Pathol. *184*, 18–27. https://doi.org/10.1016/j.ajpath.2013.08.029.

71. Dunn, G.P., Bruce, A.T., Sheehan, K.C.F., Shankaran, V., Uppaluri, R., Bui, J.D., Diamond, M.S., Koebel, C.M., Arthur, C., White, J.M., et al. (2005). A critical function for type I interferons in cancer immunoediting. Nat. Immunol. *6*, 722–729. https://doi.org/10.1038/ni1213.

72. Critchley-Thorne, R.J., Simons, D.L., Yan, N., Miyahira, A.K., Dirbas, F.M., Johnson, D.L., Swetter, S.M., Carlson, R.W., Fisher, G.A., Koong, A., et al. (2009). Impaired interferon signaling is a common immune defect in human cancer. Proc. Natl. Acad. Sci. USA *106*, 9010–9015. https://doi.org/10.1073/pnas.0901329106.

73. Weichselbaum, R.R., Ishwaran, H., Yoon, T., Nuyten, D.S.A., Baker, S.W., Khodarev, N., Su, A.W., Shaikh, A.Y., Roach, P., Kreike, B., et al. (2008). An interferon-related gene signature for DNA damage resistance is a predictive marker for chemotherapy and radiation for breast cancer. Proc. Natl. Acad. Sci. USA *105*, 18490–18495. https://doi.org/10.1073/pnas.0809242105.

74. Benci, J.L., Johnson, L.R., Choa, R., Xu, Y., Qiu, J., Zhou, Z., Xu, B., Ye, D., Nathanson, K.L., June, C.H., et al. (2019). Opposing Functions of Interferon Coordinate Adaptive and Innate Immune Responses to Cancer. Cell *178*, 933–948. https://doi.org/10.1016/j.cell.2019.07.019.

75. Cucolo, L., Chen, Q., Qiu, J., Yu, Y., Klapholz, M., Budinich, K.A., Zhang, Z., Shao, Y., Brodsky, I.E., Jordan, M.S., et al. (2022). The interferon-stimulated gene RIPK1 regulates cancer cell intrinsic and extrinsic resistance to immune checkpoint blockade. Immunity *55*, 671–685.e10. https://doi.org/10.1016/j.immuni.2022.03.007.

76. Leaman, D.W., Chawla-Sarkar, M., Vyas, K., Reheman, M., Tamai, K., Toji, S., and Borden, E.C. (2002). Identification of X-linked inhibitor of apoptosis-associated factor-1 as an interferon-stimulated gene that augments trail Apo2L-induced apoptosis. J. Biol. Chem. *277*, 28504–28511. https://doi.org/10.1074/jbc.M204851200.

77. Kristiansen, H., Scherer, C.A., McVean, M., Iadonato, S.P., Vends, S., Thavachelvam, K., Steffensen, T.B., Horan, K.A., Kuri, T., Weber, F., et al. (2010). Extracellular 2′-5′ oligoadenylate synthetase stimulates RNase L-independent antiviral activity: a novel mechanism of virus-induced innate immunity. J. Virol. *84*, 11898–11904. https://doi.org/10.1128/JVI.01003-10.

78. Zhao, C., Collins, M.N., Hsiang, T.Y., and Krug, R.M. (2013). Interferon-induced ISG15 pathway: an ongoing virus-host battle. Trends Microbiol. *21*, 181–186. https://doi.org/10.1016/j.tim.2013.01.005.

79. Basters, A., Knobeloch, K.P., and Fritz, G. (2018). USP18 - A multifunctional component in the interferon response. Biosci. Rep. *38*, BSR20180250. https://doi.org/10.1042/BSR20180250.

80. Boys, I.N., Xu, E., Mar, K.B., De La Cruz-Rivera, P.C., Eitson, J.L., Moon, B., and Schoggins, J.W. (2020). RTP4 is a potent IFN-inducible anti-Flavivirus effector engaged in a host-virus arms race in bats and other mammals. Cell Host Microbe *28*, 712–723.e9. https://doi.org/10.1016/j.chom.2020.09.014.

81. Yang, L., Liu, C.C., Zheng, H., Kanekiyo, T., Atagi, Y., Jia, L., Wang, D., N'songo, A., Can, D., Xu, H., et al. (2016). LRP1 modulates the microglial immune response via regulation of JNK and NF-KB signaling pathways. J. Neuroinflammation *13*, 304. https://doi.org/10.1186/s12974-016-0772-7.

82. Luo, L., Wall, A.A., Tong, S.J., Hung, Y., Xiao, Z., Tarique, A.A., Sly, P.D., Fantino, E., Marzolo, M.P., and Stow, J.L. (2018). TLR crosstalk activates LRP1 to recruit Rab8a and PI3Kγ for suppression of inflammatory responses. Cell Rep. *24*, 3033–3044. https://doi.org/10.1016/j.celrep.2018.08.028.

83. May, P., Reddy, Y.K., and Herz, J. (2002). Proteolytic processing of low density lipoprotein receptor-related protein mediates regulated release of its intracellular domain. J. Biol. Chem. *277*, 18736–18743. https://doi.org/10.1074/jbc.M201979200.

84. Cohen, J.C., Boerwinkle, E., Mosley, T.H., and Hobbs, H.H. (2006). Sequence variations in PCSK9, low LDL, and protection against coronary heart disease. N. Engl. J. Med. *354*, 1264–1272. https://doi.org/10.1056/NEJMoa054013.

85. McDonagh, M., Peterson, K., Holzhammer, B., and Fazio, S. (2016). A systematic review of PCSK9 inhibitors alirocumab and evolocumab.

J. Manag. Care Spec. Pharm. *22*, 641–653q. https://doi.org/10.18553/jmcp.2016.22.6.641.

86. Chan, J.C.Y., Piper, D.E., Cao, Q., Liu, D., King, C., Wang, W., Tang, J., Liu, Q., Higbee, J., Xia, Z., et al. (2009). A proprotein convertase subtilisin/kexin type 9 neutralizing antibody reduces serum cholesterol in mice and nonhuman primates. Proc. Natl. Acad. Sci. USA *106*, 9820–9825. https://doi.org/10.1073/pnas.0903849106.

87. Turrell, F.K., Orha, R., Guppy, N.J., Gillespie, A., Guelbert, M., Starling, C., Haider, S., and Isacke, C.M. (2023). Age-associated microenvironmental changes highlight the role of PDGF-C in ER+ breast cancer metastatic relapse. Nat. Cancer *4*, 468–484. https://doi.org/10.1038/s43018-023-00525-y.

88. Tarragona, M., Pavlovic, M., Arnal-Estapé, A., Urosevic, J., Morales, M., Guiu, M., Planet, E., González-Suárez, E., and Gomis, R.R. (2012). Identification of NOG as a specific breast cancer bone metastasis- supporting gene. J. Biol. Chem. *287*, 21346–21355. https://doi.org/10.1074/jbc.M112.355834.

89. Scherer, S.D., Zhao, L., Butterfield, A.J., Yang, C.H., Cortes-Sanchez, E., Guillen, K.P., Welm, B.E., and Welm, A.L. (2023). Breast cancer PDxO cultures for drug discovery and functional precision oncology. Star Protoc. *4*, 102402. https://doi.org/10.1016/j.xpro.2023.102402.

90. Godina, C., Tryggvadottir, H., Bosch, A., Borgquist, S., Belting, M., Isaksson, K., and Jernström, H. (2023). Caveolin-1 genotypes as predictor for locoregional recurrence and contralateral disease in breast cancer. Breast Cancer Res. Treat. *199*, 335–347. https://doi.org/10.1007/s10549-023-06919-x.

91. Ding, K., and Kullo, I.J. (2008). Molecular population genetics of PCSK9: A signature of recent positive selection. Pharmacogenet. Genomics *18*, 169–179. https://doi.org/10.1097/FPC.0b013e3282f44d99.

92. Fisher, R.A. (1958). The Genetical Theory of Natural Selection, Second Edition (The Clarendon Press).

93. Flatt, T., and Partridge, L. (2018). Horizons in the evolution of aging. BMC Biol. *16*, 93. https://doi.org/10.1186/s12915-018-0562-z.

94. Rashid, S., Curtis, D.E., Garuti, R., Anderson, N.N., Bashmakov, Y., Ho, Y.K., Hammer, R.E., Moon, Y.A., and Horton, J.D. (2005). Decreased plasma cholesterol and hypersensitivity to statins in mice lacking Pcsk9. Proc. Natl. Acad. Sci. USA *102*, 5374–5379. https://doi.org/10.1073/pnas.0501652102.

95. Perez-Riverol, Y., Bai, J., Bandla, C., García-Seisdedos, D., Hewapathirana, S., Kamatchinathan, S., Kundu, D.J., Prakash, A., Frericks-Zipper, A., Eisenacher, M., et al. (2022). The PRIDE database resources in 2022: A hub for mass spectrometry-based proteomics evidences. Nucleic Acids Res. *50*, D543–D552. https://doi.org/10.1093/nar/gkab1038.

96. Danecek, P., Bonfield, J.K., Liddle, J., Marshall, J., Ohan, V., Pollard, M.O., Whitwham, A., Keane, T., McCarthy, S.A., Davies, R.M., et al. (2021). Twelve years of SAMtools and BCFtools. GigaScience *10*, giab008. https://doi.org/10.1093/gigascience/giab008.

97. Deelen, P., Bonder, M.J., Van Der Velde, K.J., Westra, H.J., Winder, E., Hendriksen, D., Franke, L., and Swertz, M.A. (2014). Genotype harmonizer: automatic strand alignment and format conversion for genotype data integration. BMC Res. Notes *7*, 901. https://doi.org/10.1186/1756-0500-7-901.

98. Delaneau, O., Marchini, J., and Zagury, J.F. (2011). A linear complexity phasing method for thousands of genomes. Nat. Methods *9*, 179–181. https://doi.org/10.1038/nmeth.1785.

99. Howie, B.N., Donnelly, P., and Marchini, J. (2009). A flexible and accurate genotype imputation method for the next generation of genome-wide association studies. PLoS Genet. *5*, e1000529. https://doi.org/10.1371/journal.pgen.1000529.

100. Chang, C.C., Chow, C.C., Tellier, L.C.A.M., Vattikuti, S., Purcell, S.M., and Lee, J.J. (2015). Second-generation PLINK: rising to the challenge of larger and richer datasets. GigaScience *4*, 7. https://doi.org/10.1186/s13742-015-0047-8.

101. Dobin, A., Davis, C.A., Schlesinger, F., Drenkow, J., Zaleski, C., Jha, S., Batut, P., Chaisson, M., and Gingeras, T.R. (2013). STAR: ultrafast universal RNA-seq aligner. Bioinformatics *29*, 15–21. https://doi.org/10.1093/bioinformatics/bts635.

102. Liao, Y., Smyth, G.K., and Shi, W. (2014). featureCounts: an efficient general purpose program for assigning sequence reads to genomic features. Bioinformatics *30*, 923–930. https://doi.org/10.1093/bioinformatics/btt656.

103. Ewels, P., Magnusson, M., Lundin, S., and Käller, M. (2016). MultiQC: summarize analysis results for multiple tools and samples in a single report. Bioinformatics *32*, 3047–3048. https://doi.org/10.1093/bioinformatics/btw354.

104. Li, W., Xu, H., Xiao, T., Cong, L., Love, M.I., Zhang, F., Irizarry, R.A., Liu, J.S., Brown, M., and Liu, X.S. (2014). MAGeCK enables robust identification of essential genes from genome-scale CRISPR/Cas9 knockout screens. Genome Biol. *15*, 554. https://doi.org/10.1186/s13059-014-0554-4.

105. Love, M.I., Huber, W., and Anders, S. (2014). Moderated estimation of fold change and dispersion for RNA-seq data with DESeq2. Genome Biol. *15*, 550. https://doi.org/10.1186/s13059-014-0550-8.

106. Sergushichev, A.A. (2016). An algorithm for fast preranked gene set enrichment analysis using cumulative statistic calculation. Preprint at bioRxiv. https://doi.org/10.1101/060012.

107. Therneau, T.M., and Grambsch, P.M. (2000). The Cox Model BT – Modeling Survival Data: Extending the Cox Model (Springer).

108. Marcus, J.H., and Novembre, J. (2017). Visualizing the geography of genetic variants. Bioinformatics *33*, 594–595. https://doi.org/10.1093/bioinformatics/btw643.

109. Tsou, C.C., Avtonomov, D., Larsen, B., Tucholska, M., Choi, H., Gingras, A.C., and Nesvizhskii, A.I. (2015). DIA-Umpire: comprehensive computational framework for data-independent acquisition proteomics. Nat. Methods *12*, 258–264. https://doi.org/10.1038/nmeth.3255.

110. Sherry, S.T., Ward, M., and Sirotkin, K. (1999). dbSNP – database for single nucleotide polymorphisms and other classes of minor genetic variation. Genome Res. *9*, 677–679. https://doi.org/10.1101/gr.9.8.677.

111. Ramilowski, J.A., Goldberg, T., Harshbarger, J., Kloppmann, E., Lizio, M., Satagopam, V.P., Itoh, M., Kawaji, H., Carninci, P., Rost, B., et al. (2015). A draft network of ligand-receptor-mediated multicellular signalling in human. Nat. Commun. *6*, 7866. https://doi.org/10.1038/ncomms8866.

112. Goldman, M.J., Craft, B., Hastie, M., Repečka, K., McDade, F., Kamath, A., Banerjee, A., Luo, Y., Rogers, D., Brooks, A.N., et al. (2020). Visualizing and interpreting cancer genomics data via the Xena platform. Nat. Biotechnol. *38*, 675–678. https://doi.org/10.1038/s41587-020-0546-8.

113. Netanely, D., Avraham, A., Ben-Baruch, A., Evron, E., and Shamir, R. (2016). Expression and methylation patterns partition luminal-A breast tumors into distinct prognostic subgroups. Breast Cancer Res. *18*, 74. https://doi.org/10.1186/s13058-016-0724-2.

114. van Leeuwen, E.M., Kanterakis, A., Deelen, P., Kattenberg, M.V., Genome; Netherlands Consortium, Slagboom, P.E., de Bakker, P.I.W., Wijmenga, C., Swertz, M.A., Boomsma, D.I., et al. (2015). Population-specific genotype imputations using minimac or IMPUTE2. Nat. Protoc. *10*, 1285–1296. https://doi.org/10.1038/nprot.2015.077.

115. Amos, C.I., Dennis, J., Wang, Z., Byun, J., Schumacher, F.R., Gayther, S.A., Casey, G., Hunter, D.J., Sellers, T.A., Gruber, S.B., et al. (2017). The oncoarray consortium: A network for understanding the genetic architecture of common cancers. Cancer Epidemiol. Biomarkers Prev. *26*, 126–135. https://doi.org/10.1158/1055-9965.EPI-16-0106.

116. Michailidou, K., Hall, P., Gonzalez-Neira, A., Ghoussaini, M., Dennis, J., Milne, R.L., Schmidt, M.K., Chang-Claude, J., Bojesen, S.E., Bolla, M.K., et al. (2013). Large-scale genotyping identifies 41 new loci associated with breast cancer risk. Nat. Genet. *45*, 353–361. https://doi.org/10.1038/ng.2563.

117. Sandén, E., Khazaei, S., Tryggvadottir, H., Borgquist, S., Isaksson, K., Jirström, K., and Jernström, H. (2020). Re-evaluation of HER2 status in 606 breast cancers—gene protein assay on tissue microarrays versus routine pathological assessment. Virchows Arch. *477*, 317–320. https://doi.org/10.1007/s00428-020-02768-x.

118. Staaf, J., Häkkinen, J., Hegardt, C., Saal, L.H., Kimbung, S., Hedenfalk, I., Lien, T., Sørlie, T., Naume, B., Russnes, H., et al. (2022). RNA sequencing-based single sample predictors of molecular subtype and risk of recurrence for clinical assessment of early-stage breast cancer. npj Breast Cancer *8*, 94. https://doi.org/10.1038/s41523-022-00465-3.

119. Győrffy, B. (2023). Discovery and ranking of the most robust prognostic biomarkers in serous ovarian cancer. GeroScience *45*, 1889–1898. https://doi.org/10.1007/s11357-023-00742-4.

120. Tang, Z., Kang, B., Li, C., Chen, T., and Zhang, Z. (2019). GEPIA2: an enhanced web server for large-scale expression profiling and interactive analysis. Nucleic Acids Res. *47*, W556–W560. https://doi.org/10.1093/nar/gkz430.

121. Huang, R., Gao, Y., Duan, Q., Zhang, Q., He, P., Chen, J., Ma, G., Wang, L., Zhang, Y., Nie, K., et al. (2023). Endothelial LRP1-ICD accelerates cognition-associated alpha-synuclein pathology and neurodegeneration through PARP1 activation in a mouse model of Parkinson's disease. Mol. Neurobiol. *60*, 979–1003. https://doi.org/10.1007/s12035-022-03119-4.

122. Tyanova, S., Temu, T., Sinitcyn, P., Carlson, A., Hein, M.Y., Geiger, T., Mann, M., and Cox, J. (2016). The Perseus computational platform for comprehensive analysis of (prote)omics data. Nat. Methods *13*, 731–740. https://doi.org/10.1038/nmeth.3901.

123. Subramanian, A., Tamayo, P., Mootha, V.K., Mukherjee, S., Ebert, B.L., Gillette, M.A., Paulovich, A., Pomeroy, S.L., Golub, T.R., Lander, E.S., et al. (2005). Gene set enrichment analysis: A knowledge-based approach for interpreting genome-wide expression profiles. Proc. Natl. Acad. Sci. USA *102*, 15545–15550. https://doi.org/10.1073/pnas.0506580102.

124. Joung, J., Konermann, S., Gootenberg, J.S., Abudayyeh, O.O., Platt, R.J., Brigham, M.D., Sanjana, N.E., and Zhang, F. (2017). Genome-scale CRISPR-Cas9 knockout and transcriptional activation screening. Nat. Protoc. *12*, 828–863. https://doi.org/10.1038/nprot.2017.016.

125. Wang, T., Yu, H., Hughes, N.W., Liu, B., Kendirli, A., Klein, K., Chen, W.W., Lander, E.S., and Sabatini, D.M. (2017). Gene essentiality profiling reveals gene networks and synthetic lethal interactions with oncogenic Ras. Cell *168*, 890–903.e15. https://doi.org/10.1016/j.cell.2017.01.013.

STAR★METHODS

KEY RESOURCES TABLE

REAGENT or RESOURCE	SOURCE	IDENTIFIER
Antibodies		
Rabbit anti-HPRT1	Proteintech	Cat#15059-1-AP; RRID: AB_10638622
Mouse anti-HSC70	Santa Cruz Biotech	Cat# sc-7298; RRID: AB_627761
Mouse anti-alpha-TUBULIN	Cell Signaling	Cat#3873; RRID: AB_1904178
Goat anti-mouse PCSK9	R&D System	Cat#AF3985; RRID: AB_2044717
Rabbit anti-human PCSK9	GeneTex	Cat#GTX129859; RRID: AB_2886111
Rabbit anti-LRP1	Abcam	Cat#EPR3724; RRID: AB_2234877
Rabbit anti-LDLR	Proteintech	Cat#10785-1-AP; RRID: AB_2281164
Rabbit anti-NFκB	Cell Signaling	Cat#8242; RRID: AB_10859369
Rabbit anti-phospho-NFκB	Cell Signaling	Cat#3033; RRID: AB_331284
Rabbit anti-ERK1/2	Cell Signaling	Cat#4695; RRID: AB_390779
Rabbit anti-phospho-ERK1/2	Cell Signaling	Cat#4370; RRID: AB_2315112
Rabbit anti-JNK	Cell Signaling	Cat#9252; RRID: AB_2250373
Rabbit anti-phospho-JNK	Cell Signaling	Cat#4668; RRID: AB_823588
Rabbit anti-p38	Cell Signaling	Cat#8690; RRID: AB_10999090
Rabbit anti-phospho-p38	Cell Signaling	Cat#4511; RRID: AB_2139682
Rabbit anti-p70S6K	Cell Signaling	Cat#9202; RRID: AB_331676
Rabbit anti-phospho-p70S6K	Cell Signaling	Cat#9205; RRID: AB_330944
Rabbit anti-S6	Cell Signaling	Cat#2217; RRID: AB_331355
Rabbit anti-phospho-S6	Cell Signaling	Cat#2211; RRID: AB_331679
Rabbit anti-4E-BP1	Cell Signaling	Cat#9644; RRID: AB_2097841
Rabbit anti-phospho-4E-BP1	Cell Signaling	Cat#2855; RRID: AB_560835
Rabbit anti-mTOR	Cell Signaling	Cat#2983; RRID: AB_2105622
Rabbit anti-phospho-mTOR	Cell Signaling	Cat#5536; RRID: AB_10691552
Rabbit anti-AKT	Cell Signaling	Cat#4685; RRID: AB_2225340
Rabbit-anti-phospho-AKT	Cell Signaling	Cat#4060; RRID: AB_2315049
Rabbit anti-PRAS40	Cell Signaling	Cat#2691; RRID: AB_2225033
Rabbit anti-phospho-PRAS40	Cell Signaling	Cat#2997; RRID: AB_2258110
Rabbit anti-HA	Cell Signaling	Cat#3724; RRID: AB_1549585
Mouse anti-V5	Cell Signaling	Cat# 80076; RRID: AB_2920661
Mouse anti-Lamin A/C	Cell Signaling	Cat#4777; RRID: AB_10545756
Mouse anti-beta IV TUBULIN	Abcam	Cat#ab11315; RRID: AB_297919
Rabbit IgG	Cell Signaling	Cat#2729; RRID: AB_1031062
Mouse IgG2b	Cell Signaling	Cat#53484; RRID: AB_2799435
Mouse anti-His	ThermoFisher Scientific	Cat#MA1-21315; RRID: AB_557403
Rabbit anti-His	Abcam	Cat#ab9108; RRID: AB_307016
Evolocumab	TargetMol	Cat#T9920
Human IgG2 isotype control	Bio X Cell	Cat#BE0301; RRID: AB_2715459
anti-CD45-BV785	BioLegend	Cat#103149; RRID: AB_2564590
anti-CD4-BV605	BioLegend	Cat#100451; RRID: AB_2564591
anti-CD8α-AF700	BioLegend	Cat#100730; RRID: AB_493702
anti-CD45-PECy7	ThermoFisher Scientific	Cat#25-0451-82; RRID: AB_2734986
anti-MHCII-AF700	ThermoFisher Scientific	Cat#56-5321-80; RRID: AB_494010
anti-F4/80-FITC	BioLegend	Cat#123108; RRID: AB_893502

(*Continued on next page*)

Continued

REAGENT or RESOURCE	SOURCE	IDENTIFIER
anti-CD24-PE	BioLegend	Cat#101807; RRID: AB_312840
mouse anti-LRP1-PE	BD Biosciences	Cat#550497; RRID: AB_393709
Anti-mouse CD4	Bio X Cell	Cat#BE0003-1; RRID: AB_1107636
Anti-mouse CD8α	Bio X Cell	Cat#BE0004-1; RRID: AB_1107671
Rat IgG2b isotype control	Bio X Cell	Cat#BE0090; RRID: AB_1107780
Bacterial and virus strains		
Endura ElectroCompetent Cells	Lucigen	Cat#60242-1
Biological samples		
Patient-derived organoid HCI-012	Scherer et al.[89]	N/A
Chemicals, peptides, and recombinant proteins		
BSA	Sigma-Aldrich	Cat#A9576
PCSK9	Sino Biological	Cat#29698-H08H
PCSK9 D374Y V474I G670E	Sino Biological	Cat#10594-H08H1
Custom-made PCSK9 V474I	Sino Biological /This paper	N/A
Custom-made PCSK9 F379A	Sino Biological /This paper	N/A
Critical commercial assays		
VivoGlo™ Caspase 3/7 Substrate	Promega	Cat#PAP1781
TruSeq RNA Library Prep Kit	Illumina	Cat#RS-122-2001
Standard Macrophage Depletion Kit	Encapsula NanoSciences	Cat#: CLD-8901
Deposited data		
RNA sequencing data of *Lrp1* depleted (and control) EO771 cells	This paper	GSE255559.
RNA sequencing data of recombinant PCSK9 or BSA treated EO771 cells	This paper	GSE255558.
RNA sequencing data of primary breast tumors formed by implanted EO771 cells in wildtype versus *Pcsk9* knockout mice	This paper	GSE255560.
RNA sequencing data of primary breast tumors formed by implanted EO771 cells in h*PCSK9*$^{V474I/V474I}$ and h*PCSK9*$^{+/+}$ mice	This paper	GSE273936.
Mass cytometry data of the plasma membrane fraction of recombinant PCSK9 or BSA treated EO771 cells	This paper	ProteomeXchange: PXD049279
Raw western blot data	This paper	https://data.mendeley.com/preview/32369gyznm?a=34ba66b3-a90f-4c36-9b44-a653bf3cfd7b
Experimental models: Cell lines		
HEK293	ATCC	Cat#CRL-1573; RRID: CVCL_0045
4T1	ATCC	Cat#CRL-2539; RRID: CVCL_0125
EO771	ATCC	Cat#CRL-3461; RRID: CVCL_GR23
MDA-MB-231	ATCC	Cat#HTB-26; RRID: CVCL_0062
EMT6	ATCC	Cat#CRL-2755; RRID: CVCL_1923
SKBR3	ATCC	Cat#HTB-30; RRID: CVCL_0033
EO771-LM2	This paper	N/A
MDA231-LM3	This paper	N/A
Experimental models: Organisms/strains		
C57BL/6J mouse	Jackson laboratories	Strain 000664
BALB/cJ mouse	Jackson laboratories	Strain 000651
FVB/N-Tg(MMTV-PyVT)634Mul/J mouse	Jackson laboratories	Strain 002374

(*Continued on next page*)

Continued

REAGENT or RESOURCE	SOURCE	IDENTIFIER
B6.FVB-Tg(MMTV-PyVT)634Mul/LellJ mouse	Jackson laboratories	Strain 022974
NOD.Cg-Prkdc^{scid} Il2rg^{tm1Wjl}/SzJ mouse	Jackson laboratories	Strain 005557
Pcsk9 knockout mouse	This paper	N/A
hPCSK9 KI mouse	Biocytogen /This paper	N/A
hPCSK9 V474I KI mouse	Biocytogen /This paper	N/A
Oligonucleotides		
Primer, sgRNA and shRNA list	This paper	See Table S2 for the list of sequences
ON-TARGETplus Human XAF1 siRNA	Horizon Discovery	Cat#L-004357-00-0005
ON-TARGETplus Human USP18 siRNA	Horizon Discovery	Cat#L-004236-00-0005
control siRNA sictrl	Horizon Discovery	Cat#D-001810-01-05
Recombinant DNA		
pLKO.1-puro	Addgene	Cat#8453; RRID: Addgene_8453
pLKO.1-blast	Addgene	Cat#26655; RRID: Addgene_26655
pLKO.1-hygro	Addgene	Cat#24150; RRID: Addgene_24150
TLCV2	Addgene	Cat#87360; RRID: Addgene_87360
lentiCRISPR v2	Addgene	Cat#52961; RRID: Addgene_52961
lenti-sgRNA blast	Addgene	Cat#104993; RRID: Addgene_104993
pHR-SFFV-dCas9-BFP-KRAB	Addgene	Cat#46911; RRID: Addgene_46911
lenti-sgRNA puro	Addgene	Cat#104990; RRID: Addgene_104990
pCVL-ires-hygro	This paper	N/A
MI-Luciferase-IRES-mCherry	Addgene	Cat#75020; RRID: Addgene_75020
pHIV-Luc-ZsGreen	Addgene	Cat#39196; RRID: Addgene_39196
pLV-mCherry	Addgene	Cat#36084; RRID: Addgene_36084
Software and algorithms		
samtools/bcftools v1.9	Danecek et al.[96]	https://github.com/samtools/samtools
GenotypeHarmonizer v1.4.23	Deelen et al.[97]	https://cambridge-ceu.github.io/csd3/applications/Genotype-Harmonizer.html
ShapeIt v2	Dalaneau et al.[98]	https://mathgen.stats.ox.ac.uk/genetics_software/shapeit/shapeit.html
Impute2	Howie et al.[99]	https://mathgen.stats.ox.ac.uk/impute/impute_v2.html
plink v1.9	Chang et al.[100]	https://www.cog-genomics.org/plink/
Picard v2.22.3	N/A	https://broadinstitute.github.io/picard/
STAR v2.7.10b	Dobin et al.[101]	https://github.com/alexdobin/STAR
featureCounts v2.0.6	Liao et al.[102]	https://subread.sourceforge.net/featureCounts.html
MultiQC v1.11	Ewels et al.[103]	https://multiqc.info/
MAGeCK v0.5.9.4	Li et al.[104]	https://sourceforge.net/p/mageck/wiki/Home/
DESeq2 v1.32.0	Love et al.[105]	https://bioconductor.org/packages/release/bioc/html/DESeq2.html
fgsea v1.12.0	Sergushichev[106]	https://bioconductor.org/packages/release/bioc/html/fgsea.html
msigdbr v7.5.1	N/A	https://github.com/igordot/msigdbr
forestmodel v0.6.2	N/A	https://github.com/NikNakk/forestmodel
survival v3.4-0	Therneau and Grambsch[107]	https://cran.r-project.org/web/packages/survival/index.html
survminer v0.4.9	N/A	https://github.com/kassambara/survminer

(*Continued on next page*)

Continued

REAGENT or RESOURCE	SOURCE	IDENTIFIER
pheatmap v1.0.12	N/A	https://cran.r-project.org/web/packages/pheatmap/index.html
RGGV v2016-09-07	Joseph H Marcus and John Novembre[108]	https://github.com/NovembreLab/RGGV
R 3.6.3	The R Foundation	https://www.r-project.org
Rstudio 2022.12.0 Build 353	Posit Software	https://posit.co/
Spectronaut v17	Biognosys	https://biognosys.com/software/spectronaut/
DIA-Umpire	Tsou et al.[109]	https://github.com/Nesvilab/DIA-Umpire
ImageJ v1.54h	NIH	http://imageJ.org/
FCS Express 7	De Novo Software	https://denovosoftware.com/
Other		
Regular chow diet	Research Diets	Cat#D12492
High cholesterol diet	Envigo	Cat#TD08464
Custom-made 0.01% atorvastatin diet	Envigo/This paper	N/A
Control diet with no statin	Envigo	Cat#TD220626

EXPERIMENTAL MODEL AND STUDY PARTICIPANT DETAILS

Animal studies

All animal experiments were conducted in accordance with the Institutional Animal Care and Use Committee at The Rockefeller University. All mice were housed in a specific pathogen free facility. The following mouse strains were obtained from Jackson Laboratories: BALB/cJ (stock no. 000651), C57BL/6J (stock no. 000664), MMTV-PyMT on a FVB background (FVB/N-Tg(MMTV-PyVT)634Mul/J, stock no. 002374), MMTV-PyMT on a C57BL/6 background (B6.FVB-Tg(MMTV-PyVT)634Mul/LellJ, stock no. 022974), NSG (NOD.Cg-Prkdc^{scid} Il2rg^{tm1Wjl}/SzJ mouse, stock no. 005557). *Pcsk9* knockout mice were generated at the Transgenic and Reproductive Technology Center at Rockefeller University. Human *PCSK9* and *PCSK9* (V474I) targeted-replacement (knock-in) mice were generated by Beijing Biocytogen Co., Ltd. *Pcsk9* knockout mice were crossed to wild-type C57BL/6J mice to generate *Pcsk9*$^{+/-}$ mice, which were subsequently intercrossed to generate *Pcsk9*$^{-/-}$ and *Pcsk9*$^{+/+}$ littermates. *Pcsk9* knockout mice were also crossed with C57BL/6 background *MMTV-PyMT* mice to generate MMTV-PyMT; *Pcsk9*$^{+/-}$ progeny. These were then bred to generate both MMTV-PyMT; *Pcsk9*$^{+/+}$ and MMTV-PyMT; *Pcsk9*$^{-/-}$ mice. Female mice were used in experiments as this study focused on female human breast cancer. For transplantable models, female mice aged 7-9 weeks were used. For MMTV-PyMT model on a FVB background, experiments started on 5-week-old female mice. For MMTV-PyMT model on a C57BL/6 background, experiments started on 10-week-old female mice.

Tissue culture

4T1, EO771, HEK293T, EMT6, SKBR3 and MDA-MB-231 cells were obtained from American Tissue Type collection (ATCC). EO771 and EMT6 cells were maintained in RPMI (Life Technologies, 11875-093) with 10% FBS (Sigma-Aldrich, F4135), and 10 mM HEPES (ThermoFisher Scientific, 15-630-080). HEK293T, 4T1 and MDA-MB-231 cells were maintained in DMEM (Gibco, 11995065) with 10% FBS. SKBR3 cells were maintained in McCoy's 5A Medium (ATCC, 30–2007) with 10% FBS. The highly metastatic EO771-LM2 and MDA-MB-231-LM3 subclones were *in vivo* selected as previously described.[62] Contamination with mycoplasma was ruled out on a quarterly basis using a PCR-based protocol.

Three-dimensional culture

Patient-derived organoid HCI-012[89] was a gift from Alana L. Welm from University of Utah. Organoids were embedded in 2,000-4,000 organoids/ml of growth factor reduced Matrigel (Corning, 354320). The complete medium for organoid cultures included Advanced DMEM/F12 (Gibco, 12-634-010), 10 mM HEPES (ThermoFisher Scientific, 15-630-080), 5% FBS (ThermoFisher Scientific, A3840101), 1% Glutamax (ThermoFisher Scientific, 35050061), 1μg/ml Hydrocortisone (Sigma-Aldrich, H0888), 50μg/ml Gentamicin (ThermoFisher Scientific, 15750060), 10ng/ml hEGF (Sigma-Aldrich, E9644) and 10nM Y-27632 (Selleck Chemicals, S1049).

METHOD DETAILS

Selection of candidate SNPs

The NIH database dbSNP[110] was used to select common missense SNP candidates with known disease associations with the following filter: a global minor allele frequency > 0.1, classified as a missense variant and possessing a clinical significance

annotation. A list of genes encoding ligands, receptors and transporters was compiled from the ligand-receptor list curated by Ramilowski et al.[111] and the transporter database available at https://tcdb.org/. This gene list was then cross-referenced with dbSNP to select common missense mutations. This approach yielded 3361 candidate SNPs.

Analysis of the TCGA cohort

Aligned whole-exome sequencing BAM files from normal tissue samples (blood, solid tissue or buccal cells) of the TCGA-BRCA, TCGA-SKCM, TCGA-LUAD and TCGA-LUSC cohorts were obtained from the GDC data portal (https://portal.gdc.cancer.gov/). Germline variants were called with samtools/bcftools v1.9. $Log_2(x+1)$ transformed RSEM normalized RNASeq count table, curated survival time and other clinical information including cancer stage and age at diagnosis were downloaded from UCSC Xena (https://xena.ucsc.edu/[112]). PAM50 subtype information was curated by Natanely et al.[113] In order to harmonize the analysis across breast cancer datasets with different patient age distributions, females over 50-year-old at diagnosis with stage II or III breast cancer were included in analysis, which also enriched patients with high risk of metastasis. For SKCM, LUAD and LUSC, patients with stage II or III cancer were included in analysis. Survival times were censored at 10 years to ensure a sufficient patient count in each group. To assess the effect of germline variants on overall survival, survival analyses were performed, employing the log-rank test for statistical significance using the survival v3.4-0 and survminer v0.4.9 packages in R. Hazard ratios (HRs) were calculated according to a Cox proportional hazard regression model using the survival package. Each candidate variant was tested under three genetic models: additive (coded 0, 1, or 2 for the number of alternative alleles), dominant (alternative allele carriers coded as 1, wild-type homozygotes as 0) and recessive (alternative allele homozygotes coded as 1, wild-type carriers as 0). Models with fewer than 50 genotyped patients in one group were excluded from the analysis. Common confounding clinical variables were tested for significance in a multivariable Cox proportional hazard model with R package forestmodel v0.6.2.

Pair-wise Pearson's correlations were calculated between the genes in the 5-gene signature (*XAF1*, *RTP4*, *USP18*, *OAS1*, *and ISG15*) and the correlations were visualized using R package pheatmap v1.0.12.

Analysis of the Bertucci et al. cohort

Aligned whole-exome sequencing BAM files from normal tissue samples and clinical information were downloaded from the original Bertucci et al. study[26] and https://www.ebi.ac.uk/ega/ (EGAS00001003290). Germline variants were called with samtools/bcftools v1.9. As all patients in this study had metastatic breast cancer, survival time was censored at 2 years to ensure a sufficient patient count in each group. Subsequent analysis of the association between clinical variables and germline variants was performed as described in the TCGA-BRCA study above.

Analysis of the Nik-Zainal et al. cohort

Aligned whole-exome sequencing BAM files from normal tissue samples and clinical information were downloaded from the original Nik-Zainal et al. study[29] and https://www.ebi.ac.uk/ega/ (EGAS00001001178). Germline variants were called with SAMtools/bcftools v1.9. Imputation was done as described[114] to increase the genotyping rate of PCSK9 variant rs562556. Briefly, genotyping data were filtered using plinkv1.9 to exclude variants with a minor allele frequency less than 1%, a genotyping rate less than 75% and a departure from the Hardy–Weinberg equilibrium at P<1e-6. Strands were aligned using GenotypeHarmonizer v1.4.23 and the 1000 Genomes Project reference genome downloaded from (https://ftp.1000genomes.ebi.ac.uk/vol1/ftp/release/20130502/). Pre-phasing was performed using ShapeIt v2. Variants in the genomic region chr1:55495944-55540946 were imputed with Impute2 with parameters used in a previous study[24]: -NE 20000 -iter 100 -call_thresh 0.8.

For consistency with the analysis of TCGA-BRCA, European females over 50-year-old at diagnosis with grade II or III breast cancer were included in analysis. Survival time was censored at 10 years to maintain sufficient patient counts in each group. Subsequent analysis of the association between clinical variables and rs562556 was performed as described in TCGA-BRCA study above.

Analysis of the Hartwig Medical Foundation (HMF) cohort

Germline information VCF files and clinical data were downloaded from Hartwig data bucket on Google Cloud with gsutil v5.24. For consistency, females over 50-year-old at biopsy were included in the analysis. As there were no overall survival time annotations available in the clinical information, we defined survival time based on time between biopsy date and date of death (when applicable). 569 female patients had available biopsy date and germline information. 415 of them were older than 50 when biopsied. 285 of 415 (69%) who were included in the analysis had date of death information and their overall survival time was measured from biopsy date to date of death. As all patients in this study had metastatic breast cancer, survival time was censored at 2 years to ensure a sufficient patient count in each group. This was the same endpoint used in the Bertucci et al. metastatic breast cancer cohort. Subsequent analysis of the association between clinical variables and rs562556 was performed as described in the TCGA-BRCA study above.

Analysis of the UK Biobank

To assess the effect of rs562556 on survival of non-breast cancer populations, we downloaded germline information VCF files and clinical data, including cancer diagnosis, year of birth and date of death on October 3, 2020. Females over 50 years old without breast cancer were included in the analysis (data field 40006 not equal to 'C500','C501', 'C502', 'C503', 'C504', 'C505', 'C506', 'C508' and 'C509'). Survival time was measured as the number of years from the participant's birth year to the year of death, loss of follow-up, or

to the year 2020 for participants who were still alive. Analysis of the association between rs562556 and death was performed with R package forestmodel v0.6.2.

Analysis of population structure

To assess if population structure impacted the clinical association, we sought to select SNP markers with high genotyping quality in the TCGA-BRCA, Bertucci et al., Nik-Zainal et al., HMF cohorts as well as the 1000 genome reference. We first pruned variants in the 1000 genome reference to generate a list of common variants in approximate linkage disequilibrium using plink v1.9 with the following setting: –maf 0.10 –indep 50 5 1.5. We then selected biallelic SNP markers with >90% genotyping rate in the four clinical cohorts. 285 common variants and 5375 people were included in the principal component analysis with plink. The genomic coordinates of TCGA-BRCA data were converted from hg38 to hg19 with LiftoverVcf of Picard v2.22.3 by the Broad Institute. Individuals from the clinical cohorts were plotted along with 1000 genome participants with known ancestral information and European ancestry was defined as PC1 < 0.00779496 and PC2 < 0.0104922. The first five principal components were also included in a multivariable Cox proportional hazard model with R package forestmodel v0.6.2 to account for population structure in each clinical cohort. The geographical distribution of rs562556 allele frequency (Figure 1A) was plotted with RGGV.[108]

Analysis of the BC-Blood cohort

We investigated whether a *PCSK9* SNP (rs562556) was associated with prognosis in the BCblood cohort from Lund University, which comprised patients treated for primary breast cancer at Skåne University Hospital, Lund, Sweden.[90] Patient enrollment spanned from diagnosis to pre-surgery, with eligibility limited to those with a first diagnosis of primary breast cancer and no other primary cancer diagnoses in the preceding 10 years. At enrollment, participants completed a questionnaire regarding lifestyle and reproductive factors, underwent anthropometric measurements by research nurses, and provided EDTA plasma for genotyping. Clinical data were obtained from medical records, pathology reports, and registries. Genotype information was available for patients enrolled from 2002 to 2016. The cohort was refined by excluding individuals with carcinoma *in situ*, those who received preoperative treatment, and those with distant metastasis within 0.3 years of enrollment, resulting in 1701 eligible patients. A further exclusion of patients < 50 years old or with Grade I tumors yielded a cohort of 1032 patients. The univariable and multivariable survival analysis included the patients that were LN negative (668 of 1032). An additional 152 patients with large tumors (pT2/3/4) were also excluded in the analyses. The cutoff for the last follow-up was June 30, 2019. The Lund University Ethics Committee approved this study and all patients signed written informed consent.

SNP genotyping was performed by the Centre for Translational Genomics at Lund University using Infinium OncoArray-500K BeadChip by Illumina.[115] Details on the genotyping calling have been previously described.[115] Standard quality control was performed on all scans. All samples with low call rates (< 1 × 1e-5) were excluded, as were SNPs with minor allele frequency < 1% or call rate < 99%. For rs562556, genotype intensity cluster plots were examined manually to judge reliability and manual clustering was performed.[116]

Per Swedish clinical routine, the ER and PR positivity cut-offs were >10% stained nuclei. For patients with missing HER2 status, HER2 status was obtained from dual gene protein staining of HER2 on tissue microarrays, which showed 97.7% agreement with available pathological assessment.[117]

The endpoints used for survival analyses were breast cancer-free interval (BCFI) and distant metastasis-free interval (DMFI). DMFI was defined as time from enrollment until distant metastasis. BCFI was defined as time between enrollment and the first breast cancer event, or last follow-up, i.e., the period during which the patient has not experienced any recurrence of the disease. The endpoint, breast cancer event, includes any of the following: locoregional recurrence, distant metastasis, or contralateral breast cancer. Patients without any breast cancer event were censored at time of emigration, death, or the last follow-up date of June 30, 2019. Cox proportional hazards regression was used to estimate crude and adjusted Hazard ratios (HRs) with 95% CI. The multivariable models were adjusted for age (continuous), tumor characteristics (Grade (III), estrogen receptor positivity (ER), and adjuvant treatments; tamoxifen, aromatase inhibitors, radiotherapy chemotherapy, and trastuzumab. To account for death from other causes as a competing risk, competing risk regression (Fine-Gray) model was used to assess the cumulative incidence of the DMFI. Subdistribution hazard ratios (SHRs) with 95% CI were calculated.

Analysis of the SCAN-B cohort

SCAN-B data were downloaded from the supplementary information and Data from Staaf et al.[118] Expression levels were expressed in fragments per kilobase of exon per million mapped reads (FPKM) in an expression matrix. To all FPKM data an offset of +0.1 was added, and then the data was $\log_2$ transformed. Patients with gene expression profiles (GEXs) only from noninvasive cancer or lymph nodes, bilateral cancer, or who had no available follow-up for distant metastasis were excluded. In cases where multiple GEXs from a single tumor passed quality control, the GEX profile with the highest RNA concentration measured by NanoDrop spectrophotometry was chosen, leaving one GEX per patient for analysis. This procedure left a total of 5326 patients. The Lund University Ethics Committee approved this study and all patients signed written informed consent.

The expression of the 5 gene signature was calculated as the mean expression of the five included genes (*XAF1*, *RTP4*, *USP18*, *OAS1*, and *ISG15*). Pair-wise Pearson's correlations were calculated between the genes in the 5-gene signature and the correlations were visualized using pheatmap. The Kaplan-Meier estimator and Log-rank test were used for univariable survival analyses of the

5-gene signature in relation to distant metastasis-free interval (DMFI). Crude Hazard ratios (HRs) with 95% confidence intervals (CI) were obtained from Cox proportional hazards models. The R packages survival and survminer were used.

KM plotter

The association between the expression of the 5-gene signature and the distant metastasis-free survival (DMFS) was also assessed with the KM plotter (https://kmplot.com/analysis/),[119] a database with microarray-based gene expression of human breast cancer. The expression of the 5-gene signature was calculated as the mean expression of the probes of the five genes (*XAF1*, *RTP4*, *USP18*, *OAS1*, and *ISG15*). The DMFS of the upper and lower expression quantile (Q1 vs Q4) were compared using Cox proportional hazards model with the default setting.

Expression of PCSK9 in human tissues

The expression dot plot of human PCSK9 in multiple normal and cancerous tissues was generated with GEPIA2[120] (http://gepia2.cancer-pku.cn/). TCGA tumor, matched normal tissue and GTEx data were used. "LIMMA" differential method was chosen to compare tumor and normal tissue expression.

Generation of *Pcsk9* knockout mice

Two gRNA targets were designed to target exon 1 (CTACTGTGCCCCACCGGCGC TGG) and intron 11 (CCACGAGTGTCCAT TCTGGT GGG) of the *Pcsk9* gene to generate a large deletion. The selected gRNAs were evaluated for their off-target potential with the web-based tool CRISPOR (http://crispor.tefor.net). Their on-target efficiency was assessed by electroporating gRNA/Cas9 reagents (2 μM) into 0.5-day fertilized zygotes and then analyzing the percentage of mouse embryos with indels on target. 24 hours after electroporation each 2-cell embryo was transferred to 6ul of QuickExtract buffer (Lucigen, QE09050), heated to 68℃ for 6 minutes, and then 98℃ for 2 minutes. The lysate of each embryo was used to amplify the genomic target by PCR, followed by sequencing to score indels.

Synthetic crRNA and tracrRNA from IDT (Integrated DNA Technology) were used to assemble the gRNA. crRNA and tracrRNA were annealed by heating to 98°C for 2 minutes and cooling at room temperature for 5 minutes. Cas9 protein (0.2 μM) was added to the solution containing both gRNAs (0.1 μM), incubated at 37℃ for 15 minutes to form the riboprotein complex, purified by Millipore Ultrafree column (Millipore, UFC30VV25), and placed on ice until microinjection.

Microinjection using zygotes prepared by *in vitro* fertilization (IVF) followed a well-established protocol (https://www.cosmobiousa.com/content/document/cosmo-bio-ltd/kyd-manual_en-chap1-in-vitro-fertilization.pdf43). C57BL/6J male mice and super-ovulated female C57BL/6J mice were purchased from Jackson Laboratories and used to extract spermatozoa and oocytes for IVF.

Mouse genomic DNA was extracted from tail biopsies using the QIAamp Fast DNA Tissue kit (Qiagen, 51404). PCR primers Pcsk9E1-F1 (5'-GTAACAGGTCCCGTTTGCAG) and Pcsk9I-11-R2 (5'-CCCAGCCATCCATCCTACTT) were designed to flank each gRNA target. The genomic DNA with a targeted deletion was expected to amplify a DNA fragment of around 800 bp. The PCR reaction was performed with 200 ng of genomic DNA, primers (0.25 μM), and 0.2 μM of dNTPs using PrimeSTAR HS DNA polymerase (TekaRa Bio, R010B). The PCR amplicons from positive mice were then sequenced to confirm the deletion junctions.

Generation of human PCSK9 KI mice

C57BL/6J mice were purchased from Beijing Vital River Laboratory Animal, Co., Ltd. All mice were housed in a specific-pathogen-free facility. For generating h*PCSK9 KI (V474I)* and h*PCSK9 KI(WT)* mice, sgRNAs were designed to target the region exon1 with the CRISPR design tool (http://www.sanger.ac.uk/htgt/wge/). Guide RNAs were screened for on-target activity using UCATM (Universal CRISPR Activity Assay), a sgRNA activity detection system developed by Biocytogen. The Cas9 mRNA and sgRNA were transcribed by T7 RNA polymerase *in vitro*. For Cas9 mRNA and sgRNA production, the T7 promoter sequence was added to the Cas9 or sgRNA template by PCR amplification. The T7-Cas/sgRNA PCR products were gel purified and served as the template for *in vitro* transcription using the MEGAshortscript T7 kit (Life Technologies). The Cas9 mRNA and sgRNA were purified using the MEGAclear kit and eluted with RNase-free water. To minimize random integrations, a circular donor vector was used. For the h*PCSK9 KI (V474I)*, the gene targeting vector contained human *PCSK9* CDS (c.1420G>A p.V474I)-WPRE-bGHpA-STOP and 2 homology arms of left (1300 bp) and right (1100 bp). For the h*PCSK9 KI (WT)*, the gene targeting vector contained human *PCSK9* CDS-WPRE-bGHpA-STOP and 2 homology arms of left (1300 bp) and right (1100 bp). The human *PCSK9* CDS was inserted after the ATG start codon of the murine *Pcsk9* gene. C57BL/6J females were used as embryo donors and pseudopregnant foster mothers. Superovulated C57BL/6J mice (4–5 weeks old) were mated to C57BL/6J stud males, and fertilized embryos were collected from the ampullae. Cas9 mRNA, sgRNA and donor vectors were mixed at different concentrations and co-injected into the cytoplasm of fertilized eggs at the one-cell stage. After injection, surviving zygotes were transferred into the oviducts of C57BL/6J pseudopregnant females.

Genotyping of the tail biopsies from progenies was done to screen for mice with the human *PCSK9* knockin. Southern blotting was done to confirm the knockin. Genomic DNA extracted from tail biopsies was digested with NsiI or BglII (NEB), separated on a 1% agarose gel, and transferred to a positively charged nylon membrane (Hybond N+; Amersham International plc). The membrane was hybridized using DIG Easy Hyb Granules (Roche Applied Science Inc.) at 42°C overnight containing a PCR-generated probe, labeled by the PCR DIG probe synthesis kit (Roche Applied Science Inc.). Hybridization signals were detected using the DIG Luminescent Detection Kit (Roche Applied Science Inc.). For probe labeling, 3'-external and internal DIG-labeled probes were prepared by

PCR using Taq DNA polymerase and incorporated DIG-11-dUTP according to the manufacturer's instruction. The following primers were used to amplify the 3'-external (350 bp) probes: 5'- GTAAAGCTTAGGTCTGATCTGACTC-3' (forward primer) and 5'-GAGACAGAGGCGCGCCTGGTAG-3' (reverse primer). For the internal (500 bp) probe, the following primers were used: 5'-GTGGA TACGCTGCTTTAATGCC-3' (forward primer) and 5'- AAGGGAGATCCGACTCGTCTG-3' (reverse primer).

Genotyping of transgenic mouse lines

Genotyping of various mouse colonies was performed after extracting DNA from an ear skin biopsy. The PCR primers of mice generated in this study are:

Pcsk9 knockout mice:
Pcsk9IE1-SA-F1: 5'-GTAACAGGTCCCGTTTGCAG-3'
Pcsk9I11-SA-R2: 5'-CCCAGCCATCCATCCTACTT-3'
Pcsk9IE1-SA-R1: 5'-TGCCACTAGAGTTCTCAGCC-3'
Pcsk9IE1-SA-F1+Pcsk9I11-SA-R2 848bp (KO band); Pcsk9IE1-SA-F1+R1 909bp (WT band)
PCSK9 Hu KI(V474I) and *PCSK9* Hu KI(WT) knock-in mice:
hPCSK9 KI WT-F: 5'-CGGGGCCCGTTAATGTTTAATCAGA-3'
hPCSK9 KI WT-R: 5'-AGAGACCACCAGACGGCTAGATGAG -3'
hPCSK9 KI Mut-R: 5'-CTCGGAACGCAAGGCTAGCACCAGC-3'
hPCSK9 KI WT-F+ hPCSK9 KI WT-R 590bp (murine Pcsk9 band); hPCSK9 KI WT-F+ hPCSK9 KI Mut-R 429 (human PCSK9 band).
hPCSK9 KI GT-F: 5'-CAAAGATGTCATCAATGAGGCCTGG-3'
hPCSK9 KI GT-R: 5'-GTAGACACCCTCACCCCCAAAAG-3'
hPCSK9 KI GT-F + hPCSK9 KI GT-R 304bp. Sanger sequencing was done at GENEWIZ, Inc. to distinguish *PCSK9* and *PCSK9:V474I* allele. Sanger sequencing traces were visualized with SnapGene Viewer 5.2.5.1.

In vivo selection of PDO

For *in vivo* selection of metastatic subclones, we intravenously injected 400,000 HCI-012 cells resuspended in PBS into 8-week-old NSG female mice. Organoids were resuspended in Cell Recovery Solution (Corning, 354253), digested with TrypLE Express (ThermoFisher Scientific, 12605010) for 5 minutes at room temperature, filtered through 70um Cell Strainer (ThermoFisher Scientific, 08-771-2) to generate single cell suspension for injection. Lung metastases formed by HCI-012 were dissected out, digested at 37°C on a benchtop shaker at 180 rpm for 40 minutes and embedded into Matrigel to generate metastatic subclones. The medium for metastasis digestion included RPMI-1640, 4 mg/ml collagenase (Sigma-Aldrich, C2139), 1% Pen-Strep (Sigma-Aldrich, P4333), 5% FBS and 10 mM HEPES. Contamination with mycoplasma was ruled out on a quarterly basis using PCR-based protocol.

Vector Construction

To knockdown murine *Pcsk9*, *Ldlr*, *Lrp1* and human *XAF1*, *USP18* shRNA vectors (pLKO.1-puro, Addgene #8453; pLKO.1-blast, Addgene #26655; pLKO.1-hygro, Addgene #24150) were used. The following shRNA sequences were cloned into pLKO.1 vectors:

shctrl:
F 5'-CGGCAACAAGATGAAGAGCACCAACTCGAGTTGGTGCTCTTCATCTTGTTGTTTTTG-3'
R 5'-AATTCAAAAACAACAAGATGAAGAGCACCAACTCGAGTTGGTGCTCTTCATCTTGTTG-3'
shPcsk9:
F 5'-CCGGCCATGTCCACTGCCACCAGAACTCGAGTTCTGGTGGCAGTGGACATGGTTTTTG-3'
R 5'-AATTCAAAAACCATGTCCACTGCCACCAGAACTCGAGTTCTGGTGGCAGTGGACATGG-3'
shLrp1-1:
F 5'-CCGGAGGCGCCTGTGTGGTCAATAACTCGAGTTATTGACCACACAGGCGCCTTTTTTG-3'
R 5'-AATTCAAAAAAGGCGCCTGTGTGGTCAATAACTCGAGTTATTGACCACACAGGCGCCT-3'
shLrp1-2:
F 5'-CCGGCGGAGTCACTTACATCAATAACTCGAGTTATTGATGTAAGTGACTCCGTTTTTG-3'
R 5'- AATTCAAAAACGGAGTCACTTACATCAATAACTCGAGTTATTGATGTAAGTGACTCCG-3'
shLdlr:
F 5'-CCGGCACCTGTCAGTCCAATCAATTCTCGAGAATTGATTGGACTGACAGGTGTTTTTG-3'
R 5'-AATTCAAAAACACCTGTCAGTCCAATCAATTCTCGAGAATTGATTGGACTGACAGGTG-3'
shXAF1:
F 5'- CCGGACTCACGTATCATCTCAATAGCTCGAGCTATTGAGATGATACGTGAGTTTTTTG-3'
R 5'-AATTCAAAAAACTCACGTATCATCTCAATAGCTCGAGCTATTGAGATGATACGTGAGT-3'
shUSP18:
F 5'-CCGGCTTGATTCAGGTGTTCGTAATCTCGAGATTACGAACACCTGAATCAAGTTTTTG-3'
R 5'-AATTCAAAAACTTGATTCAGGTGTTCGTAATCTCGAGATTACGAACACCTGAATCAAG-3'

To knockout murine *Pcsk9*, *Lrp1*, human *PCSK9* and *LRP1*, lentiCRISPR v2 (Addgene #52961) and lenti-sgRNA blast (Addgene #104993) were used. The following sgRNA sequences were cloned into the lentiCRISPR v2 vector:

sgctrl (mouse):
F 5'-CACCGGTTCCAGGGAACAGCACTGA-3'
R 5'-AAACTCAGTGCTGTTCCCTGGAACC-3'
sgPcsk9-1:
F 5'-CACCGACTGCTCTGCGTGGCTGCGG-3'
R 5'-AAACCCGCAGCCACGCAGAGCAGTC-3'
sgPcsk9-2:
F 5'-CACCGCCAGTGCGTTGGCCACCAGG-3'
R 5'-AAACCCTGGTGGCCAACGCACTGGC-3'
sgLrp1-1:
F 5'-CACCGCGTGGACCAGACTCGCCCAG-3'
R 5'-AAACCTGGGCGAGTCTGGTCCACGC-3'
sgLrp1-2:
F 5'-CACCGGGGAAACTCCTGGACAACGG-3'
R 5'-AAACCCGTTGTCCAGGAGTTTCCCC-3'
sgctrl1 (human):
F 5'-CACCGACCGGCTCTCACAACAGCAG-3'
R 5'-AAACCTGCTGTTGTGAGAGCCGGTC-3'
sgPCSK9-1:
F 5'-CACCGGCAGCGGTGGAAGGTGGCTG-3'
R 5'-AAACCAGCCACCTTCCACCGCTGCC-3'
sgPCSK9-2:
F 5'-CACCGGTTGCCTGGCACCTACGTGG-3'
R 5'-AAACCCACGTAGGTGCCAGGCAACC-3'
The following sgRNA sequences were cloned into lenti-sgRNA blast vector:
sgctrl2 (human):
F 5'-CACCGGTCCCGGCCGCGCTAATGTG-3'
R 5'-AAACCACATTAGCGCGGCCGGGACC-3'
sgLRP1-1:
F 5'-CACCGGCCCGATCCACAGACAGACG-3'
R 5'-AAACCGTCTGTCTGTGGATCGGGCC-3'
sgLRP1-2:
F 5'-CACCGCCATCACACCTACGAGCACG-3'
R 5'-AAACCGTGCTCGTAGGTGTGATGGC-3'

To knockdown murine Ldlr, we used CRISPRi system. pHR-SFFV-dCas9-BFP-KRAB (Addgene #46911) and lenti-sgRNA puro (Addgene #104990) were used. The following sgRNA sequences were cloned into the lenti-sgRNA puro vector:
sgctrl (CRISPRi):
F 5'-CACCGTTTTACCTTGTTCACATGGA-3'
R 5'-AAACTCCATGTGAACAAGGTAAAAC-3'
sgLdlr:
F 5'-CACCGCACTCAAACAGCAACGCGGG-3'
R 5'-AAACCCCGCGTTGCTGTTTGAGTGC-3'

For LRP1-ICD stable overexpression study, murine LRP1-ICD (NM_008512, a.a. 4446–4545)[121] was cloned into a custom pCVL-IRES-hygro vector, carrying an SFFV promoter, HA-tag and hygromycin selection marker. pCVL-IRES-hygro empty vector was used as control. The pCVL-IRES-hygro was generated as following: starting from Addgene plasmid #31476, an IRES-hygro sequence was introduced flanked by NsiI restriction sites. After confirming the IRES-hygro insertion in the correct orientation, the region downstream of the SFFV promoter and upstream of the IRES was cut out using XhoI and SbfI and replaced by a short filler sequence.

For Xaf1 and Usp18 overexpression, the CDS of murine *Xaf1* (CCDS24984.2) followed by an HA-tag and the CDS of *Usp18* (CCDS20489.1) followed by a V5 tag separated by P2A sequence were cloned into the pCVL-IRES-hygro vector similarly as described above. To minimize the immunogenicity in *in vivo* experiments, we also cloned the same sequence without tags into pCVL-IRES-hygro.

For LRP1-ICD inducible overexpression study, murine LRP1-ICD followed by an HA-tag was cloned into TLCV2 (Addgene #87360) in place of the Cas9 sequence using AgeI and NheI. The region downstream of the U6 promoter was cut out using KpnI and EcoRI and replaced by a short filler sequence.

Lentiviral production, transduction and cell line construction

The second-generation lentivirus system was used to produce virus from HEK293T cells grown in 6-well plates. HEK293 cells were cultured in DMEM with 10% FBS and plated at 70% confluency the night before transfection. Cells were transfected with 260 ng of

pMD2.G (Addgene #12259), 500 ng of psPAX2 (Addgene #12260), and 680 ng of target vector, using 10 μl of Lipofectamine 2000 (ThermoFisher Scientific, 11668019) diluted in Opti-MEM (ThermoFisher Scientific, 51985034). After an overnight incubation, the medium was replaced with fresh medium. Virus-containing medium was collected 48- and 72-hours post-transfection. The viral supernatant was filtered through a 0.45 μm filter (Pall, 4614), mixed 1:1 with fresh medium and 8 μg/ ml polybrene (Sigma-Aldrich, TR-1003-G) to transduce pre-plated target cells at 50% confluency. To increase PDO transduction efficiency, spin transduction was used. 50-100,000 resuspended HCI-012 cells were plated in low-attachment 6-well plates (Corning, 07-200-601) with viral supernatant and complete media (1:1 mixture) and 8 μg/ml polybrene. The plates were centrifuged at 800g for 1 hour at room temperature. Cells were recovered for 6 hours at 37°C before being embedded into Matrigel. For vectors containing antibiotic selection marker, selection was conducted 48 hours post-transduction. For vectors containing a fluorescent marker, cells were sorted on a BD FACSAria II cell sorter 72 hours post-transduction. For EO771 cells, 2μg/ml puromycin (ThermoFisher Scientific, A1113803) was used for 3 days; 10 μg/ml blasticidin (ThermoFisher Scientific, A1113903) for 7 days; 100 μg/ml hygromycin (ThermoFisher Scientific, 10687010) for 7 days. For MDA-MB-231 cells, 2μg/ml puromycin were used for 3 days; 8μg/ml blasticidin for 7 days; 600 μg/ml hygromycin for 7 days. Gene knockdown or knockout was validated using Western Blotting 3 days after selection. For the LRP1-inducible overexpression, EO771 cells transduced with the TLCV2 vector were treated with varying concentrations and duration of doxycycline (Sigma-Aldrich, D9891) as indicated in Figure 6D.

siRNA transfection

Transient knockdown of *XAF1* and *USP18* was performed using a mixture of four siRNAs (ON-TARGETplus SMARTpool siRNA) purchased from Horizon Discovery. The catalog numbers were: siXAF1 (L-004357-00-0005), siUSP18 (L-004236-00-0005) and control siRNA sictrl (D-001810-01-05). 2nmol siRNA and LipofectamineTM RNAiMAX transfection reagent (ThermoFisher Scientific, 13778150) were diluted in Opti-MEM and added to MDA231-LM3-sgPCSK9-2 cells at ~60% confluency in a 10cm plate. After an overnight incubation, the culture medium was replaced with fresh medium. Successful knockdown was validated with qPCR 72 hours after transfection.

Protein isolation

Cell lines were washed with and scraped into ice-cold PBS (without any Ca^{2+} or Mg^{2+}), centrifuged for 5 minutes at 300 g (4°C). The cell pellet was resuspended in an appropriate volume of RIPA-based lysis buffer (G Biosciences, 786-490) with cOmplete™ Protease Inhibitor Cocktail (Roche, 11697498001), vortexed and left on ice for 15 minutes before a 17,900g centrifugation for 10 minutes. Supernatants were collected as protein solution. For mouse tissues, ~10 mg of tissue was homogenized in ~500 μl ice-cold lysis buffer using Bead Ruptor (OMNI International, SKU 19-040E). Samples were centrifuged at 17,900 g (4°C) for 10 minutes and the supernatants were transferred to new, prechilled Eppendorf tubes. A BCA assay kit (Thermo Scientific, PI23225) was used to quantify the amount of protein in each sample. Samples were stored at -80°C.

Nuclear and cytoplasmic fractionation

Cell lines were washed with and scraped into ice-cold PBS (without any Ca^{2+} or Mg^{2+}, ThermoFisher Scientific, 14190144), centrifuged for 5 minutes at 300g (4°C). The cell pellet was resuspended in an appropriate volume of ice-cold CER I buffer and cytoplasmic and nuclear proteins were extracted with NE-PER Nuclear and Cytoplasmic Extraction Kit (ThermoFisher Scientific, 78835) according to manufacturer's instruction. A BCA assay kit was used to quantify the amount of protein in each sample. Samples were stored at -80°C.

Western blotting

Protein lysates were thawed on ice for 30 minutes before use. Samples were diluted with 4x protein loading buffer (Li-Cor, 928-40004) and 10x sample reducing agent (ThermoFisher Scientific, NP0009). Equal amounts of protein were loaded in 4-12% Bis-tris Mini Protein Gels (Fisher Scientific, NP0336PK2). SDS-Page was performed in MOPS-SDS running buffer (20x, ThermoFisher Scientific, NP000102) at 180 V for ~1 hour or until the dye front had run off the gel. The gels were transferred at 100 V for 1.5 hours at 4°C in transfer buffer (ThermoFisher Scientific, NP0006) onto PVDF membranes (ThermoFisher Scientific, 88520). Membranes were blocked in 5% BSA (Millipore, A2153) in TBS-T (TBS (Cell Signaling Technology, 12498S) + 0.2% Tween (Millipore, P2287) for 1 hour at room temperature. Primary antibodies were diluted in 5% BSA / TBS-T and incubated overnight at 4°C. Membranes were washed thrice with 0.2% TBS-T and incubated for 1 hour at room temperature with corresponding HRP-linked secondary antibodies, added at a dilution of 1:4000. Membranes were then washed thrice with 0.2% TBS-T and activated by an ECL blotting solution (ThermoFisher Scientific, 32106). X-Ray films (Imaging Solutions Company, 110102) were exposed to the membrane for 5 seconds to 10 minutes and developed afterwards. Western blot images were analyzed with ImageJ v1.54h. Mean intensity of the target band was normalized to the loading control band. Primary antibodies used included rabbit anti-HPRT1 (1:8000; Proteintech, 15059-1-AP), mouse anti-HSC70 (1:10000; Santa Cruz Biotechnology, sc-7298), mouse anti-TUBULIN (1:10000; Cell Signaling, 3873), goat anti-PCSK9 (1:400; R and D Systems; AF3985), rabbit anti-PCSK9 (1:1000; GeneTex, GTX129859), rabbit anti-LRP1 (1:20000; Abcam, EPR3724), rabbit anti-LDLR (1:1000; Proteintech, 10785-1-AP), rabbit anti-NFκB (1:1000; Cell Signaling, 8242), rabbit anti-phospho-NFκB (1:1000; Cell Signaling, 3033), rabbit anti-ERK1/2 (1:1000; Cell Signaling, 4695), rabbit anti-phospho-ERK1/2 (1:1000; Cell Signaling, 4370), rabbit anti-JNK (1:1000; Cell Signaling, 9252), rabbit anti-phospho-JNK (1:1000; Cell Signaling, 4668), rabbit

anti-p38 (1:1000; Cell Signaling, 8690), rabbit anti-phospho-p38 (1:1000; Cell Signaling, 4511), rabbit anti-p70S6K (1:1000; Cell Signaling, 9202), rabbit anti-phospho-p70S6K (1:1000; Cell Signaling, 9205), rabbit anti-S6 (1:1000; Cell Signaling, 2217), rabbit anti-phospho-S6 (1:1000; Cell Signaling, 2211), rabbit anti-4E-BP1 (1:1000; Cell Signaling, 9644), rabbit anti-phospho-4E-BP1 (1:1000; Cell Signaling, 2855), rabbit anti-mTOR (1:1000; Cell Signaling, 2983), rabbit anti-phospho-mTOR (1:1000; Cell Signaling, 5536), rabbit anti-AKT (1:1000; Cell Signaling, 4685), rabbit-anti-phospho-AKT (1:1000; Cell Signaling, 4060), rabbit anti-PRAS40 (1:1000; Cell Signaling, 2691), rabbit anti-phospho-PRAS40 (1:1000; Cell Signaling, 2997), rabbit anti-HA (1:1000; Cell Signaling, 3724), mouse anti- Lamin A/C (1:2000; Cell Signaling, 4777), mouse anti-beta IV TUBULIN (1:4000; Abcam, ab11315), rabbit anti-His (1:1000; Abcam, ab9408), mouse anti-V5 (1:1000; Cell Signaling, 80076) and mouse anti-His (1:4000; ThermoFisher Scientific, MA1-21315).

Quantitative reverse transcription PCR

Total RNA from cells cultured in quadruplicate was isolated with the Total RNA Purification Kit (Norgen Biotek, 17200) with 10μl/ml of 2-mercaptoethanol (Sigma-Aldrich, M6250) added to buffer RL. RNA quality was checked on an Agilent 2100 Bioanalyzer and samples with RNA integrity number (RIN) smaller than 8 were excluded. The SuperScript III First-Strand Synthesis System (ThermoFisher Scientific, 18080051) was used to reverse transcribe 1-5μg of total RNA into cDNA according to the manufacturer's instructions using oligo(dT) primers. Subsequently, quantitative real-time PCR was performed using Fast SYBR Green Master Mix (Applied Biosystems) and an Applied Biosystems 7900HT system. Data were analyzed with the pcr R package (v1.2.2). Amplicons were visualized on 2% agarose gel (Lonza Bioscience, 50004) with 0.01% SYBR Safe (ThermoFisher Scientific, S33102). Primer sequences used were as follows:

Murine genes:
Gapdh:
F 5'-AGGTCGGTGTGAACGGATTTG -3'
R 5'-TGTAGACCATGTAGTTGAGGTCA -3'
Xaf1:
F 5'-AGCCATGTGTCTGAGTGCAAA -3'
R 5'- GCAAAGATCACAACGGGTTTTTC -3'
Oas1a:
F 5'-GCCTGATCCCAGAATCTATGC -3'
R 5'-GAGCAACTCTAGGGCGTACTG -3'
Isg15:
F 5'-GGTGTCCGTGACTAACTCCAT -3'
R 5'-TGGAAAGGGTAAGACCGTCCT -3'
Usp18:
F 5'- TTGGGCTCCTGAGGAAACC -3'
R 5'-CGATGTTGTGTAAACCAACCAGA -3'
Rtp4:
F 5'-TGGGAGCAGACATTTCAAGAAC-3'
R 5'-ACCTGAGCAGAGGTCCAACTT -3'
Pcsk9:
F 5'- GAGACCCAGAGGCTACAGATT -3'
R 5'- AATGTACTCCACATGGGGCAA -3'
Human genes:
XAF1:
F 5'- GCTCCACGAGTCCTACTGTG -3'
R 5'- GTTCACTGCGACAGACATCTC-3'
USP18:
F 5'- CCTGAGGCAAATCTGTCAGTC-3'
R 5'- CGAACACCTGAATCAAGGAGTTA-3'
GAPDH:
F 5'- GCCCAATACGACCAAATCC-3'
R 5'- AGCCACATCGCTCAGACAC-3'

Analysis of cell surface protein expression

MDA231-LM3-sgPCSK9-2 cells were seeded in quadruplicates and treated with 2μg/ml BSA (Sigma-Aldrich, A9576), PCSK9 (Sino Biological, 29698-H08H), PCSK9 D374Y V474I G670E (Sino Biological, 10594-H08H1), PCSK9 V474I or PCSK9 F379A. PCSK9 V474I and PCSK9 F379A were produced by Sino Biological in HEK293 cells using the same pipeline for PCSK9 wildtype production. Cells were resuspended in PBS, washed once and diluted in flow buffer (DPBS without calcium and, 1% FBS and 25 mM HEPES). Cells were stained with primary antibodies for 40 minutes on ice, washed twice in PBS and stained with secondary antibodies for

30 minutes on ice in flow buffer with 1μg/ml DAPI. Cells were washed twice and analyzed with Attune NxT Flow Cytometer. Dead cells with compromised membrane (DAPI+) were excluded from the analysis. The following antibodies were used: rabbit anti-LDLR (1:100; Proteintech, 10785-1-AP), mouse anti-LRP1-PE (1:5; BD Biosciences, 550497), and secondary AlexaFluor conjugates (1:200, ThermoFisher Scientific).

Co-immunoprecipitation (co-IP) analysis

MDA231-LM3-sgPCSK9-2 cells were seeded in 15 cm plates 24 hours before the experiment and starved in serum-free Opti-MEM for 2 hours. Cells were then treated with 2μg/ml PCSK9, PCSK9 V474I or PCSK9 D374Y V474I G670E for 1 hour in the presence of 0.1 mM chloroquine (Sigma-Aldrich, C6628). Plates were washed with ice-cold PBS twice and the cells were scraped off from the plate. Cells were lysed in 1% digitonin lysis buffer (20 mM HEPES, 150 mM NaCl, 1 mM MgCl2, and cOmplete™ Protease Inhibitor Cocktail and 1% digitonin (Sigma-Aldrich, 300410)) for 10 minutes on ice before a 17,900g centrifugation for 10 minutes. Supernatants were collected as protein solution. 1μg extracted protein (a total volume of 400-500μl) was subjected to co-IP with Dynabeads™ Protein G (ThermoFisher Scientific, 10003D) following manufacturer's instructions. 5μg rabbit IgG (Cell Signaling, 2729), rabbit anti-LRP1 (Abcam, EPR3724), mouse IgG2b (Cell Signaling, 53484) or mouse anti-His (ThermoFisher Scientific, MA1-21315) were used in the co-IP solution. The bead-bound protein was eluted with Laemmli Sample Buffer (Bio-RAD, 1610747) following manufacturer's instruction. The subsequent western blot was performed as described above.

Matrigel Invasion Assay

EO771 shPcsk9 or MDA231 sgPCSK9-2 cells were serum-starved in 0.2% FBS media for 24 hours. Trans-well invasion chambers (BD Biosciences, 354480) were pre-equilibrated prior to the beginning of the assay by adding 0.5 ml of starvation media to the top and bottom chambers. After 30 minutes, the media in the top chamber was removed, and 0.5 ml of media with 2μg/ml BSA (diluted from Sigma-Aldrich, A9576) or PCSK9 (Sino Biological, 29698-H08H) containing 100,000 cancer cells was added into each matrigel-coated trans-well insert. Cells were allowed to invade through the matrigel-coated inserts for 24 hours at 37°C. Upon completion of the assay, matrigel-coated inserts were washed with PBS, the cells at the top side of each insert were scraped off, and the inserts were fixed in 4% paraformaldehyde (VWR, AA43368-9M) for 15 minutes, washed with PBS and stained with DAPI (Roche, 10236276001) at 1mg/ml for 15 minutes. The inserts were then cut out and mounted onto slides with Prolong Gold (Fisher Scientific, P36930). The basal side of each insert was imaged using an inverted fluorescence microscope (Zeiss Axiovert 40 CFL) at 5X magnification, taking six representative images for each insert. The number of cells that had invaded was quantified using ImageJ.

Cell Proliferation Assay

To determine the effects of *LRP1* knockdown and recombinant PCSK9 treatment on cell proliferation, 50,000 EO771 cells were seeded in quadruplicate in 6-well plates, and viable cells were counted after 2 and 4 days using the trypan blue dead cell exclusion dye (Sigma-Aldrich, T8154). For recombinant protein treatment experiments, 2μg/ml BSA or PCSK9 were added to the media.

Anoikis Assay

800,000 EO771 shPcsk9 or MDA231 sgPCSK9-2 cells were seeded in quadruplicate in Ultra-Low Attachment Surface 6-well plates (Corning, 3471) containing cell media supplemented with 0.2% methylcellulose (Sigma-Aldrich, M7140) with 2μg/ml BSA or PCSK9. Following 48 hours in suspension, the numbers of dead versus viable cells were counted using the trypan blue dead cell exclusion dye.

Colony initiation in the absence of substratum attachment

EO771 or MDA231 cells were sorted with a BD FACSAria II cell sorter at a clonal density of one cell per well into Ultra-Low Attachment Surface 96-well plates (Corning, 3474) in media containing a 1:1 mixture of RPMI or DMEM supplemented with 10% FBS, and 2x RPMI or DMEM mixed 1:1 with 3% methylcellulose stock solution (R&D, HSC001). For recombinant protein treatment experiments, 2μg/ml BSA or PCSK9 were added to the media. The plates were imaged with Incucyte S3 (Sartorius) and the number of cells in each well were counted in the subsequent days. Wells with cells out of focus were excluded from the analysis.

Experimental metastasis assay

To monitor metastasis *in vivo* through bioluminescence imaging, cancer cells were transduced with a lentiviral vector expressing a luciferase reporter and fluorescent marker (MI-Luciferase-IRES-mCherry, Addgene #75020 for EO771-LM2-DR, 4T1, EMT6 and SKBR3; pHIV-Luc-ZsGreen, a gift from B. Welm (Addgene #39196), for MDA231-LM3-TR or HCI012). To stain mCherry+ metastasis in immunofluorescence, EO771 cells were transduced with a lentiviral vector expressing mCherry (pLV-mCherry. Addgene #36084), which exhibited stronger mCherry expression than MI-Luciferase-IRES-mCherry. Fluorescent cells were sorted with a BD FACSAria II cell sorter. Cells were resuspended in PBS and injected into the tail veins of 7–9-week-old female mice. The number of cells injected and the corresponding mice were: 100,000 EO771 cells into mice on C57BL/6 background, 100,000 4T1 cells or 50,000 EMT6 cells into BALB/c mice, 200,000 MDA231 cells or 400,000 HCI012 cells into NSG mice. To measure bioluminescence signal, mice were injected with 16.67 mg/ml d-luciferin (Goldbio LUCK) in 100 μl PBS retro-orbitally and imaged using an IVIS spectrum machine (PerkinElmer). BALB/c and NSG mice were imaged for 60s and C57BL/6 mice were imaged for 300s. Bioluminescence imaging

was performed approximately twice a week, and each lung signal was normalized to the same animal's signal obtained on day 1 after injection. Mice with failed injections were excluded from experiments. Experiments were terminated when the signal of mice in either group reached 100-fold compared to day 1 or mice appeared morbid. Lungs were harvested at the end of the experiments, perfused with PBS via right ventricle injection, fixed with 4% paraformaldehyde (Fisher Scientific, AA433689M) overnight at 4°C, stored in 70% ethanol and sent to Histoserv, Inc for sectioning. The number of lung metastasis nodules and their sizes were quantified from H&E-stained lung brightfield 40x scanning sections prepared by Histoserv. The sizes of metastases were quantified with ImageJ. Experimental group labels were masked during quantification.

In vivo caspase activity was measured by retro-orbital injections of VivoGlo Caspase 3/7 Substrate (1.5mg/mouse of Z-DEVD-aminoluciferin sodium salt; Promega, PAP1781) and the bioluminescence signal was normalized to cancer cell luciferase signal. For recombinant protein treatment experiments, cancer cells were treated with 2μg/ml BSA or PCSK9 for 24 hours prior injection.

Mouse diet and serum chemistry

For high cholesterol diet studies, 7-week-old female wildtype or *Pcsk9* knockout mice were fed regular chow diet (Research Diets, D12492) or high cholesterol diet (Envigo, TD08464, 0.425% cholesterol) 10 days prior to experimental metastasis experiments. For the statin diet study, 7-week-old female C57BL/6J mice were fed control diet (Envigo, TD220626) or 0.01% atorvastatin diet 14 days prior to experimental metastasis experiments. The 0.01% atorvastatin diet was prepared by adding atorvastatin calcium (PCCA, 30-5153) to the control diet.

At the endpoint, blood was collected from mice by submandibular bleeding into dipotassium EDTA Tubes (ThermoFisher Scientific, 02-669-33). Following centrifugation, serum was collected and analyzed on a Beckman Coulter AU680 clinical chemistry analyzer for the following parameters: cholesterol, triglycerides, low-density lipoproteins and high-density lipoproteins.

T cell depletion

For T cell depletion studies, 400μg each of anti-CD4 (Bio X Cell, BE0003-1) and anti- CD8α (Bio X Cell, BE0004-1) antibodies were injected intraperitoneally on days 4 and 11 after cancer cell injection. Control mice received isotype control (Bio X Cell, BE0090) injections on the same days. Efficient depletion was verified by flow cytometry with an Attune NxT Flow Cytometer at the end of the experiments (day 18). Specifically, spleens, lymph nodes and lungs were dissected, chopped into pieces, and incubated in HBSS2+ (HBSS with calcium and magnesium (Gibco, 24020) supplemented with 2% FBS, 1 mM sodium pyruvate (Gibco, 11360), 25 mM HEPES (Gibco, 15630), 500 U/ml collagenase IV (Worthington, LS004188), 100 U/ml collagenase I (Worthington, LS004196) and 0.2 mg/ml DNAse I (Roche, 10104159001) for 30 minutes at 37 °C on an orbital shaker (80 rpm). After thorough trituration, the mixture was passed through a 70 μm strainer and washed with flow buffer (DPBS without any Ca^{2+} or Mg^{2+}, 1% FBS and 25 mM HEPES). Samples were incubated with ACK lysing buffer (Gibco, A1049201) for 5 minutes at room temperature before another wash with flow buffer. Samples were diluted in flow buffer with FC block (BioLegend, 101320) and incubated for 10 minutes on ice. Cells were then incubated with antibodies diluted in flow buffer for 20 minutes, washed with PBS, incubated with Zombie NIR Fixable Live/Dead Stain (BioLegend, 423105) or 1μg/ml DAPI for 20 minutes at room temperature and washed twice with staining buffer. The cells were then analyzed with an Attune NxT Flow Cytometer and FCS Express 7 (De Novo Software). The following anti-mouse fluorophore-conjugated antibodies were used: anti-CD45-BV785 (1:3000; BioLegend, 103149), anti-CD4-BV605 (1:200; BioLegend, 100451) and anti-CD8α-AF700 (1:1000; BioLegend, 100730).

Macrophage depletion

For macrophage depletion studies, the Standard Macrophage Depletion Kit (Encapsula NanoSciences, CLD-8901) was used as described.[48] Specifically, 0.2ml clodronate or control liposomes were injected retro-orbitally into mice 2 days before tumor implantation and every 4 days afterwards. 4 days after the last treatment, spleen and lungs were examined for macrophage abundance as similarly described in the **T cell depletion** section. The following anti-mouse fluorophore-conjugated antibodies were used: anti-CD45-PECy7 (1:200; ThermoFisher Scientific, 25-0451-82), anti-F4/80-FITC (1:200; BioLegend, 123108), anti-CD24-PE (1:200; 101807), anti-MHCII-AF700 (1:200; ThermoFisher Scientific, 56-5321-80).

Intracardiac injection

To study metastasis to organs beyond lung, 100,000 EO771 shPcsk9 cells or SKBR3 cells resuspended in PBS were injected into the left ventricle of 7-9-week-old *Pcsk9* knockout and wildtype mice or NSG mice. Bioluminescence imaging was performed approximately twice a week as described above and the photon flux from the whole body was quantified. Mice with failed injections were excluded from experiments.

Primary tumor growth and spontaneous metastasis

Cancer cells (4T1 and EO771 LM2) were resuspended in a 1:1 mix of PBS and Matrigel (Corning, 354320) at a concentration of 2,000,000 cells/ ml before being injected into the 4^{th} mammary fat pads on the left sides of 7-9-week-old female mice. 200,000 cells were injected per mouse. Mice with failed injections were excluded from experiments. Animals were palpated weekly for tumor formation, after which sizeable tumors were measured with a caliper twice a week. Tumor volume was calculated as $(\text{small diameter})^2 \times (\text{large diameter})/2$. Lungs were harvested and processed at the end of experiments as described in experimental metastasis assay.

MMTV-PyMT mice of the C57BL/6 background developed mammary gland tumors with a mean latency of 13 weeks of age, compared to 7 weeks for FVB background mice. Weekly tumor palpation started at 14 weeks for C57BL/6 and at 6 weeks for FVB mice. The largest measurable tumors were measured with calipers weekly in C57BL/6 and biweekly in FVB mice. Tumor volume was calculated as (small diameter)^2 × (large diameter)/2. Lungs were harvested and processed similarly at the end of the experiments.

PCSK9 inhibition therapeutics

To evaluate the efficacy of PCSK9 inhibition, 200μg human IgG2 monoclonal antibody evolocumab (TargetMol, T9920) were injected intraperitoneally in each mouse approximately twice a week with exact schemes indicated in figures or legends. Control mice received 200μg isotype control (Bio X Cell, BE0301) injections on the same days.

Immunofluorescence

Lungs harvested from mice were fixed in 4% paraformaldehyde overnight at 4℃ and then transferred into 25% sucrose (Sigma-Aldrich, S0389), 0.1% sodium azide (Fisher Scientific, 71448–16) in PBS for 24 hours at 4℃. Tissues were embedded in Tissue-Tek O.C.T. Compound (VWR, 4583) and frozen at -80℃. Sections (20-50 μm thick) were cut using a cryostat set to -20℃ cutting temperature. The sections were collected onto Superfrost Plus microscope Slides (Fisher Scientific, 12-550-15). Prior to immunofluorescent staining, O.C.T. was removed by incubating the slides in PBS for 1 hour. Sections were then permeabilized using 0.5% Triton-X-100 (Millipore, T9284). Slides were blocked in 10% FBS, 1% BSA (Millipore, A2153), 0.1% Tween-20 (Millipore, P2287) in PBS for up to 2 hours at room temperature. Slides were then incubated in primary or secondary antibodies diluted in 1% FBS, 1% BSA, 0.1% Tween-20, 1μg/ml DAPI overnight at 4℃ or for 2-3 hours at room temperature. Slides were mounted with ProLong Gold (ThermoFisher Scientific, P36930). Primary antibodies used in the study include rat anti-mCherry (1:1000, ThermoFisher Scientific, M11217) and rabbit anti-Ki67 (1:1000, Abcam, ab15580). All secondary antibodies were AlexaFluor conjugates (1:200, ThermoFisher Scientific). Confocal microscopy was performed using A1R confocal microscope (Nikon). For each mouse lung, 6 sections and 141-431 fields of view were examined.

Mass spectroscopy of plasma membrane protein

EO771-LM2-shPcsk9 cells were plated in quadruplicates, treated with 2μg/ml BSA or PCSK9 for 24 hours before plasma membrane protein extraction with the Minute™ Plasma Membrane Protein Isolation and Cell Fractionation Kit (Invent Biotechnologies, SM-005). A total of 20μg of each sample was withdrawn and reduced/alkylated with DTT/IAA. Proteins were precipitated with ice-cold acetone and the pellet was digested with sequencing grade trypsin (Promega, V5111). The samples were analyzed by data independent acquisition (DIA) using a 60-minute linear gradient at 900nL/min using a Dionex 3000 HPLC system connected to a Q-Exactive mass spectrometer (both Thermo Scientific). The resulting spectra were analyzed in DirectDIA[109] (https://github.com/Nesvilab/DIA-Umpire) using the mouse proteome (downloaded from uniprot.org) concatenated with common contaminants. The database search and quantification were performed using Spectronaut v.17 (Biognosys) and cross-run normalization was applied. The resulting protein quantification results were further handled within the Perseus statistical environment.[122] Protein quantitative values were $\log_2$ transformed and it was required that a value be present in at least 4 replicates in at least one group to be accepted. Missing values were imputed with random low-abundant signals from a normal distribution. Significance was tested using an FDR-corrected t-test.

Bulk RNASeq

EO771 cells were plated in quadruplicates 24 hours before RNA extraction (treated with 2μg/ml BSA or PCSK9; shctrl or shLrp1). EO771 tumors formed by mammary fat pad injection in wildtype, *Pcsk9* knockout, h*PCSK9*$^{V474I/V474I}$ or h*PCSK9*$^{+/+}$ mice were dissected when their sizes reached 1000mm^3 and disaggregated with a Bead Ruptor. Total RNAs were isolated from cancer cells and tumors using the Total RNA Purification Kit with 5μl/ml of RNasin Plus and 10μl/ml of 2-mecarptoethanol added to buffer RL. RNA quality was checked on an Agilent 2100 Bioanalyzer and samples with RNA integrity number (RIN) smaller than 8 were excluded. Libraries were constructed from 1μg of total RNAs using the TruSeq RNA Library Prep Kit (Illumina, RS-122-2001) with $\geq$ 4 replicates per condition. Constructed libraries were sequenced using an Illumina NextSeq (High Output, 75 SR) at the Rockefeller University Genomics Center. Sequencing reads were mapped to the mouse genome (GRCm38) using STAR aligner v2.7.10b at default settings. Downstream analyses were done in R 3.6.3. Expression levels of genes were quantified with featureCounts v2.0.6. Quality control was conducted with MultiQC v1.11. Differential gene expression analysis was performed with DESeq2 (v1.32.0). For shLrp1 experiments, differentially expressed genes (DEG) were defined as p-adj (Benjamini-Hochberg Procedure) < 0.1 and log2FoldChange > 0.4. For recombinant protein treatment and primary tumor growth experiments, given the smaller effect size, a relaxed threshold was used: DEG were defined as $p < 0.05$. For differential gene expression analysis with the TCGA-BRCA RNASeq data, a two-sided Wilcoxon rank test was applied to each gene comparing patients grouped by rs562556 genotype. Genes were ranked by the -log(p-value) and Gene Set Enrichment Analysis (GSEA)[123] was performed with fgsea v1.12.0 on the Hallmark gene set from MSigDB (https://www.gsea-msigdb.org/gsea/msigdb) with R package msigdbr v7.5.1.

In vivo CRISPR competition assay

The CRISPR competition assay was conducted as previously described.[124] Briefly, a custom library of 60 CRISPR guides targeting the 5 genes (*Isg15*, *Oas1a*, *Rtp4*, *Usp18* and *Xaf1*) was synthesized by IDT with sequences from a previously benchmarked library,[125] amplified by PCR and cloned into lentiCRISPR v2. The library was amplified in liquid culture via electroporation of Endura ElectroCompetent Cells (Lucigen, 60242-1) according to manufacturer's instructions. Miseq-Nano (Illumina) sequencing of the library was performed to ensure a balanced representation of all guides (10 guides per gene plus 10 guides targeting the intergenic regions). Viral supernatant was titrated in EO771 by infecting target cells at increasing amounts of virus and by assessing cell survival after 3 days of selection with puromycin. Two million EO771 cells were infected at an MOI (multiplicity of infection) of 0.105 (calculated from an infection rate of 0.1) 2 days before selection with puromycin for 3 days. At day 12 after transduction of the library, EO771 cells were treated with 2μg/ml PCSK9 *in vitro* for 24 hours before being injected intravenously into 7-week-old C57BL/6J female mice. 100,000 cells were injected per mouse with 5 mice in total, reaching a representation of >1666 cells per guide per mouse. An initial pool of two million cells was collected prior to injection. On day 17 after injection, lungs were harvested. Two million EO771 cells passaged *in vitro* were collected on the same day. Genomic DNA samples were extracted with Quick-DNA MidiPrep Plus Kit (Zymo Research, 11-317MD). For amplification of sgRNA inserts, we performed PCR using specific primers for each condition. PCR amplicons were then purified and sequenced on a Miseq-Nano (Illumina). Reads were mapped and the abundance of each guide was measured. Gene score was defined as the median $\log_2$ fold change in the abundance between the initial and final population of all guides targeting a particular gene and visualized with R package pheatmap. A permutation test was used to determine if guides targeting a gene significantly dropped out compared to control guides with MAGeCK[104] v0.5.9.4. Benjamini-Hochberg Procedure was performed and false discovery rate was reported.

QUANTIFICATION AND STATISTICAL ANALYSIS

Unless otherwise noted, all data are expressed as mean ± standard error of the mean. Sample numbers are indicated in the figures or their legends. Group comparisons were made using significance tests as described in the figure legends and text. Specifically, a Shapiro–Wilk test was conducted first to assess the normality of the data when comparing the means of two groups. Data that passed the normality test were analyzed using Welch's t-test, while non-normally distributed data were evaluated using the Wilcoxon rank-sum test. For qPCR analysis and flow cytometry quantification, equal variance among groups was assumed and Student's t-test was used. For growth curve analysis in experimental metastasis assays, logarithmic fold changes in bioluminescence relative to day 1 were modeled using linear regression. An F test (anova function) compared the null model (fitting all data irrespective of group) with the grouped model (fitting data by grouped label). A P-value of less than 0.05 was considered statistically significant. All statistics were performed in R version 3.6.3 and RStudio 2022.12.0 Build 353.

Supplemental figures

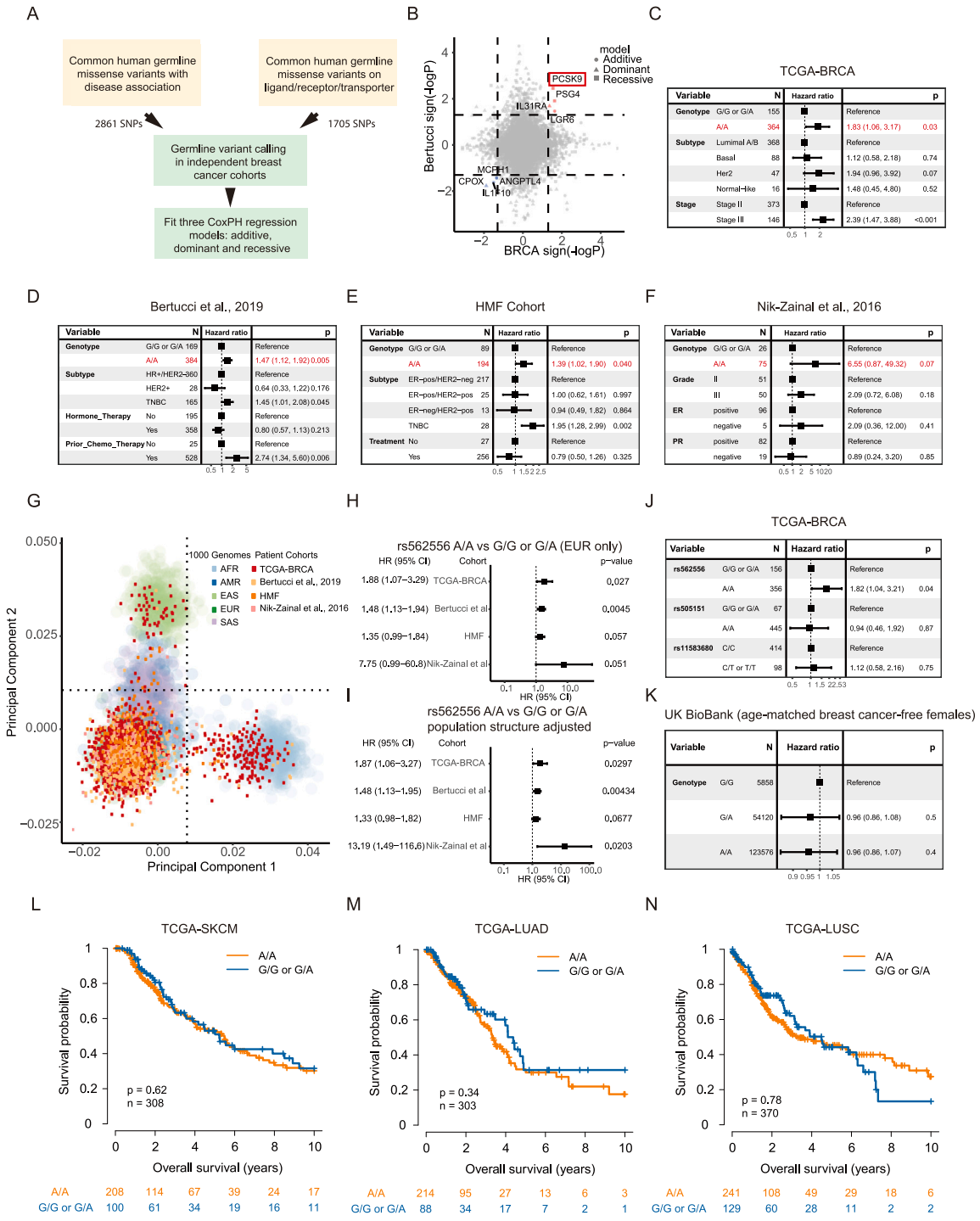

Figure S1. Bioinformatic pipeline and quality controls to identify common germline variants associated with breast cancer survival, related to Figure 1

(A) Bioinformatic pipeline of variant candidate selection, SNP calling, and statistical models.

(B) Dot plot showing −log *p* values with sign of β coefficient (>0 being detrimental to prognosis, <0 being protective to prognosis) in independent breast cancer datasets. Each dot represents a SNP tested in one model labeled with the gene name. Different statistical models are marked with distinct shapes.

(legend continued on next page)

(C–F) Multivariate analysis of rs562556 genotype and common clinical covariates in association with breast cancer survival in TCGA-BRCA (C), Bertucci et al.[26] (D), HMF cohort (E), Nik-Zainal et al.[29] (F). Hazard ratios (HRs) and *p* values were calculated with two-sided Cox proportional hazard model.

(G) Dot plot of genetic principal components of breast cancer patients from cohorts analyzed in this study and participants in the 1000 genome project colored by cohort or ancestry. The dotted line indicates the cutoff to determine European ancestry. AFR, African; AMR, admixed American; EAS, East Asian; EUR, European; SAS, South Asian.

(H and I) Hazard ratios and *p* values of rs562556 association with breast cancer survival in different cohorts limited to European ancestry (H) or adjusted with the first five genetic principal components (I).

(J) Multivariate analysis of rs562556, rs505151, or rs11583680 associations with breast cancer survival in TCGA-BRCA.

(K) Hazard ratios of distinct rs562556 genotypes in breast cancer-free females older than 50 years old in the UK Biobank. Hazard ratios (HRs) and *p* values were calculated with two-sided Cox proportional hazard model.

(L–N) Kaplan-Meier curves of patients with stage II/III melanoma or lung cancer stratified by rs562556 genotype in TCGA-SKCM (L), TCGA-LUAD (M), and TCGA-LUSC (N). *p* values were calculated with two-sided log-rank test.

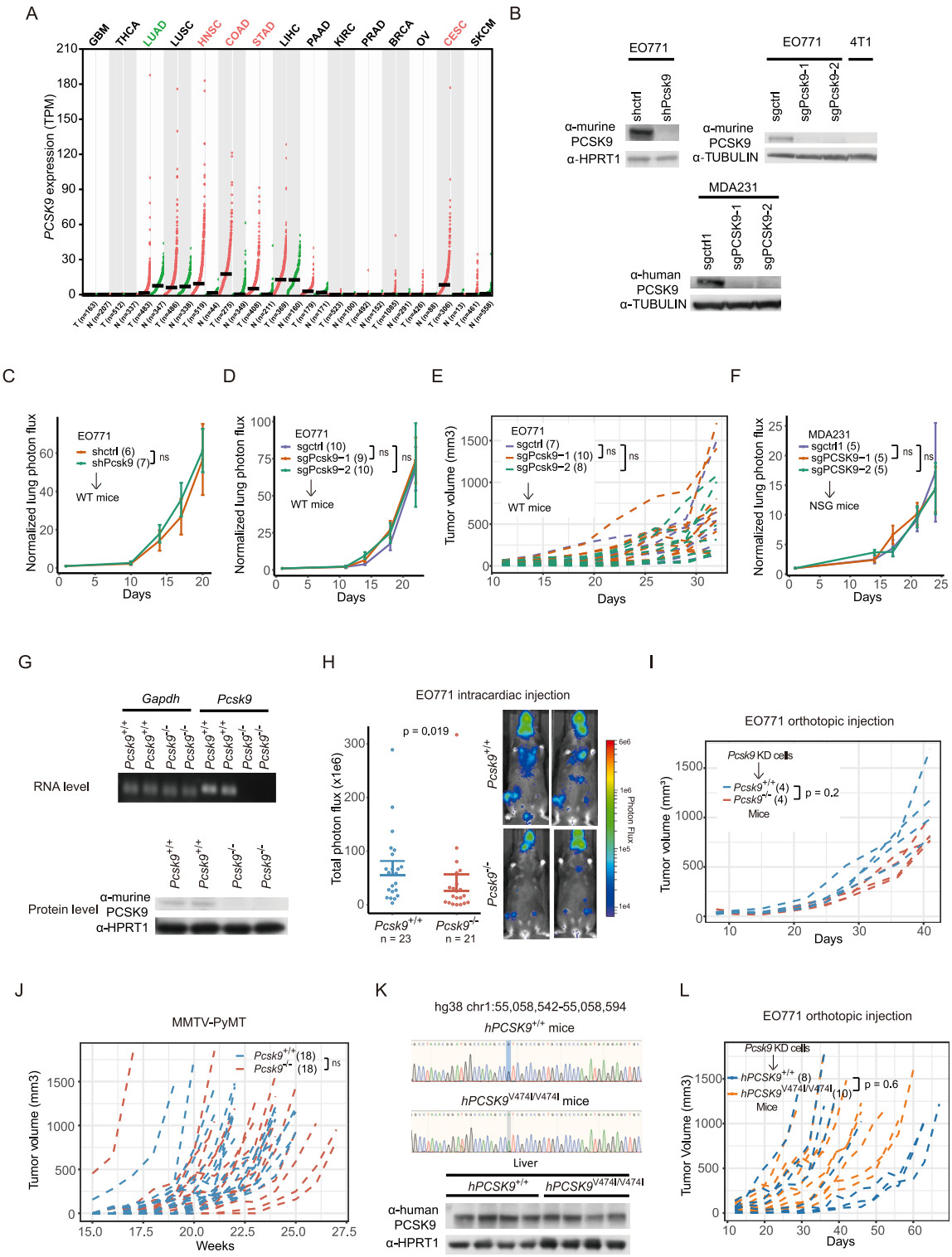

Figure S2. *PCSK9* expression and its function in tumors, related to Figure 2

(A) RNA levels of *PCSK9* in normal tissues (N) and tumors (T) in GTEx and TCGA. PCSK9 upregulated (downregulated) cancer type is marked in red (green).

(B) Protein levels of PCSK9 in EO771-LM2-shPcsk9 cells, EO771-LM2-sgPcsk9 cells, wild-type 4T1 cells, and MDA231-LM3-sgPCSK9 cells.

(C) Bioluminescence imaging of metastatic progression of murine breast cancer EO771-shPcsk9 and shctrl cells intravenously injected into C57BL/6J mice (F test).

(legend continued on next page)

(D) Bioluminescence imaging of metastatic progression of murine breast cancer EO771-LM2-sgPcsk9 and sgctrl cells intravenously injected into C57BL/6J mice (F test).
(E) Growth of murine breast cancer EO771-LM2-sgPcsk9 and sgctrl cells orthotopically injected in C57BL/6J mice (two-sided Wilcoxon rank-sum test on tumor volume at day 34).
(F) Bioluminescence imaging of metastatic progression of human breast cancer MDA231-LM3-sgPCSK9 and sgctrl cells intravenously injected into NSG mice (F test).
(G) RT-PCR (top) and western blot (bottom) validation of *Pcsk9* knockout mice (liver tissue was examined, two mice per group).
(H) Bioluminescence imaging of EO771-LM2-shPcsk9 cells intracardially injected into wild-type or *Pcsk9* knockout mice, 14 days after injection (two-sided Wilcoxon rank-sum test).
(I) Growth of murine breast cancer EO771-LM2-shPcsk9 cells orthotopically injected into wild-type or *Pcsk9* knockout mice (two-sided Wilcoxon rank-sum test on tumor volume at day 41).
(J) Growth of the largest spontaneous tumors in wild-type or *Pcsk9* knockout mice with MMTV-PyMT transgene (two-sided Wilcoxon rank-sum test on tumor volume at week 21).
(K) Sanger sequencing (top) and protein level (bottom) of human PCSK9 of human *PCSK9* knockin mice (liver tissue was examined).
(L) Growth of murine breast cancer EO771-LM2-shPcsk9 cells orthotopically injected into h*PCSK9*$^{+/+}$ or h*PCSK9*$^{V474I/V474I}$ mice (two-sided Wilcoxon rank-sum test on tumor volume at day 29).
In (C)–(F), (H)–(J), and (L), mice numbers per group are indicated.

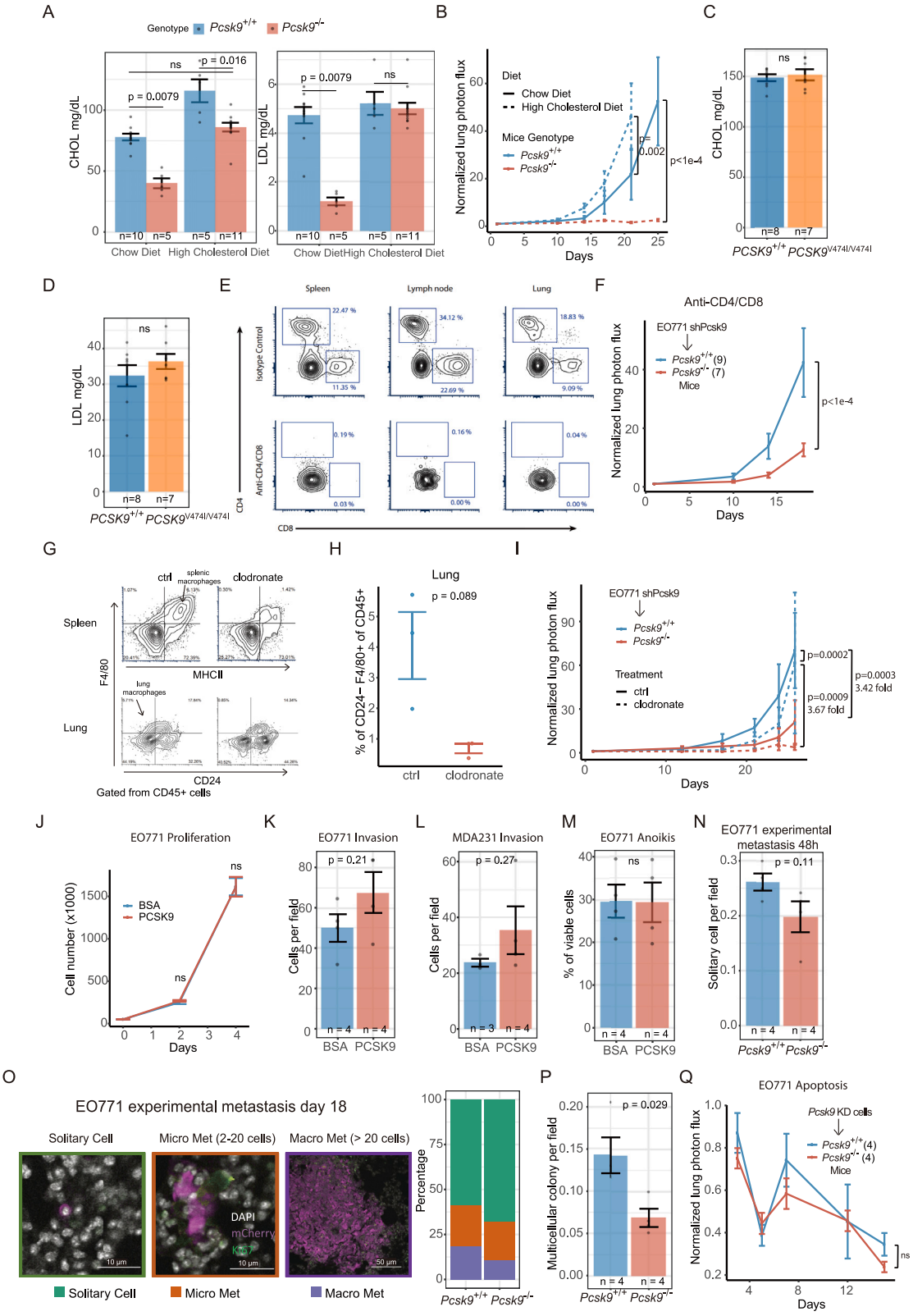

(legend on next page)

Figure S3. PCSK9 specifically promotes metastatic initiation independent of cholesterol or immune regulatory roles, related to Figure 3

(A) Plasma cholesterol (CHOL) and LDL level of *Pcsk9* knockout and wild-type mice fed a high cholesterol or chow diet (two-tailed Welch's t test). Mice numbers per group are indicated.

(B) Bioluminescence imaging of metastatic progression of EO771-LM2-shPcsk9 cells intravenously injected into wild-type or *Pcsk9* knockout mice on high cholesterol diet and chow diet (F test). $Pcsk9^{-/-}$ on HCD: $n = 5$, $Pcsk9^{+/+}$ on chow diet: $n = 10$, $Pcsk9^{+/+}$ on HCD: $n = 10$.

(C and D) Plasma cholesterol (C) and LDL (D) levels of human *PCSK9* knockin mice fed chow diet (two-tailed Welch's t test). Mice numbers per group are indicated.

(E) Representative flow cytometry plots of samples from spleens, lymph nodes, and lungs of mice treated with isotype control versus anti-CD4 and anti-CD8 antibodies.

(F) Bioluminescence imaging of metastatic progression of EO771-LM2-shPcsk9 cells intravenously injected into T cell-depleted wild-type or *Pcsk9* knockout mice (F test, mice numbers per group are indicated).

(G) Representative flow cytometry plots of samples from the spleens and lungs of mice treated with control liposomes versus clodronate liposomes.

(H) Quantification of lung macrophages (CD45+CD24−F4/80+) of mice under control or clodronate liposome treatment.

(I) Bioluminescence imaging of metastatic progression of EO771-LM2-shPcsk9 cells intravenously injected into macrophage-depleted wild-type or *Pcsk9* knockout mice (F test). Number of replicates: control liposomes + wild-type mice $n = 8$; control liposomes + *Pcsk9* knockout mice $n = 6$; clodronate liposomes + wild-type mice $n = 9$; clodronate liposomes + *Pcsk9* knockout mice $n = 8$.

(J) Proliferation of EO771-LM2-shPcsk9 *in vitro* treated with 2 μg/mL BSA or PCSK9 ($n = 4$ per group).

(K and L) Quantification of number of EO771-LM2-shPcsk9 (K) and MDA231-LM3-sgPCSK9-2 (L) cells that invaded into Matrigel *in vitro* under the treatment of 2 μg/mL BSA or PCSK9 (number of replicates per group is indicated).

(M) Percentage of viable EO771-LM2-shPcsk9 cells when detached for 48 h under the treatment of 2 μg/mL BSA or PCSK9 ($n = 4$ per group).

(N) Related to Figures 3A–3C. Quantification of solitary EO771-LM2-shPcsk9 cells in the lung 48 h after injection.

(O) Representative immunofluorescence images and quantification of single, micro (2–20 cells), and macro (>20 cells) lung metastases formed by EO771-LM2-shPcsk9 cells intravenously injected into wild-type or *Pcsk9* knockout mice (18 days after injection). DAPI staining in white, Ki-67 staining in green, and mCherry staining in purple.

(P) Multicellular lung metastasis quantification in wild-type and *Pcsk9* knockout mice ($n = 4$ per group).

(Q) Quantification of apoptotic cells monitored by measurement of a luciferase-based caspase-3/-7 reporter normalized to total EO771-LM2-shPcsk9 cell luciferase signal after intravenous injection into wild-type or *Pcsk9* knockout mice (mice numbers per group are indicated).

p values were calculated with two-sided Wilcoxon rank-sum test. The number of fields of view of each mouse examined in (O) and (P) were: $Pcsk9^{+/+}$ (211, 418, 249, and 270), $Pcsk9^{-/-}$ (372, 431, 389, and 317).

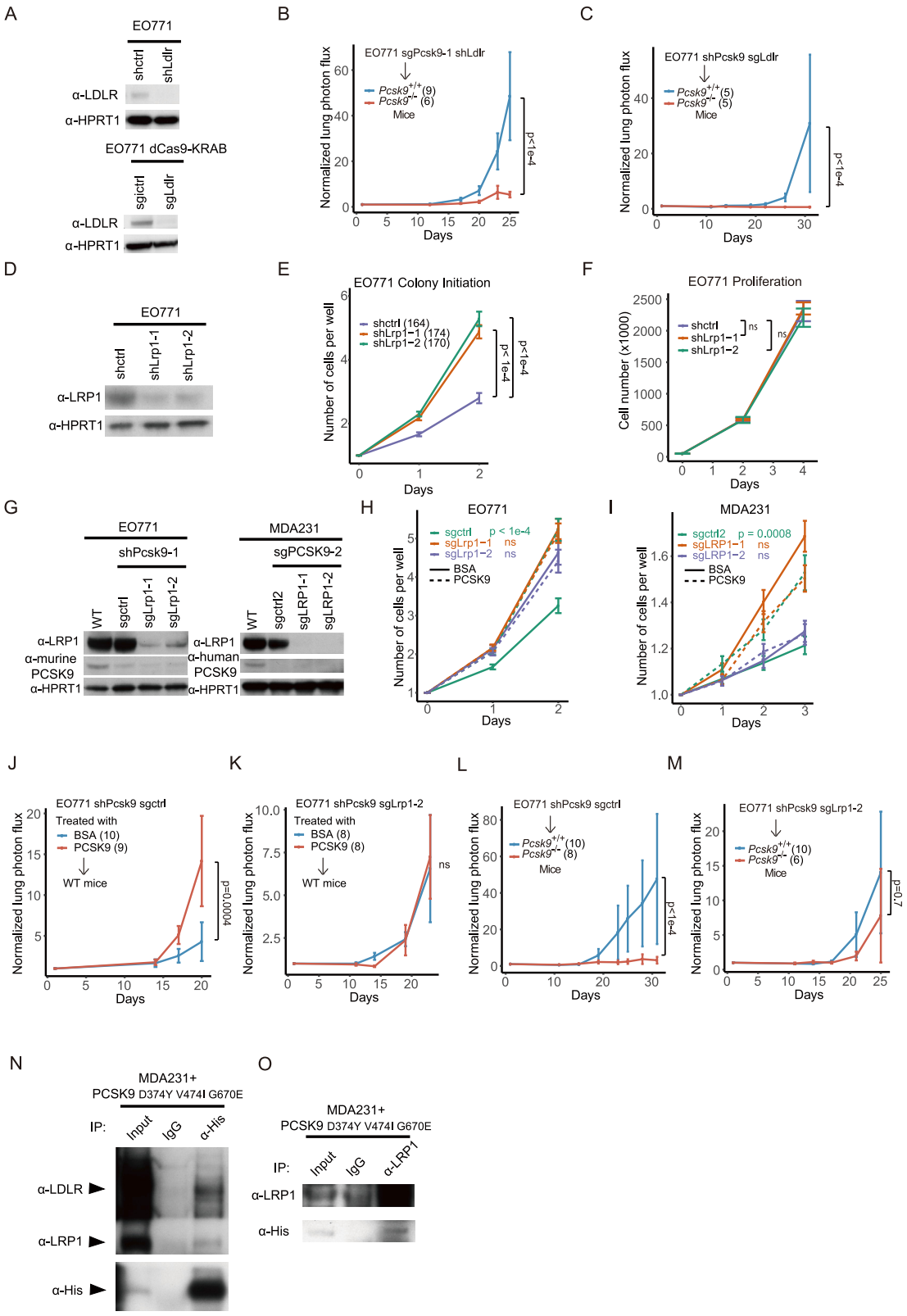

(legend on next page)

Figure S4. PCSK9 targets tumoral LRP1 and drives breast cancer metastasis, related to Figure 4

(A) Protein expression of *Ldlr* in EO771-LM2-sgPcsk9-1 shctrl or shLdlr cells (top) and EO771-LM2-shPcsk9-dCas9KRAB sgctrl or sgLdlr cells (bottom).

(B and C) Bioluminescence imaging of metastatic progression of EO771-LM2-sgPcsk9-1-shLdlr (B) and EO771-LM2-shPcsk9-dCas9KRAB-sgLdlr cells (C) intravenously injected into wild-type or *Pcsk9* knockout mice.

(D) Protein expression of *Lrp1* in EO771-LM2-sgPcsk9-1 shctrl or shLrp1 cells.

(E) Number of EO771-LM2-sgPcsk9-1 shctrl or shLrp1 cells per well in colony initiation assay in low-attachment 96-well plates.

(F) Proliferation of EO771-LM2-sgPcsk9-1 shctrl or shLrp1 cells *in vitro* ($n = 4$ per group).

(G) LRP1 and PCSK9 protein levels in EO771-LM2-shPcsk9 sgctrl or sgLrp1 (left), and MDA231-LM3-sgPCSK9-2 sgctrl or sgLRP1 (right).

(H and I) Number of EO771 (H) or MDA231 (I) cells per well in colony initiation assay in low-attachment 96-well plates with 2 μg/mL BSA or PCSK9 treatment. Number of replicates (wells) are: EO771-LM2-shPcsk9-sgctrl + BSA (160); EO771-LM2-shPcsk9-sgctrl + PCSK9 (161); EO771-LM2-shPcsk9-sgLrp1-1 + BSA (171); EO771-LM2-shPcsk9-sgLrp1-1 + PCSK9 (161); EO771-LM2-shPcsk9-sgLrp1-2 + BSA (160); EO771-LM2-shPcsk9-sgLrp1-2 + PCSK9 (141); MDA231-LM3-sgPCSK9-2-sgctrl + BSA (145); MDA231-LM3-sgPCSK9-2-sgctrl + PCSK9 (142); MDA231-LM3-sgPCSK9-2-sgLRP1-1 + BSA (137); MDA231-LM3-sgPCSK9-2-sgLRP1-1 + PCSK9 (139); MDA231-LM3-sgPCSK9-2-sgLRP1-2 + BSA (142); and MDA231-LM3-sgPCSK9-2-sgLRP1-2 + PCSK9 (134). *p* values indicate comparison between BSA- and PCSK9-treated cells.

(J and K) Related to Figure 4H. Bioluminescence imaging of metastatic progression of EO771-LM2-shPcsk9 sgctrl (J) or sgLrp1 cells (K) treated with 2 μg/mL BSA or PCSK9 for 24 h before being intravenously injected into C57BL/6J mice.

(L and M) Related to Figure 4I. Bioluminescence imaging of EO771-LM2-sgPcsk9-1 sgctrl (L) or sgLrp1 (M) cells intravenously injected into wild-type or *Pcsk9* knockout mice.

(N and O) Co-immunoprecipitation of LRP1 and exogenously added 2 μg/mL His-tagged PCSK9 D374Y V474I G670E protein from MDA231-LM3-sgPCSK9-2 cells. Arrows indicate the expected sized band.

p values in (E), (F), (H), and (I) were calculated with two-sided Wilcoxon rank-sum test. *p* value in (B), (C), and (J)–(M) was calculated with F test. Number of replicates per group was indicated.

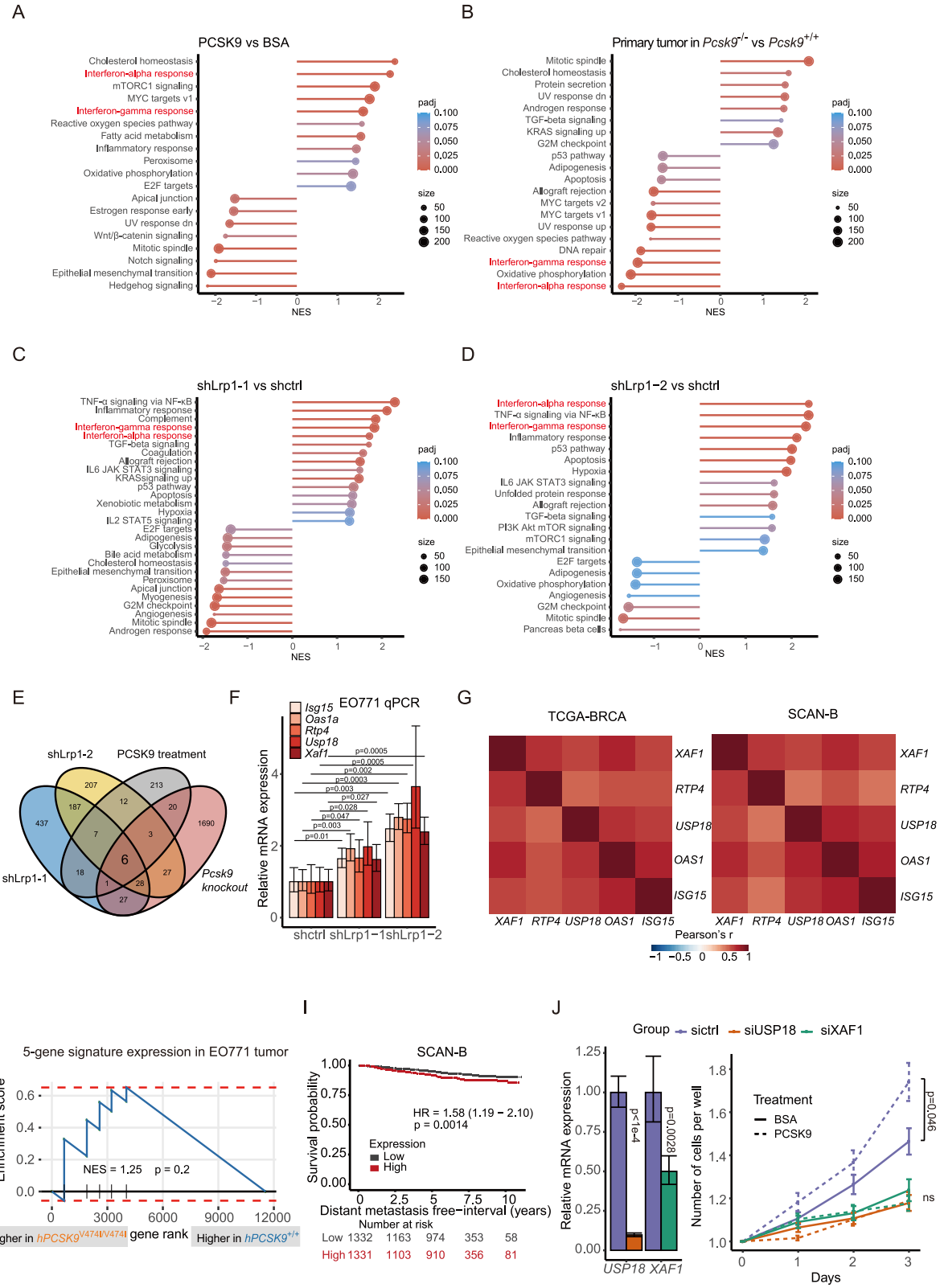

(legend on next page)

Figure S5. PCSK9 targets tumoral LRP1 and de-represses the expression of IFN-associated genes, related to Figure 5

(A–D) Normalized enrichment score (NES) of the top differentially expressed pathways revealed by GSEA in RNA-seq experiments. Each dot represents a Hallmark pathway. Color indicates adjusted *p* values obtained in permutation test. Shape indicates the size of the gene set. (A) Comparing EO771-LM2-shPcsk9 cells treated with 2 μg/mL BSA or PCSK9 *in vitro*. (B) Comparing size-matched EO771-LM2-shPcsk9 primary tumors in *Pcsk9* knockout to wild-type mice. (C and D) Comparing EO771-LM2-sgPcsk9-1 shLrp1-1 (C) or shLrp1-2 (D) to shctrl cells *in vitro*.

(E) Venn diagram showing the overlap of significantly upregulated genes in different experiments.

(F) qPCR quantification of the 5-gene signature expression in EO771 cells upon Lrp1 knockdown (n = 4 per group). Two-tailed Student's t test.

(G) Heatmap depicting the Pearson correlation coefficients among the 5-gene signature expression in TCGA-BRCA and SCAN-B primary tumors. Red indicates Pearson's r close to 1.

(H) Gene set enrichment analysis of the 5-gene signature in EO771-LM2-shPcsk9 primary tumors when implanted into the mammary fat pads of h*PCSK9*$^{+/+}$ or h*PCSK9*$^{V474I/V474I}$ mice. NES, normalized enrichment score. *p* value was calculated with permutation test.

(I) Kaplan-Meier curve of distant metastasis-free interval of breast cancer patients in SCAN-B cohort stratified by the mean expression of the 5-gene signature (bottom quantile versus top quantile). Hazard ratio (HR) and *p* value were calculated with two-sided Cox proportional hazard model.

(J) qPCR quantification of XAF1 and USP18 expression (left) (n = 4 per group; two-tailed Student's t test) and colony initiation assay (right) of MDA231-LM3-sgPCSK9-1 cells transfected with sictrl, siUSP18, or siXAF1 treated with 2 μg/mL recombinant PCSK9 or BSA in low-attachment 96-well plates. Number of wells (replicates): sictrl: BSA (n = 140) and PCSK9 (n = 131); siUSP18: BSA (n = 140) and PCSK9 (n = 127); and siXAF1: BSA (n = 122) and PCSK9 (n = 136). *p* values were calculated with two-sided Wilcoxon rank-sum test.

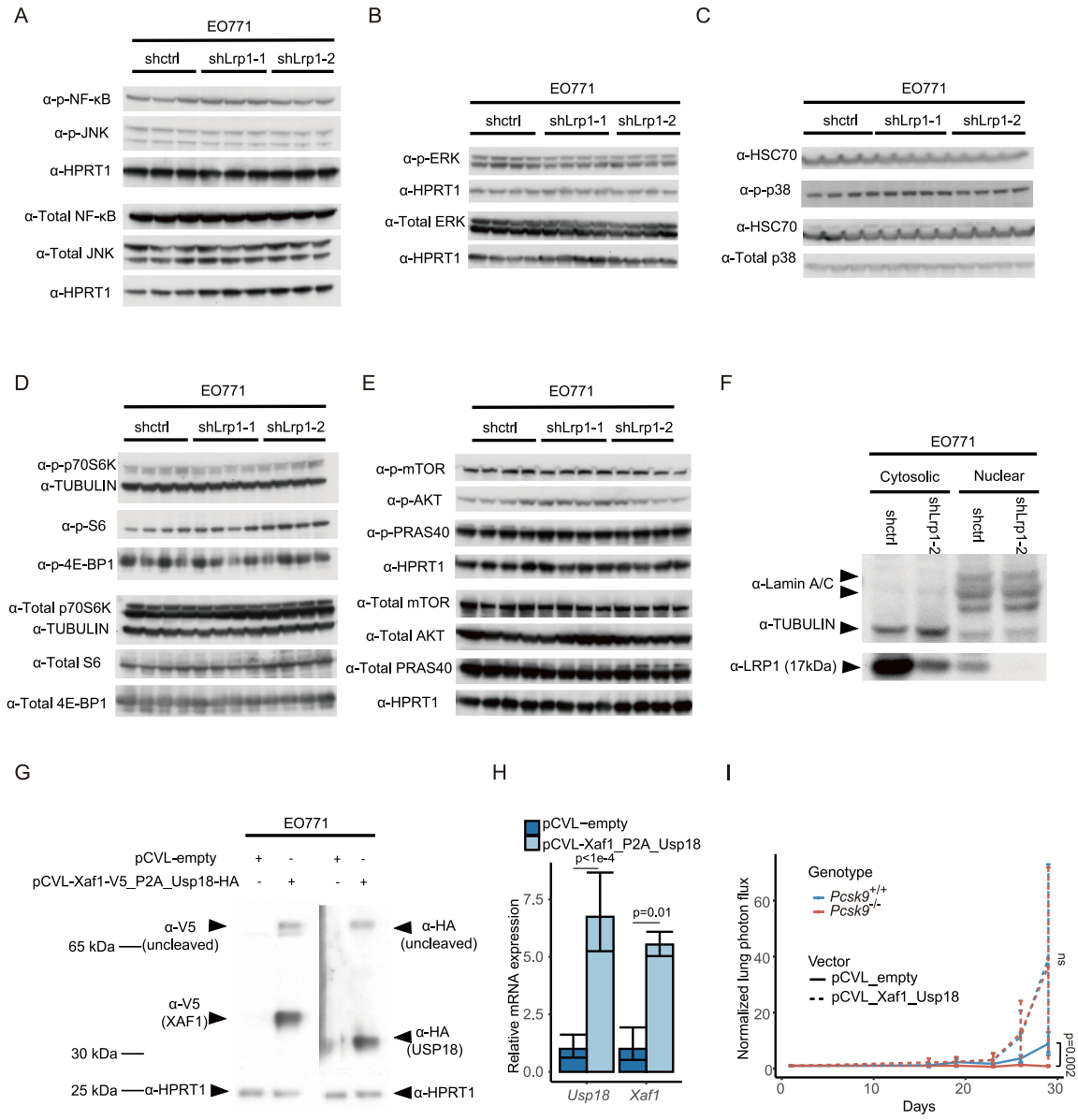

Figure S6. LRP1 depletion does not affect the activity of NF-κB, MAPK, or Akt/mTOR pathway; knockdown of LRP1-ICD and overexpression of its targets, related to Figure 6

(A) Levels of total and phosphorylated NF-κB and JNK in EO771-LM2-sgPcsk9-1-shctrl or shLrp1 cells (3 replicates per group).

(B and C) Levels of total and phosphorylated ERK (B) and p38 (C) in EO771-LM2-sgPcsk9-1-shctrl or shLrp1 cells (4 replicates per group).

(D and E) Levels of total and phosphorylated Akt, mTOR, and their downstream targets in EO771-LM2-sgPcsk9-1-shctrl or shLrp1 cells (4 replicates per group).

(F) Protein expression of LRP1-ICD (17 kDa) in EO771-LM2-sgPcsk9-1 shctrl or shLrp1-2 cells. Western blotting with antibodies against lamin A/C (nuclear marker), beta-IV-TUBULIN (cytosolic marker), and LRP1. Arrows indicate the expected sized band.

(G) Protein products of *Xaf1* and *Usp18* overexpression. Arrows indicate the expected cleaved and uncleaved-tagged XAF1 and USP18 protein products.

(H) qPCR quantification of *Xaf1* and *Usp18* overexpression (two-tailed Student's t test). 4 replicates per group.

(I) Bioluminescence imaging of metastatic progression of EO771-LM2-shPcsk9 cells with empty vector or *Xaf1* and Usp18 overexpression injected intravenously into wild-type or *Pcsk9* knockout mice (F test). Number of replicates: pCVL-empty + *Pcsk9* wild type (n = 5); pCVL-empty + *Pcsk9* knockout (n = 2); pCVL_Xaf1_Usp18 + *Pcsk9* wild type (n = 6); pCVL_Xaf1_Usp18 + *Pcsk9* knockout (n = 4).

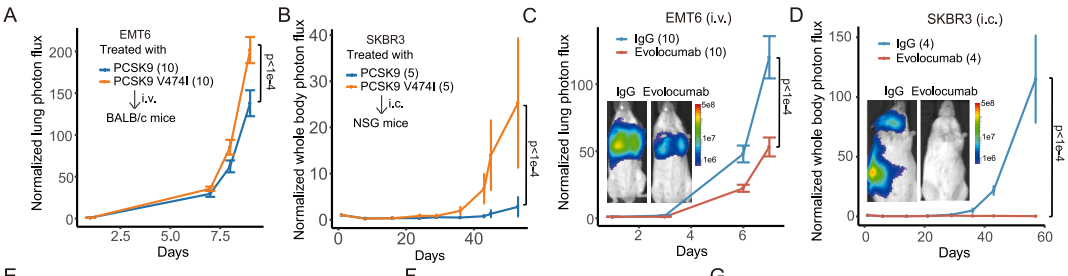

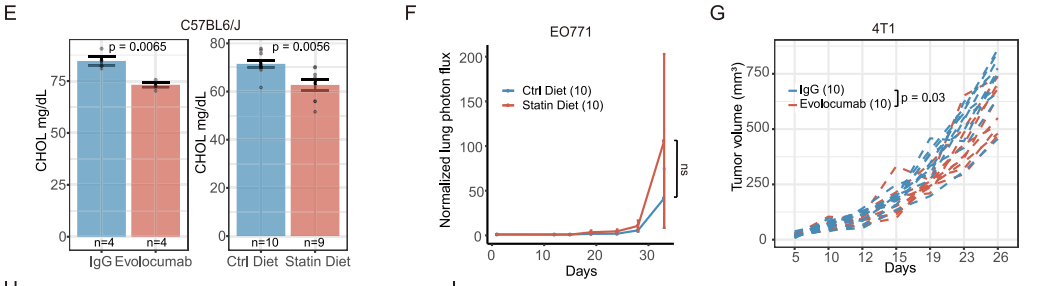

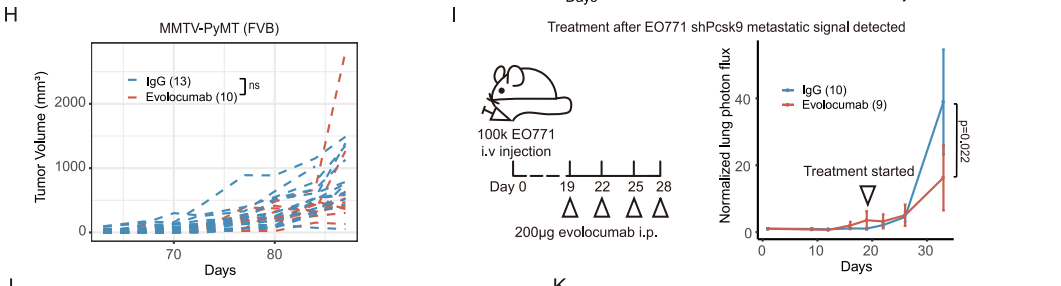

J

DMFI

Variable		N	Hazard ratio	p
Genotype	G/G or A/A	180	Reference	
	A/A	336	7.66 (1.78, 32.90)	0.006
Age.at.Inclusion		516	0.98 (0.92, 1.03)	0.430
ER.Status	Negative	66	Reference	
	Positive	450	0.33 (0.09, 1.18)	0.089
Grade	I or II	363	Reference	
	III	153	1.42 (0.52, 3.93)	0.496
Chemotherapy	No	415	Reference	
	Yes	101	0.13 (0.01, 1.16)	0.068
Radiotherapy	No	179	Reference	
	Yes	337	1.03 (0.42, 2.48)	0.954
Trastuzumab	No	479	Reference	
	Yes	37	5.56 (0.46, 67.62)	0.178
Tamoxifen	No	254	Reference	
	Yes	262	0.54 (0.20, 1.44)	0.218
Aromatase.Inhibitor	No	339	Reference	
	Yes	177	1.05 (0.35, 3.20)	0.928

K

BCFI

Variable		N	Hazard ratio	p
Genotype	G/G or A/A	180	Reference	
	A/A	336	2.44 (1.20, 4.97)	0.01
Age.at.Inclusion		516	0.98 (0.94, 1.02)	0.23
ER.Status	Negative	66	Reference	
	Positive	450	0.79 (0.27, 2.33)	0.67
Grade	I or II	363	Reference	
	III	153	1.17 (0.53, 2.60)	0.69
Chemotherapy	No	415	Reference	
	Yes	101	0.13 (0.02, 1.10)	0.06
Radiotherapy	No	179	Reference	
	Yes	337	0.97 (0.53, 1.79)	0.93
Trastuzumab	No	479	Reference	
	Yes	37	6.11 (0.60, 62.40)	0.13
Tamoxifen	No	254	Reference	
	Yes	262	0.53 (0.28, 1.01)	0.05
Aromatase.Inhibitor	No	339	Reference	
	Yes	177	0.75 (0.34, 1.66)	0.48

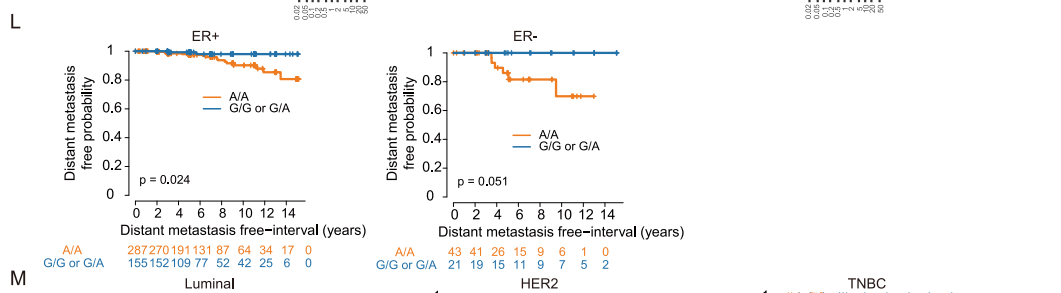

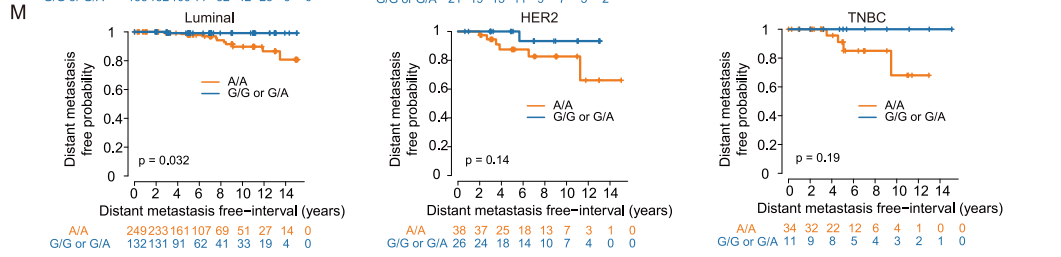

(legend on next page)

Figure S7. Evolocumab treatment, the effect of statin, and rs562556 as a biomarker of breast cancer, related to Figure 7

(A) Bioluminescence imaging of metastatic progression of EMT6 cells treated with 2 μg/mL PCSK9 wild type or V474I for 24 h before being intravenously injected into BALB/c mice (F test).

(B) Bioluminescence imaging of metastatic progression of SKBR3 cells treated with 2 μg/mL PCSK9 wild type or V474I for 24 h before being intracardially injected into NSG mice (F test).

(C) Bioluminescence imaging of metastatic progression of EMT6 cells intravenously injected into BALB/c mice treated with evolocumab or isotype control (F test). Treatment started 2 days before tumor cell injection and continued twice a week.

(D) Bioluminescence imaging of metastatic progression of SKBR3 cells intracardially injected into NSG mice treated with evolocumab or isotype control (F test). Treatment started 2 days before tumor cell injection and continued twice a week.

(E) Plasma cholesterol levels of C57BL/6J mice under evolocumab or isotype control treatment (left) or control diet and statin diet (right) (two-tailed Welch's t test).

(F) Bioluminescence imaging of metastatic progression of EO771-LM2-shPcsk9 cells intravenously injected into C57BL/6J mice on control diet or statin diet (F test).

(G) Growth of 4T1 cells orthotopically injected into BALB/c mice treated with evolocumab or isotype control. *p* values were calculated with two-sided Wilcoxon rank-sum test at the endpoint.

(H) Growth of the largest spontaneous tumors in FVB/NJ mice with MMTV-PyMT transgene treated with evolocumab or isotype control. *p* values were calculated with two-sided Wilcoxon rank-sum test at the endpoint.

(I) Treatment scheme after metastasis signal of EO771-LM2-shPcsk9 cells was detected. Bioluminescence imaging of metastatic progression of EO771-LM2-shPcsk9 cells intravenously injected into C57BL/6J mice treated with evolocumab or isotype control started as indicated (F test).

(J and K) Multivariate analysis of rs562556 genotype and common clinical covariates in association with distant metastasis-free interval (DMFI) (J) and breast cancer-free interval (BCFI) (K) of early-stage breast cancer patients (defined as stage I, lymph node negative, and grades 2 or 3, older than 50 when diagnosed) from the BC-blood cohort.

(L and M) Kaplan-Meier survival curve of breast cancer patients in BC-blood cohort divided by ER status (L) or molecular subtype (M) (two-sided log-rank test).

In (A)–(I), mice numbers per group are indicated.